NASA Contractor Report 185601

# National Aeronautics and Space Administration (NASA)/American Society for Engineering Education (ASEE) Summer Faculty Fellowship Program–1989

*Volume 2*

William B. Jones, Jr., Editor
Texas A&M University
College Station, Texas

Stanley H. Goldstein, Editor
University Programs Office
Lyndon B. Johnson Space Center
Houston, Texas

Grant NGT 44-001-800
December 1989

# PREFACE

The 1989 Johnson Space Center (JSC) National Aeronautics and Space Administration (NASA)/ American Society for Engineering Education (ASEE) Summer Faculty Fellowship Program was conducted by Texas A&M University and JSC. The 10-week program was operated under the auspices of the ASEE. The program at JSC, as well as the programs at other NASA Centers, was funded by the Office of University Affairs, NASA Headquarters, Washington, D.C. The objectives of the program, which began nationally in 1964 and at JSC in 1965, are

1. To further the professional knowledge of qualified engineering and science faculty members
2. To stimulate an exchange of ideas between participants and NASA
3. To enrich and refresh the research and teaching activities of participants' institutions
4. To contribute to the research objective of the NASA Centers

Each faculty fellow spent at least 10 weeks at JSC engaged in a research project commensurate with his/her interests and background and worked in collaboration with a NASA /JSC colleague. This document is a compilation of the final reports on the research projects performed by the faculty fellows during the summer of 1989. Volume 1 contains reports 1 through 11, and Volume 2 contains reports 12 through 26.

# CONTENTS

## *Volume 1*



## *Volume 2*

# OPTICAL CALCULATION OF CORRELATION FILTERS FOR A ROBOTIC VISION SYSTEM

Final Report

NASA/ASEE Summer Faculty Fellowship Program--1989

Johnson Space Center


| | |
|---|---|
| Prepared By: | Jerome Knopp |
| Academic Rank: | Associate Professor |
| University & Department: | University of Missouri-Columbia<br>(Truman Campus)<br>Dept. of Electrical & Computer Engineering<br>600 West Mechanic<br>Independence, MO 64050 |
| NASA/JSC | |
| Directorate: | Engineering |
| Division: | Tracking and Communications |
| Branch: | Tracking Techniques |
| JSC Colleague: | Richard D. Juday |
| Date Submitted: | September 19, 1989 |
| Contract Number: | NGT 44-001-800 |

## ABSTRACT

A method is presented for designing optical correlation filters based on measuring three intensity patterns: the Fourier transform of a filter object, a reference wave and the interference pattern produced by the sum of the object transform and the reference. The method can produce a filter that is well matched to both the object, its transforming optical system and the spatial light modulator used in the correlator input plane. A computer simulation was presented to demonstrate the approach for the special case of a conventional binary phase-only filter. The simulation produced a workable filter with a sharp correlation peak.

## INTRODUCTION

The location and recognition of objects such as handtools drifting in space, boulders on the surface of Mars and the recognition and alignment of docking mechanisms using computer vision are typical of mission requirements in several NASA programs. These include the unmanned Mars mission, the EVA (Extra-Vehicular Activity) retriever and autonomous rendezvous and docking. In most of these cases the speed involved in the recognition process must exceed that of human vision. Even the fastest available digital computing systems cannot process data fast enough to compete with the eye-brain. An interesting alternative to using digital computation is a hybrid system that uses a combination of optical and digital computing. Among several promising schemes being studied by NASA for implementation is an optical computer that uses a "matched filtering" technique[1] for the recognition tasks. The key element in this approach is the design of a correlation filter; a new approach to designing filters is described.

## MATCHED FILTERING

Matched filtering is based on computing the optical Fourier transform using a lens and then multiplying the transform by a filter that approximates the conjugate of the object transform under match conditions. This product is then inverse Fourier transformed using another lens. If the filter and the object are matched to each other then a strong correlation peak (an intense point of light) can be detected at the output of the optical system. An object is identified by testing it against a bank of previously calculated filters for an intense correlation peak. This testing can be carried out at extraordinary speeds using a special optical-digital chip designed for NASA by Texas Instruments in Dallas known as the Deformable Mirror Device (DMD). The DMD consists of an array of more than 16,000 microscopic mirror elements arranged in a square array only one quarter of an inch on a side. This array is mounted on an integrated circuit chip and is controlled by a small computer (an IBM clone). During the past 4 years, NASA has been working on a robotic vision system that uses the DMD to sequence through a set of test filters. The filters are stored and written to the DMD by the computer. One of the problems using this approach is the precise design of the test filters. At present the filter designs are based on computer models or digitized television camera images of the objects of interest. Unfortunately in a real system what an object will "look like" to the optical computer depends on the precise details of the spatial light modulator (SLM)[2] used in the input plane of the optical correlator. There are many different types of candidate SLM's available. These include liquid crystal light valves, modified liquid crystal televisions and even the DMD. It is exceedingly difficult to accurately model the image these devices would produce. An alternative to computer modeling is a more direct optical approach that uses the input SLM as well as the correlator optical system to make a precise in situ calculation of a correlating filter.

## OPTICAL FILTER CALCULATION: GENERAL APPROACH

The ideal filter is one computed directly from images presented by the input SLM. This would provide precisely the filter needed based on the correct image rather than an approximate model. This can be done using an optical approach that collects the information directly using the same lens system that is used in the optical filtering operation. This approach has the additional advantages that it can account for certain shift invariant aberrations in the optical system as well as provide data quickly enough for real-time filter design. The latter

property is of use in building tracking systems that can lock onto arbitrary targets.

In order to explain the optical approach, a one dimensional model will be analyzed for convenience. First consider the intensity pattern produced I(x) by the sum of the fields of the Fourier transform of an object t(x) and a reference field R(x) exp[jΘ(x)]:

$$I(v) = \{F\{t(x)\} + R(v)\exp[j\Theta(v)]\}\{F\{t(x)\} + R(v)\exp[j\Theta(v)]\}^*$$

Here F{ } represents the Fourier transform operator, exp( ) represents exponentiation and the asterisk superscript represents conjugation. Letting

$$T(v)\exp[j\psi(v)] = F\{t(x)\}$$

and carrying out the previous product gives

$$I(v) = R^2 + T^2 + 2RT\cos(\Theta - \psi) \qquad (1)$$

Equation (1) is the key to the filter design. Before discussing a general case, we will examine a simple case where Θ is constant. This implies the reference is locally a plane wave, although the amplitude is not necessarily a constant. If I, $R^2$ and $T^2$ are measured by separate intensity measurements it is possible to solve for the magnitude of the cosine term and hence the magnitude of the relative phase between the reference and the object transform. This is precisely the information needed to design a conventional binary phase-only filter. (A filter that will match provide the best match possible to a planar wavefront given the constraints that the filter will add either 0 or 180 degrees at given location v in the frequency plane.) If the relative phase magnitude is less than 90 degrees then the filter should add only 0 degrees of phase shift. Otherwise the filter should add 180 degrees of phase shift to provide the best match. To implement this approach the three intensity measurements can be made by using a camera with a frame-grabber to store the data in a computer. The processing is fairly simple and can be simplified further by avoiding the arccosine calculation of the relative angle. Since the only information that is needed is the phase range, it is only necessary to determine if

$$I(v) > T^2 + R^2 \qquad (2)$$

If this is true then it follows that the relative phase angle is less than 90 degrees and the filter will add no phase shift. If the inequality is false the filter should provide 180 degrees of phase shift. Inequality (2) provides a fast way to implement binary filter calculations using only three simple intensity measurements, addition and a simple compare operation. If a better matching than a binary filter is desired than more information than provided by inequality (2) is needed. This requires another intensity measurement.

The sign and magnitude of the relative phase can be found by making one additional measurement in which the reference wave is shifted by a known amount at every point and the intensities associated with the object wave and the reference wave are kept constant. If the reference shift is carefully chosen there are two equations for I(v) at every point that can be solved for the relative phase. If the phase magnitude and sign are known at every point then an optimal phase filter can be designed that can produce the best correlation peak signal

possible within the phase constraints of the spatial light modulator (SLM) used to implement the filter design[3]. Furthermore a more arbitrary (nonplanar) reference can be used provided its shape is the desired output of the filter. For example, it may be desired to use the filter to provide quadratic phase compensation or perhaps provide the phase shift needed to produce its own inverse Fourier transform and thus save a lens in the correlation system.

One particularly easy method to implement the additional measurement occurs in the case of a plane wave reference. If the reference is shifted by 90 degrees then the additional equation replaces the cosine term in eq. (1) by a sine term. These equations can be solved uniquely.

## SIMULATION RESULTS

It is interesting to demonstrate the method using a computer model for an arbitrary object. A one dimensional object was constructed using 64 random data points between 0 and 1 from a pseudo-random number generator that approximated a uniform distribution. A graph of the function generated is shown in Fig. 1.

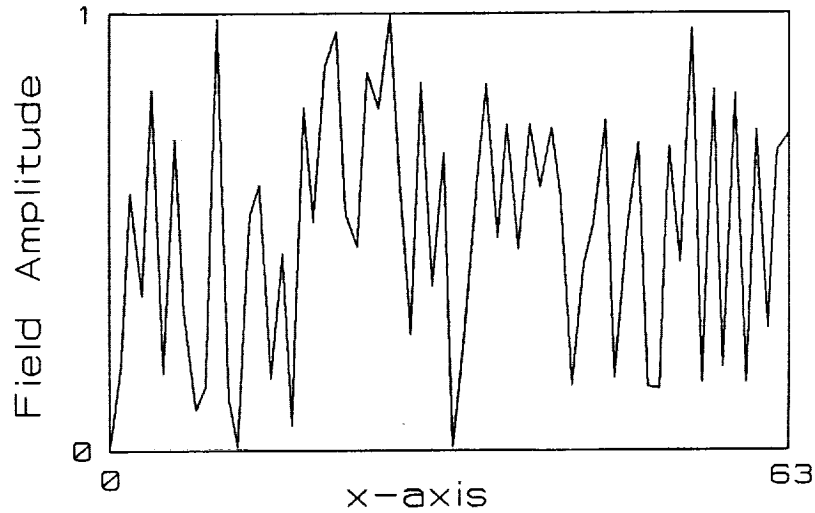


Fig. 1. Random object used for filter design.

The object was used to construct a binary correlation filter using inequality (2). The object function was zero padded with an additional 64 points and digitally Fourier transformed. An on-axis reference wave of amplitude 1 and 0 degrees phase shift was assumed. The binary filter shown in Fig. 2 was produced.

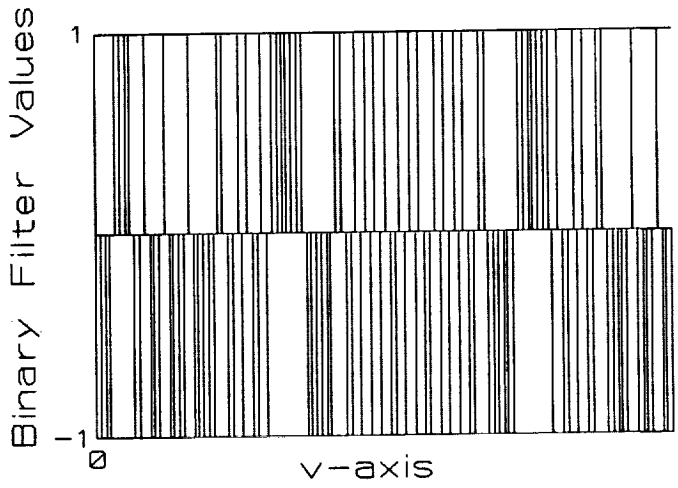


Fig. 2. The binary filter calculated from intensity measurements.

This filter was then applied to the Fourier transform of the random object and inverse transformed. The magnitude of the inverse transform was squared to produce the output correlation. The output is shown in Fig. 3 as a function of x', the output plane coordinates.

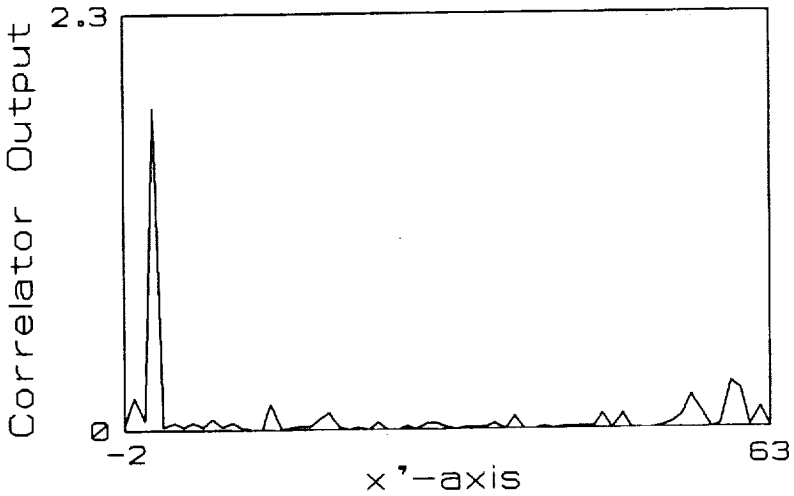


Fig. 3. Output plane correlation for binary filter.

This plot was slightly shifted using some frequency plane tilt and truncated to 66 points to show the region around the correlation peak clearly. This peak shows the typical sharpness expected from binary filters.

## CONCLUSIONS

A method has been presented for designing optical correlation filters based on measuring intensity patterns. A computer simulation was carried out for the special case of a binary phase-only filter using an on-axis uniform plane wave. The simulation produced a workable filter with a sharp correlation peak.

## FUTURE WORK

Plans have already been made for laboratory demonstrations of the approach outlined. These plans include trials with the DMD and a liquid crystal television (LCTV). The DMD is phase-mostly SLM; it acts primarily on the phase with a small (usually insignificant) amount of amplitude modulation. It will be tried using phase-only filters. Previous experimentation with LCTVs at NASA has yielded fruit. A high contrast LCTV has been found that can be used both in the input plane and the filter plane. This device can be used for both amplitude and phase controlled binary filters. The amplitude only filter simply blocks the terms that normally require 180 degrees phase shift in a binary filter. This produces the same type correlation profile as a binary phase filter (i.e., All the phasors at the filter output are constrained to a 180 degree phase window.) but with a reduction in peak strength on the order of 4. In order to use the LCTV as a phase-only filter it is necessary to produce either 0 or 180 degrees phase shift at each pixel at the analyzing polarizer output. This can be done by putting the analyzer's polarization axis orthogonal to a polarization angle half way between the two angles associated with a maximally transmitting or blocking pixel. This method has low throughput unless an efficient (i.e. high contrast) LCTV is used.

In addition to the laboratory work, new schemes for optimizing the filters are being studied. Although it should be possible to digitally calculate an optimal filter using the intensity data, it would be interesting to consider optically methods to rapidly carry out these calculations. One simple scheme would be to vary the reference phase while monitoring the peak strength to search out an optimal design. This is reasonable using SLMs that are easy to write on via computer control. In the case of binary filters it makes sense to consider using optical subtraction and thresholding to calculate filters in real-time.

## REFERENCES

1. J.W. Goodman, Introduction to Fourier Optics, p. 178, Mc-Graw-Hill, New York (1960).
2. D.G. Feitelson, Optical Computing for Computer Scientists, p. 24, MIT Press, Cambridge MA (1988)
3. J. Knopp and R.T. Wingerter, "A Comparison of Binary and Continuous Phase-Only Filters With Restricted Range", Proc. of the SPIE, V1098 (1989).

N90-24987

# KNOWLEDGE-BASED CONTROL OF AN ADAPTIVE INTERFACE

Final Report

NASA/ASEE Summer Faculty Fellowship Program-1989

Johnson Space Center


| | |
|---|---|
| Prepared By: | Roy Lachman, Ph.D. |
| Academic Rank: | Professor of Psychology |
| University & Department: | University of Houston<br>Department: Psychology<br>Houston, Texas 77204 |
| NASA/JSC | |
| Directorate: | Space and Life Sciences |
| Division: | Man-Systems Division |
| Branch: | Crew Station Branch |
| JSC Colleague: | Frances E. Mount, MS |
| Date Submitted: | August 25, 1989 |
| Contract Number: | NGT 44-005-803 |

## ABSTRACT

The analysis, development strategy, and preliminary design for an intelligent, adaptive interface is reported. The design philosophy couples knowledge-based system technology with standard human factors approaches to interface development for computer workstations. An expert system has been designed to drive the interface for application software. The intelligent interface will be linked to application packages, one at a time, that are planned for multiple-application workstations aboard Space Station Freedom. Current requirements call for most Space Station activities to be conducted at the workstation consoles. One set of activities will consist of standard data management services (DMS). DMS software includes text processing, spreadsheets, data base management, etc. Text processing was selected for the first intelligent interface prototype because text-processing software can be developed initially as fully functional but limited with a small set of commands. The program's complexity then can be increased incrementally. The intelligent interface includes the operator's psychometric profile, prior performance history, and a current keystroke performance stack within a conventional expert system database. Error detection and other productions in the form of conditionals between the operator's behavior and three types of instructions to the underlying application software are included in the rule base. A conventional expert-system inference engine searches the data base for antecedents to rules and sends the consequents of fired rules as commands to the underlying software. Plans for putting the expert system on top of a second application, a database management system, will be carried out following behavioral research on the first application. The intelligent interface design is suitable for use with ground-based workstations now common in government, industrial, and educational organizations.

## INTRODUCTION

Integrated computer work stations are now under development at major U.S. corporations and at NASA. It is likely that in the 1990s, a variety of professionals will practice most aspects of their craft at an integrated work station. The most ambitious program, in this regard, is the Multipurpose Applications Console that will be used by the crew of U.S. Space Station Freedom. Scientific research as well as standard operations aboard the Space Station will require new approaches to human performance. Crews will operate and maintain equipment of unprecedented technological sophistication and complexity. Simultaneous monitoring of multiple systems, documentation access, data management, and command and control will be routinely conducted at integrated work-station consoles. Significant components of Space Station design now incorporate machine intelligence in the form of expert systems, robotics, and advanced automation. One aspect of machine intelligence in Space Station Program Requirements is of particular interest to cognitive psychologists: standard computer services with knowledge-based components and an interface that adapts to the unique characteristics of individual crew members.

This paper explores approaches to instantiating intelligence in the computer-human interface in the form of specific knowledge-based technologies. The initial effort to conceptualize an approach to this problem, formulate a design philosophy, and to develop a prototype is described. The relatively slow pace of research on adaptive systems and its significance is considered. Cognitive psychology provides one major orientation. The emerging fields of cognitive science and cognitive engineering are also a major source of concepts and methodology in this study of basic and applied problems in human and machine cognition.

## NEEDS

The need is particularly acute for adaptive capacities in the integrated work stations of manned spacecraft. The logistics and costs of habitation aboard Space Station, for example, necessitates a minimum size of crew. Each crew member, therefore, will be assigned multiple responsibilities. Crew skill levels will vary with frequency of performance of particular tasks and native ability. The interface for a computer-based activity that is most suitable for peak skills can be highly unsuitable when that skill has diminished. Extended habitation in space may require that computers adapt to fixed and variable human characteristics. Intelligent machines, with knowledge-based control of the computer-human interface, are essential to the effective deployment of advanced computer-human interactive technologies as well as to raising productivity

for computer based tasks that are now commonplace. A number of cognitive science problems are related to developing an intelligent interface that adapts its displays and command structure to each individual system user. Psychometric and performance data of an individual must provide the knowledge base as well as the rule-driving data base to adapt the control structure and command dialogue of work-station services to fixed characteristics and the current performance level of the user. Individual capacities measured previously and performance collected continuously at the operator-system interface have the potential for interpreting human performance, competency levels, errors and other unsuitable performance patterns. Information obtained unobtrusively from embedded performance measures and directly from queries to the human operator serves as the input to expert-system software modules. Elements of this information are the antecedents to the firing of rules in a production-system architecture. A knowledge-based work-station interface possesses the potential for reducing errors and significantly enhancing system performance and human productivity on Space Station and elsewhere.

## DESIGN PHILOSOPHY

The design and development of any engineering artifact, including software systems, entails an implicit design philosophy. It is useful to articulate the philosophy so that inadequacies can be recognized and corrected before changes become too costly. The current design philosophy is consistent with proven approaches reported in the literature (Rouse, Geddes, and Curry, 1987-88) and is summarized as follows.

- o Develop operator centered design, leave the crew in charge
- o Overcome human sensory and cognitive limitations
- o Amplify existing human abilities
- o Automate where human performance is below an acceptable level
- o Sophistication of support for each application can vary from simple methods to large scale knowledge-based systems
- o Develop support systems incrementally within a range of the application subsystems.
- o Map expert-system technology on to the problem

The major justification for an operator-centered approach stems from the impossibility of ruling out the need for human intelligence to solve problems. Unanticipated events happen; only human intelligence can deal with unanticipated events. Automated systems including robotics and expert systems can only deal with events that were anticipated, and then only when plans were specifically enacted to deal with those events. There are numerous examples of the failure to anticipate potentially

catastrophic events. The examples include the fuel cell failure on STS-2 and the false warning of an impending Soviet nuclear attack in 1960 due to unanticipated radar reflections from a moon rise.

An incremental approach with more than one application is the recommended method of development because cognitive variables interact with tasks and the tasks interact with each other to change difficulty levels, error types, and other performance parameters. The last item in the statement of design philosophy calls for the development of expert systems. Expert systems are the technology of choice for an adaptive interface because of their power and flexibility and their capacity to capture the heuristics of operator performance.

## RESEARCH IN COGNITIVE PSYCHOLOGY

Contemporary theories of intelligence view adaptability as essential to intelligent behavior; this likewise must be part of any reasonable concept of machine intelligence. Understanding the processes by which adaptability is incorporated into a knowledge-based system requires more than AI system building; basic research in cognitive psychology is also needed. Research to isolate the heuristics that facilitate machine adaptation to the human user's fixed and variable capacities requires combining research in Artificial Intelligence and Psychology. Part of this project is devoted to the study of general human expertise and skilled performance in selected work-station tasks. Developing an adaptive interface requires inquiry into a machine's ability to recognize user and task properties. In order to effectively guide a person through a complicated task, a machine (or even a human helper) must possess specific sets of knowledge of the person and the task. The expert system knowledge base must possess detailed information as to the current stage of the task and the user's performance. At certain machine-state operator-input cycles, it is essential to determine the user's intentions, at least partially, for effective machine intervention. The system will provide more realistic and improved guidance if it possesses rules and facts dealing with user characteristics related to performance such as general task knowledge, aptitude, and motivation.

Precisely formulating the user's task state knowledge, and the user's intentions relative to the current machine state (i.e. what the user is trying to do right now) is the goal of continuing cognitive research that is important to the project. Machine-detectable user information from keystrokes is currently the primary basis for formulating rules that, when fired, produce the adaptation of a work station's display and command structure. It is important to

detect increasing operator expertise. Anderson, Farrell, and Sawyers (1984) have shown that the development of expertise entails a shift from the use of declarative knowledge to the development of problem specific productions that are subsequently used in new situations. The acquisition of productions can be detected by a decrease in latency and recurring keystroke patterns. Automaticity, increases in quantity of knowledge, schema driven problem solving, and changes in chunking patterns are all indicative of growth of expertise (Chi, Glaser, and Reese, 1982). Several of these indices may be detectable by changes in keystroke patterns and response latencies to specific machine states.

## DATA MANAGEMENT SERVICE SIMULATIONS

Work-station hardware and software components in current Space Station specifications (NASA SSP 30261, 1989) are to be designed for modularity. The software will contain a number of modules for crew operations support. These will provide, among other things, Data Management Services. DMS will support a full spectrum of computer services including document retrieval, word processing, and data base access. Two DMS functions are selected for simulation, namely, text editing and data base management. The "simulated" text editor has been developed with a limited command set. Figure 1 (next page) shows the help screen with the limited command set currently in use. The editor is an extension of software developed to enhance comprehension of technical text (Lachman, 1989b).

## THE EXPERT SYSTEM ADAPTIVE INTERFACE

The core idea of an adaptive interface is to reverse the usual role of human and computer and to equip the computer with mechanisms to learn about the user and adapt accordingly. Several approaches to human performance, task characteristics, and adaptation methodology have been proposed in the computer-human interface literature. The approaches include statistical analyses of performance, the GOMS model (Card, Moran, and Newell, 1983), generative grammar (Hoppe, 1988; Payne and Green, 1986), production systems (Polson and Kieras, 1985) and hybrid formalisms (Tyler, 1988). The first of these approaches, statistical analysis of keystroke command selection and error performance, is insufficient by itself to drive an autoadapting system. But it is included as part of a more effective design, the current expert-system driver for work-station interfaces. A generative grammar is formally equivalent to a production system (c.f. Lachman, 1989a) but lacks the latter's extent of implementation and demonstrated utility. A psychometric approach alone is also incapable of effectively informing adaptation software but is potentially useful in combination with other methodology, primarily

SPACE STATION FREEDOM
MPAC - DMS WORD PROCESSING SERVICES -- HELP SCREEN

Alt-B Block, marks the beginning or end of a block of lines.
Alt-C Clears all text from the current file.
Alt-D Deletes the line at the cursor position.
Alt-E Erases a block of lines.
Alt-F Find text, text to be specified.
Alt-H Help, display help screen.
Alt-L Loads a different file.
Alt-P Paste block, copies a block of lines at cursor.
Alt-R Reform, reformats paragraph from the cursor line down.
Alt-S Saves the current file.
Alt-U Unmark block, unmarks a block of lines.
Alt-X Exits without saving.
Alt-W Word-wrap, toggles on or off.
Ins Insert mode, toggles on or off.
Del Deletes character at cursor position.
Ctrl-End Deletes from the cursor to the end of the line.

CURSOR, LINE, AND SCREEN MOVEMENT KEYS:
Ctrl PgUp, Ctrl PgDown: Moves cursor to start or end of file.
Arrows - Up, Down, Left, Right: Moves cursor one unit.
Home, End: Moves cursor to start or end of line.
Ctrl-Left Ctrl-Right: Moves cursor one word left or right.

Figure 1. Print out of the help screen showing the current command set of the text editor. The help screen is called by Alt-H.

consisting of a production-system expert system (Buchanan and Shortliffe, 1984; Clancey, 1985; c.f. Lachman, 1989a). The Carnegie Group (Hayes, 1988) recommends that an independent knowledge base be used to drive the interface for expert systems. The rationale for this approach includes ease of rule modification and a guaranteed consistency between the interface and the internal system in how problems are viewed. The rule-based expert system that drives the work-station interface is based on the Carnegie recommendations (Hayes, 1988). The rule-based system exercises partial control of command syntax, command execution, and the content of screen displays and advisory messages. Finally, it should be noted that despite the various articles appearing on adaptive interfaces over the last decade, no one has reported a fully functional system. This is due, in part, to the necessity of a full scale knowledge engineering effort with all the associated costs. The current approach is feasible because it starts with a scaled down but fully-functional system and proceeds incrementally.

The use of high-level domain experts has not been required for prototype development. The DMS services selected for prototyping with a knowledge-base are common computer tasks with an established literature (Carroll, 1987; Lachman, 1989b). The literature and common knowledge concerning text editors are sources of information for construction of the rule base. This is supplemented by a limited amount of direct observation of subjects performing the targeted task at a console.

Once a tentative rule base is established, the adaptive system requires facts concerning the service in use, the state of the system, and the current performance of the user. Relevant facts are stored in the data base of the expert system and are compared continuously to the antecedents of rules. When a match is obtained between the user's command entry and a rule, that rule will fire. The firing of any rule either adds a new fact to the data base or issues a command to the underlying DMS system. Firing of a set of rules designed to affect the application triggers commands that adapt the display and command structure of the interface. The user then may be presented with automatic assistance or with direct advice. The facts are obtained from several sources, including nonobtrusive and embedded speed and accuracy measures of keystrokes or mouse movements at the work-station console; rule-selected automatic queries to the operator; unsolicited operator inputs and requests for help within predefined parameters; and software monitoring of the particular state of the DMS service being used.

An example of the action produced by the firing of one

type of rule is shown in Figure 2. The advisory message is windowed over the visible screen of the text editor by Rule 7 which has the following form.

```
RULE 7

IF RESPONSE(last) = RIGHT.ARROW.KEY
AND IF RESPONSE(last - 1) = RIGHT.ARROW.KEY
AND IF RESPONSE(last - 2) = RIGHT.ARROW.KEY
AND IF RESPONSE(last - 3) = RIGHT.ARROW.KEY
AND IF RESPONSE(last - 4) = RIGHT.ARROW.KEY
AND IF RESPONSE(last - 5) = RIGHT.ARROW.KEY
AND IF LINE.LENGTH(CURRENT.LINE) - CURSOR.POSITION > 10

THEN PRINT MESSAGE RIGHT.WORD
```

The rule states that if the right arrow key was pushed during the last six keystrokes and if the cursor is now 10 or more character positions from the last character on the line, then print the window message shown in Figure 2.



## 3.0 GUIDELINES FOR INTERACTIONS BETWEEN USERS AND THE SSFP COMPUTER SYSTEMS

The int puter systems can be char sentation of information ser and the system, and in general terms, as fo mation to the user addres information, principally s category of guidelines fo by the user. Accordingly, topics as the structures that constitute a display, the organization of those structures (i.e., display syntax), methods of directing the user's attention to specific display areas, and methods of coding the meaning of display elements (i.e., display semantics). (2) The section on real-time interactions between users and the SSFP computer systems covers human-computer interfaces that involve a close conceptual and temporal relation between an information display and the user's response -- so close that the human-computer interaction cannot be easily classified as involving primarily either information processing or response output. Several of the topics covered under this category previously

```
                    ADVISORY MESSAGE

If you want to move the cursor to the right more
quickly, hold down Ctrl and press the Right
Arrow key, the cursor will jump to the right one
word at a time.
Press <ANY KEY> TO CONTINUE.
```

LINE: 19 CHAR: 48 DMS Editing File: HCI-GUID.TXT. Alt-H for Help.

Figure 2. An advisory message that is windowed onto the screen by Rule 7. The rule is described in the text.

The rule could have executed an application command instead of sending a message to the operator. Rule 8, for example, states that if the last five keystrokes moved the cursor five words to the right and there are at least 15 characters left on the line, then execute the command to jump the cursor to the end of the line. The assumption is that the operator wanted to get to or near the end of the line and forgot the command. The command execution can be accompanied by an advisory message explaining what was done and tutoring the operator on the appropriate keyboard input for the command. Obviously, command execution rules as well as rules that alter the screen display and command entry features require behavioral research to determine their effects on productivity.

Thus, an important part of the task of the knowledge-based system is to determine an astronaut's intentions when entering commands for a particular DMS service. One aspect of predicting user intentions is straightforward. If the expert system knows (has in its data base) the context for commands that are currently being entered, then the redundancy in the command structure will allow determination of the user's intentions. For a command sequence with less than total redundancy, the point is to capture the rules used by an expert or knowledgeable observer in determining the user's intentions. A domain expert cannot perfectly determine other people's intentions; this determination can only be done partially. A machine can do no better than the expert whose rules are being implemented. But people can partially predict the intentions of others and provide appropriate directions and excellent advice; an expert system machine implementation can do as well.

The positive outcome of the this proof-of-concept study and prototype development does not mean that large scale deployment is unproblematic. Intensive and well designed behavioral experimentation is essential. In particular the strategy for sampling of subjects must be developed meticulously for realistic generalization to specialized and global populations. Up scaling to highly complex commercial systems and integrating a very large rule base present significant technical problems. But, these can be solved.

To summarize the second half of this article, the architecture of the adaptive interface is similar to the three component architecture of a conventional expert system. First, there is a database with the operator's psychometric profile, prior performance history, and the output of the current keystroke performance stack. Second, there is a rule base with error detection rules and productions in the form of conditionals between the operator's behavior and three types of instructions to the

underlying application software. Third, there is an inference engine that searches the data base for antecedents to rules and sends the consequents of fired rules as commands to the underlying software. This structure appears sufficient for the construction of an adapting interface.

## REFERENCES


Anderson, J. R., Farrell, R., and Sauers, R. (1984). Learning to program in LISP. Cognitive Science, 8, 87-129.

Card, S. K., Moran, T. P., and Newell, A. (1983). The psychology of human-computer interaction. Hillsdale, NJ: Erlbaum.

Buchanan, B. G. and Shortliffe, E. H. (Eds.) (1984). Rule-based expert systems. Reading, MA: Addison-Wesley.

Carroll, J. M. (Ed.) (1987). Interfacing thought: Cognitive aspects of human computer interaction. Cambridge, MA: MIT Press.

Chi, M. T. H., Glaser, R., and Rees, E. (1982). Expertise in problem solving. In R. Sternberg (Ed.), Advances in the psychology of human intelligence. Hillsdale, NJ: Erlbaum.

Clancey, W. J. (1985). Heuristic classification. Artificial Intelligence, 27, 1-67.

Hayes, P. J. (1988). Using a knowledge base to drive an expert system interface with a natural language component. In J. A. Hendler (Ed.), Expert systems: The user interface. Norwood, NJ: Ablex Publishing.

Hoppe, (1988). Task-oriented parsing - A diagnostic method to be used by adaptive systems. In Proceedings of CHI '88 (pp. 241-247). New York: ACM.

Lachman, R. (1989a). Expert systems: A cognitive science perspective. Behavior Research Methods, Instruments, and Computers, 21, 195-204.

Lachman, R. (1989b). On-line reading and comprehension aids for expository text. Human Factors, 31, 1-15.

NASA SSP 30261 (1989). Preliminary draft: Architectural control Document, Data Management System. Draft Version 2, Revision D. Space Station Freedom Program Office.

Payne, S. J. and Green, T. R. G. (1986). Task action grammars--A model of the mental representation of task languages. Human-Computer Interaction, 2, 93-133.

Polson, P. G., and Kieras, D. (1985). A quantitative model of the learning and perform-ance of text editing knowledge. In Proceedings of CHI '85. New York: ACM.

Rouse, W. B., Geddes, N. D., and Curry, R. E. (1987-88). An architecture for intelligent interfaces: Outline of an approach to supporting operators of complex systems. Human-computer Interaction, 3, 87-122.

Tyler, S. W. (1988). SAUCI: A knowledge-based interface architecture. In Proceedings of CHI '88 (pp. 235-240). New York: ACM.

# Some Issues Related to Simulation of the Tracking and Communications Computer Network

Final Report

NASA/ASEE Summer Faculty Fellowship Program - 1989

Johnson Space Center


| | |
|---|---|
| Prepared by: | Robert C. Lacovara, Ph. D. |
| Academic Rank: | Assistant Professor |
| University and Department: | Stevens Institute of Technology<br>Dept. of Electrical Engineering<br>and Computer Science<br>Hoboken, NJ 07030 |
| NASA/JSC | |
| Directorate: | Engineering |
| Division: | Tracking And Communications |
| Branch: | Communications Performance<br>and Integration |
| JSC Colleague: | J. C. Dallas |
| Date Submitted: | August 11, 1989 |
| Contract Number: | 44-001-800 |

**Abstract**

The Communications Performance and Integration branch of the Tracking and Communications Division has an ongoing involvement in the simulation of its flight hardware for Space Station Freedom. Specifically, the communication process between central processor(s) and orbital replaceable units (ORU's) is simulated with varying degrees of fidelity.

This report presents the results of investigations into three aspects of this simulation effort. The most general area involves the use of computer assisted software engineering (CASE) tools for this particular simulation. The second area of interest is simulation methods for systems of mixed hardware and software. The final area investigated is the application of simulation methods to one of the proposed computer network protocols for space station, specifically IEEE 802.4.

## INTRODUCTION

Simulation methods represent a broad area of knowledge and technique. The investigations herein are oriented towards a specific simulation, namely that of the space to ground subsystem of the communications and tracking system for the space station.

This particular simulation consists of a set of programs written chiefly in ADA which a) emulate the state of many ORU's and b) provide fault detection, diagnosis and recovery based on the status of the various ORU's. The simulation was written by a team of about six people, and is consequently sufficiently complex to warrant the application of CASE tools. The result of application of CASE tools to the existing simulation yielded some insight into the value of CASE tools and into the simulation itself. This is deemed useful in that the present simulation (called 3B) is a forerunner to more realistic simulations to be written in the near future.

During the study of the use of CASE tools, it became apparent that the techniques used for the simulation were highly specific. For example, some actual hardware (network hardware) will be available for use during the simulation sessions, and will therefore be incorporated. Predominantly synchronous techniques were used, and little "instrumentation" (other than journal files) of the actual simulation was written into the code. This study indicates that there is some reason to believe that some commercially available asynchronous simulation tools would be of value in future efforts.

A specific area of interest to the simulation group was the performance of certain computer networks specified for use on the space station. Some effort was made towards obtaining simulations of these networks, but this work remains to be completed.

This report now presents three sections which describe the study and results of the three areas described above: CASE Tools; Simulation Tools; and Network Simulation.

## CASE TOOLS

Computer Assisted Software Engineering (CASE) tools are intended to assist the development of large and complex software systems, particularly those which involve multiple programmers and extensive physical systems. At the present

time, there are several commercial CASE systems which are similar to a great extent.

These systems accept a specification of a software system as their input data. This input specification includes descriptions of the physical inputs to the system (human or machine generated information), descriptions of the processes needed within the system, descriptions of internal storage for the system, and specifications of the output product of the system (reports and forms.) The actual form of the specification is a graphic of data flows within the software system, and graphical representation of specific resources used in the system. The overall effect is to form a picture of a complex system which shows the flow of data through processes which modify the data.

From a description of a software system, the CASE tool makes checks for consistency of data flows from process to process, and compiles information on those flows. For example, redundant data flows, or data flows which are partially specified are automatically identified. Complete descriptions of the objects used in a system may be extracted by the CASE tool. Finally, some CASE tools can build significant portions of the final code from the description. Even simple CASE tools can produce data declarations in several programming languages. (Unfortunately, ADA does not seem to be a common choice.)

Figure 1 is the representation of the simulation of the Space to Ground subsystem of the Communications and Tracking system. External sources and sinks of data (command and status) are shown as square boxes. Data flows are shown as directed lines. Processes (programs and algorithms) which modify, use or generate data are shown as rectangles with rounded corners. In this specific case, the processes shown correspond to the efforts of single programmers. Figure 2 shows an "explosion" of a single process. The explosion has the same inputs and outputs as the corresponding process of Figure 1, but shows the internal processes in greater detail.

Associated with the data flows of Figure 1 and Figure 2 are specific record structures for the data passed. These records are not described further in this report, but by examination of the records some inconsistencies were noted in the system, and corrections were facilitated thereby.

The description of the simulation system shown in Figures 1 and 2 was obtained after most of the code was written. CASE tools, however, are intended to be used before the generation of code. Nevertheless, several interesting

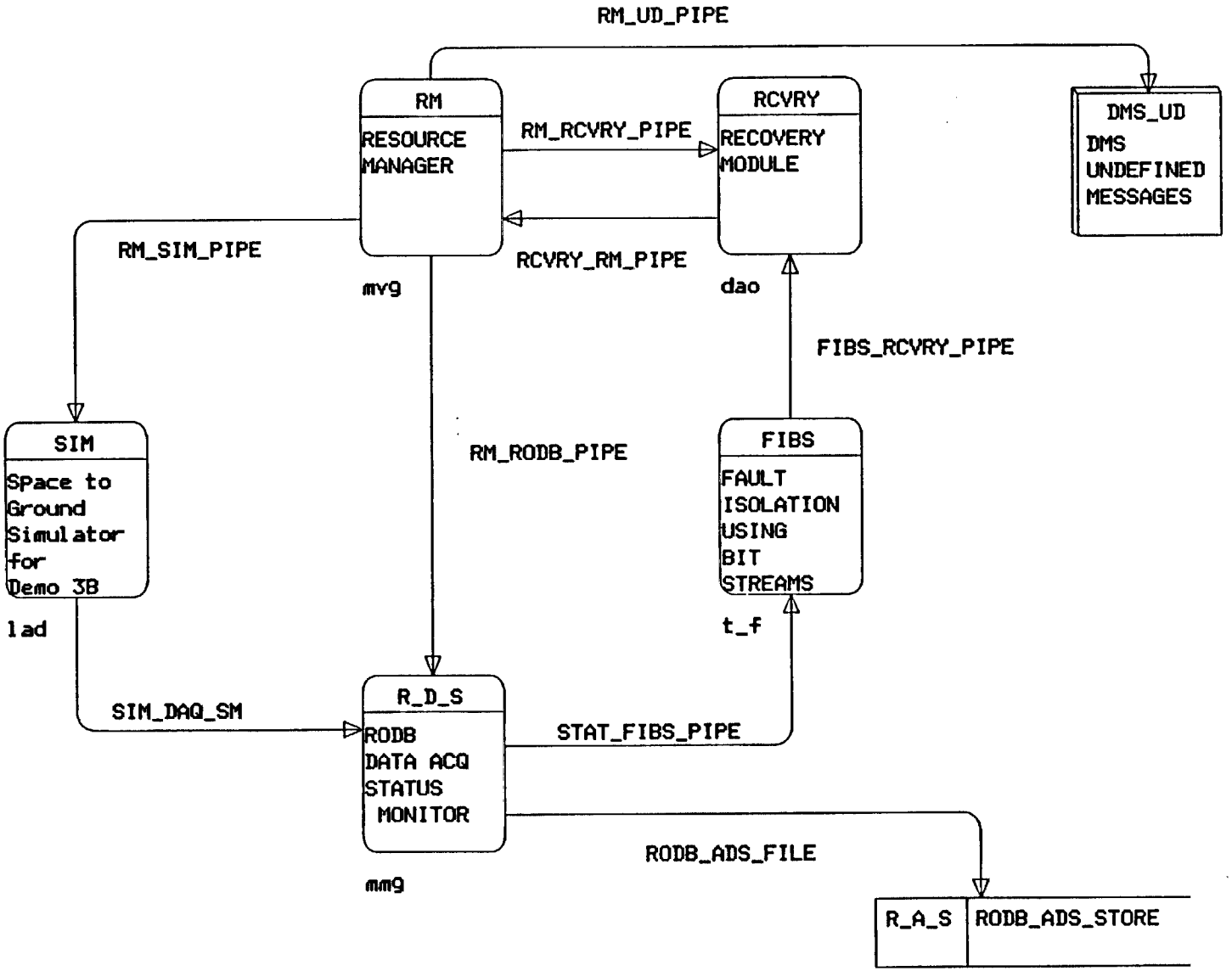


FIGURE 1: SPACE TO GROUND SIMULATION

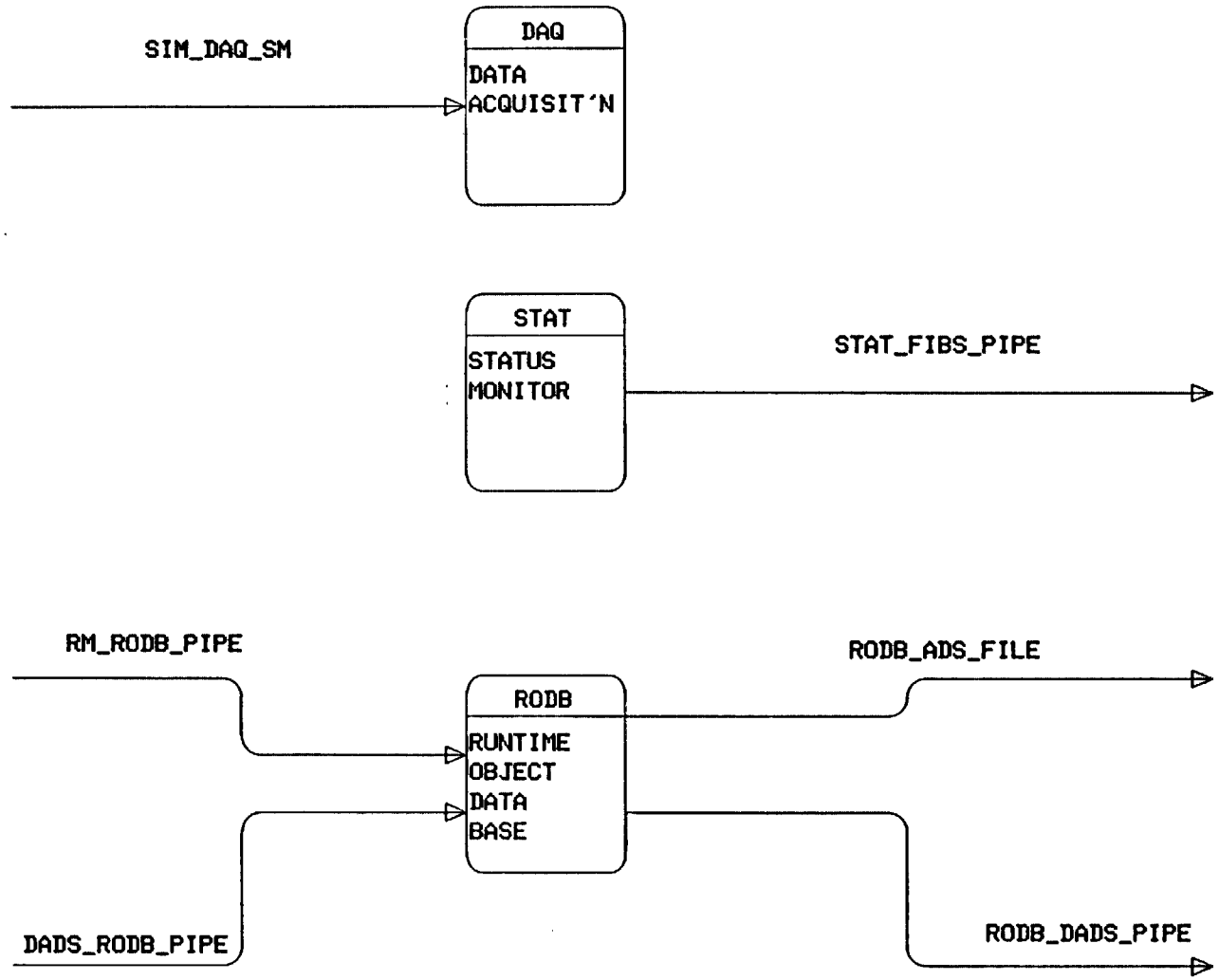


**FIGURE 2: EXPLOSION OF A PROCESS**

observations were made concerning the simulation system.

After the initial description of the simulation was distributed to programmers, several inconsistencies were noted in names of structures, and some inconsistencies in the uses of the structures were found. These faults would have surfaced readily enough at run time, but it is not clear that they would have been diagnosed quickly. The value of the CASE tool is that some types of problems which may be difficult to diagnose during debugging runs are actually explicitly visible from the output of the CASE tool. In that case, the potential error is corrected before "trial and error" runs are made.

A secondary effect of the CASE tool effort was a certain amount of interaction on the part of the programmers in an effort to standardize the use of some data structures. These changes were probably not important to the run time performance of the code. The changes tended to make different interfaces in the system look alike. Most likely, the overall clarity of the system improved by a small amount once all of the interfaces between programmers became explicit. (Prior to the use of the CASE tool, interfaces between programs were negotiated by the programmers pair-wise.)

Finally, it appeared that the existence of the CASE tool printouts provided a convenient "look and point" tool during some phases of the integration and testing of the simulation.

It seems reasonable that the use of the CASE tool even after most of the simulation was designed and written was of some concrete value. The total effort involved in the use of the CASE tool was not excessive: about 36 hours to learn to use the tool, and perhaps 8 hours to enter the description of the simulation system.

More importantly, it seems that much of the advantage of using a CASE tool will accrue from its use from the beginning of an effort. Programmers may then attend to the details of program operation from the foundation of a firm and unambiguous specification. This should speed the overall design, elaboration, and debugging process associated with a complex software system. It should also reduce the amount of time spent in "pair-wise" negotiation by the programmers.

## SIMULATION TOOLS

In the studied simulation, only one of the processes actually "simulated" anything at all. This is the module marked SIM in Figure 1. This process ran

multiple tasks which were numerical simulations of the behavior of ORU's. Other processes actually performed software tasks which will be performed in the future by flight software. Consequently, the other processes in the simulation are actually limited-scope study models of software yet to be written for flight.

The SIM module simulates some number of ORU's (about 40). Various parameters of the ORU's are simulated. However, the actual values are generated by keyboard input at a "command console." At the time of this writing, time-varying behavior of the simulation is being considered. To that end, several methods of simulation programming are considered.

There are several types of ORU in the simulation. Briefly, these may be considered only by the behavior desired of their various outputs. The simplest type of ORU has nearly static outputs and must only change for power up/down, or for gross failure. A second type of ORU reports the changes in some external event (auto-track antenna pointing, for example) and except for gross failure, may be characterized by deterministic functions of time. A third type of ORU has outputs which may be characterized best by some probability distribution function.

Individually, any of these three behaviors could be simulated by asynchronous or synchronous techniques. However, all three are needed and there are at least twenty if not forty systems which require simulation simultaneously. A reasonable method seems to be the use of a commercial simulation language such as SIMSCRIPT or GPSS, at least for the non-deterministic portions of the system. These languages hide the simulation mechanism (queues, lists, timers, etc.) from the programmer and provide access to asynchronous techniques. They are also well documented, and these two languages are both mature (more than 10 years old), and available on almost any computational platform (MS-DOS machines through supercomputers.) There is also no reason that the existing simulation (written in ADA) could not call tasks written in the formal simulation languages.

The chief benefit of the use of these languages is the ease of documentation and maintenance of the simulation. It is usually easy to change the underlying probability distribution functions in any simulation. However, changing the behavior of special purpose programs for simulation may require extensive re-writes. It appears that SIMSCRIPT or GPSS -type simulations are relatively

easy to change. This will be important as the fidelity requirement of the simulation increases.

## TOKEN BUS 802.4

At the time of writing, and prior to the August 1989 scrub exercise, the 802.4 token bus standard was to be used in flight hardware for low rate local area networks (LAN's) on Space Station. The simulations discussed above have not at the time of writing progressed to simulations of the LAN's, but this is anticipated. Accordingly, a study was initiated with the intent of identification of a means of simulation of LAN operation. As 802.4 had been specified, the simulation of this LAN was of some interest.

Interestingly, a great deal has been published on LAN simulation, and 802.4 in particular. The references which follow pertain to LAN simulation and performance. The 802.4 standard was studied extensively in the early 80's by the National Bureau of Standards (NBS) by a working group composed of both industrial concerns and the NBS.

This group did a vast amount of work in 802.4. The NBS team wrote several simulations of the standard. Further, it built an instrumented hardware implementation of a network using four or six nodes, and verified its simulation programs against the hardware systems. Results of these efforts are published in several workshops and conferences. Refer to the references.

At the present time, little commercial interest remains for 802.4 token bus. The chief reason appears to be its performance in comparison to 802.5 token ring systems and other systems of higher data rate media. In the papers surveyed and listed in the references, there appears to be no performance regime in which 802.4 is superior to 802.5 [Stuck 83]. The 802.4 standard does seem to outperform Ethernet, but this is hardly surprising, in view of the fact that Ethernet uses a collision resolution algorithm to resolve contention (specifically, CSMA-CD.) Furthermore, LAN's which employ higher rate media than 802.4, such as FDDI (at 100 Mbs as compared to 10 Mbps) seem to have leap-frogged the 802 standards for many applications. These higher rate systems provide multiples of 802 performance data rates at far under multiples of cost.

In the process of investigation, a public-domain simulation of 802.4 was discovered at the NBS. This is written in SIMSCRIPT, and has been obtained for any value it may present to simulation authors in the future. This simulation

may be useful when the details of LAN operation are desired in the Space to Ground Simulation. Further work remains in order to use the simulations.

## CONCLUSIONS

During this summer residency, the author divided his efforts along the three lines described above. The simulation efforts were particularly interesting since they have led to a consideration of mixed simulation systems. These systems will consist of hardware (probably actual LAN hardware), software written specifically to imitate flight functions, and software written in formal simulation languages.

## REFERENCES

(Alphabetically by first author)


ANSI/IEEE Standard; Draft International Standard, "802.4 Token-Passing Bus Access Method," ANSI/IEEE Std 802.4-1985; ISO/DIS 8802/4.

ANSI/IEEE Standard; ISO Draft Proposal, "802.5 Token Ring Access Method," ANSI/IEEE Std 802.5-1985; ISO/DP 8802/5.

Jean-Luc Archambault, "An IEEE 802.4 Token Bus Network Simulation," U. S. Dept. of Commerce, National Bureau of Standards, NBSIR 84-2966.

Werner Bux, "Local Area Subnetworks: A Performance Comparison," IEEE Trans. on Communications, Vol. Com-29 No. 10, Oct 1981.

Imrich Chlamtac and Raj Jain, "A methodology for building a simulation model for efficient design and performance analysis of local area networks," Simulation, Feb. 1984.

M. Alex Colvin and Alfred C. Weaver, "Performance of Single Access Classes on the IEEE 802.4 Token Bus," IEEE Trans. on Communications, Vol. Com-34 No. 12, Dec. 1986.

Rhonda Alexis Dirvin and Arthur R. Miller, "The MC68824 Token Bus Controller," IEEE Micro, June 1988.

Larry Press, "Benchmarks for LAN Performance Evaluation," Comm. of the ACM, Vol. 31 No. 8, Aug. 1988.

William Stallings, "Local Network Performance," IEEE Communications Magazine, Vol. 22 No. 3, Feb. 1984.

Bart W. Stuck, "Calculating the Maximum Mean Data Rate in Local Area Networks," IEEE Computer, May 1983.

# THE EFFECTS OF SIMULATED HYPOGRAVITY ON MURINE BONE MARROW CELLS

Final ReportNASA/ASEE Summer Faculty Fellowship Program -- 1989

Johnson Space Center


| | |
|---|---|
| Prepared by: | Brother DeSales Lawless, Ph.D. |
| Academic Rank: | Associate Professor |
| University and Deparment | Fordham University<br>Division of Science and Mathematics<br>New York, N.Y., 12023 |
| NASA/JSC | |
| Directorate: | Space and Life Sciences |
| Division: | Medical Sciences |
| Branch: | Biomedical Laboratories |
| JSC Colleague: | Steve Gonda, Ph.D. |
| Date submitted: | August 3, 1989 |
| Contract Number: | NGT 44-001-800 |

## ABSTRACT

We have compared mouse bone marrow cells grown in complete medium at unit gravity and a similar population cultured in conditions that mimic some aspects of microgravity. After the cells adjusted to the conditions that simulated micrograity they proliferated as fetal or oncogenic populations; their numbers doubled in twelve hour periods. Differentiated subpopulations were depleted from the heterogeneous mixture with time and the undifferentiated hematopoietic stem cells increased in numbers.

The cells in the control groups in unit gravity and those in the bioreactors in conditions of microgravity were monitored under a number of parameters. Each were phenotyped as to cell surface antigens using a panel of monoclonal antibodies and flow cytometry. Other parameters compared included: pH, glucose uptake, oxygen consumption and carbon-dioxide production. Nuclear DNA was monitored by flow cytometry. Functional responses were studied by mitogenic stimulation by various lectins.

The importance of these findings should have relevance to the space program. Cells should behave predictably in zero gravity; specific populations can be eliminated from diverse populations and other populations isolated. The availability of stem cell populations will enhance both bone marrow and gene transplant programs. Stem cells will permit developmental biologists study the paths of hematopoiesis.


## INTRODUCTION

This research is a study of murine bone marrow cells cultured in simulated microgravity. It has been shown by several investigators that gravity is an environmental factor which affects growth and functionality of cells. (Lorenzi, G., et al., 1986). Human lymphocytes exposed in microgravity to the mitogen Concanavalin A showed less than 3% of the activation of similar cells at unit gravity. (Cogoli, et al., 1984). The same investigators found that microgravity depresses and hypergrravity enhances cell poliferation rates. These effects were particularly strong in cells undergoing differentiation. The cellular proliferation rates of several different cell types were increased by 30% in hypergravity while the consumption per cell of glucose was lower than at unit gravity. (Tschopp, 1983).

We have undertaken this research encouraged by the work of these investigators and others who have demonstrated that a microgravity environment alters cellular behavior. We have observed murine thymus cells and hybridomas under microgravity and we report this separately. Of particular interest to us is bone marrow for reasons of the benefits that can immediately be realized by discriminate elimination of subpopulations and by the isolation of precursor cells. We estimated that bone marrow cells contain a population of cells that are essentially fetal tissue and these should proliferate indefinitely while the differentiated cells that were produced from these would have finite division numbers. Furthermore, we anticipated that the minimization of cell-cell contact and the in vitro control of many stimulating factors would increase the accomplishment of the goals .

The availability of the bioreactors developed at the Johnson Space Center gave the initial impetus to this project. We were presented with the possibility of introducting the conditions of microgravity into the study.

The study of bone marrow under conditions that could alter subtype proliferation rates and functionality has particular relevance in a number of obvious areas. Developmental biologists may be able to elucidate pathways of hematolymphoid and myeloid differentiation. The removal of cancer cells from bone marrow for autologous transplants against neoplasia or removal of T cells for allografts in severe immunodeficiencies and in prevention of graft vs host effects might by accomplished more efficiently. If human pluripotent hematopoietic stem cells could be unambiguously identified and isolated, gene inertion therapy might be advanced. (Weissman, et al., 1988).

If it is found that with time specific subpopulations are favored while others are not, we would attempt to sort and study these specific subsets within the bone marrow using the Fluorescence Activated Cell Sorter (FACS).

Since significant variance in the parameters studied in simulated hypogravity are evident from this research, we will propose that these in vitro investigations be repeated at zero gravity on a future space mission. We would ask that the study be undertaken not only with mice cells but with human cells.

The quest for the isolated clone of human hematopoietic stem cells has not been fruitful up to the present. We would like to accomplish this goal as part of a future space mission project.

## MATERIALS AND METHODS

Mice. BALB/CANN HSD 4-5 week old, female, were used. These were purchased from Trudeau Institute, Saranac Lake, New York.

Cells. Bone marrow cells were obtained from the mice by flushing the tibiae and femora of ten mice with Hanks Balanced Salt Solution (without phenol red) supplemented with 2% Fetal Calf Serum. The cells were cultured at two million cells/ml Complete Medium: RPMI-1640, 1 mM Glutamine, 100 U/ml penicillin, and 10% Fetal Calf Serum. The Fetal Calf Serum was heat inactivated at 56 deg C for 30 min. The cells were kept at 37 deg C in an atmosphere containing 5% carbon-dioxide, 95% humidity.

Monoclonal Antibodies. The panel of antibodies included the following from clones purchased from American Type Culture Collection, Rockville, MD: TIB-146, (Anti B Cell, antiB cell precursors with antigen B220), TIB-207 (anti-L3T4 expressed on T helper-inducer subsets), TIB-150 (Anti Lyt 2.2, expressed on T suppressor-cytotoxic cells); TIB-120 (Anti Ia-b,d,q haplotypes); TIB -128 (Anti-MAC-1, macrophages and granulocytes). The following were from Sigma Chemical Company:, St. Louis, Mo.: FITC-anti Thy 1.2 (cell surface differentiation antigen), and the secondary antibodies FITC-anti Rat IgG and FITC Goat anti-mouse. Obtained from Becton-Dickinson Co., Mountain View, CA.: Anti-mouse Lyt-1 and anti-mouse I-A. MoAb E13 161-7, (anti- stem cell antigen) was a gift of Dr. Shelly Heimfeld of Stanford University. MoAb 2.4G2,(anti mouse Fc-receptor) was a gift of Dr. Mary Ann Principato of the National Institutes of Health, Bethesda, Maryland.

Staining. The conjugated monoclonals were used in direct staining. The unconjugated antibodies were incubated with the bone marrow cells and followed by the fluoresceinated the secondary antibodies. In each procedure the cells were not fixed but were incubated with a solution of propidium iodide which enabled us to sort out dead cells for flow cytometry analysis.

Simulated Microgravity. The bioreactor vessel used in our research was desgined by the Engineering Department of the NASA-Johnson Space Center. The bioreactors are kept in incubators at 37 deg C, 5% carbon-dioxide, humidified atmosphere.

Flow Cytometry. Experimental data from the control cell populations grown in static culture at unit gravity and from the cells grown in microgravity in the bioreactor were obtained using Coulter Electronics EPICS V Cell Sorter (Coulter Electronics, Hialeah, FL). 10,000 events were scored on each test. Dead cells and cell aggregated were gated from the cells under study. For DNA analysis one ml suspension of cells were fixed with 2 ml 70% ethanol for 30 minutes and then incubated with a solution of propidium iodide/RNase. Cell counts were either by hemacytometer or by Coulter Counter.

Proliferative assay. Mitrogen stimulation was determined with Concanavalin-A and Lipopolysaccharide. Cells were pulsed for 16 hours with 3-H thymidine. Incorporation of radioactivity was measured by liquid scintillation counting. Cells were harvested in a multisample harvester and the data displayed as mean counts per minute.

Oxygen consumption and carbon dioxide production were determined using a Corning 166, pH Blood Gas Analyzer. (Corning, Medfield, MA, 02052).

Glucose utilization was determined on a Beckman Glucose Analyzer 2, Becton-Dickinson (Fullerton, CA, 92634).

Immunological Reestablishment: Three sets of ten mice each were irradiatead with 825 rads radiation at MD Anderson Hospital, Houston, TX. One set of the mice were kept as controls. A second set received fresh bone marrow injeactions. The test group were given 100 cells/mouse of the cells which had been circulating in the microgravity vessel for forty days. Records of animal viabilities were kept. When the animals were sacrified the colonies from from CFUs were counted.

## RESULTS

Bone marrow cells in static culture in complete medium at 37 deg decreased in numbers until day five. The cells in the flask at that time were primarily adherent cells. By daily removal of adherent cells it was possible to continue the culture. We discarded the cells grown in static culture at this time since we found that we could not maintain the non-adherent population. (16-7)

Bone marrow cells in the bioreactors also decreased in numbers until approximately day twelve. At this time there was an explosive increase in cell numbers. The increased showed some fluctuation but this was correlated with oxygen or glucose deprivation or excess carbon-dioxide production. When the culture media was changed on alternate days there was a doubling of numbers. This growth rate has been observed with three experiments beyond day forty. (16-8)

Condition of the cells was determined by monitoring glucose and oxygen use. Carbon-dioxide, pH and osmolarity also became useful parameters dor estimating the contition of the cells. (16-9) Cell counts were determined by hemacytometer and viabilities were determined by trypan blue exclusion. (16-9)

Flow cytometric data was obtained only on live cells. Dead and damaged cells were gated by use of propidium iodide. (16-10). In the reprint listed, 69.43% of the cells (those in quadrant #4) were analyzed. DNA nuclear contents studied on lysed cells with propidium iodide was normal. It showed most cells in the 2N resting phase. (16-11).

Examples of the data obtained by flow cytometry is exemplied in 16-12, 13, 14). The cells in the bioreactors on day 26 were Thy-1 and SCA-1 positive and Fc-receptor negative.

The ten mice which were given 900 rad lethal radiation and subsequent inoculation of bone marrow cells which had been growing in the microgravity environment of the bioreactor are all alive after six days. They will be continually monitored. A second group of four sets of lethally irradiated mice have been prepared. One set will receive an injection of normal bone marrow; a second will receive 100 bone marrow cells from the experimental vessels; a third set will receive amounts of cells ranging from one thousand to one million. The fourth set of mice will receive no cells.

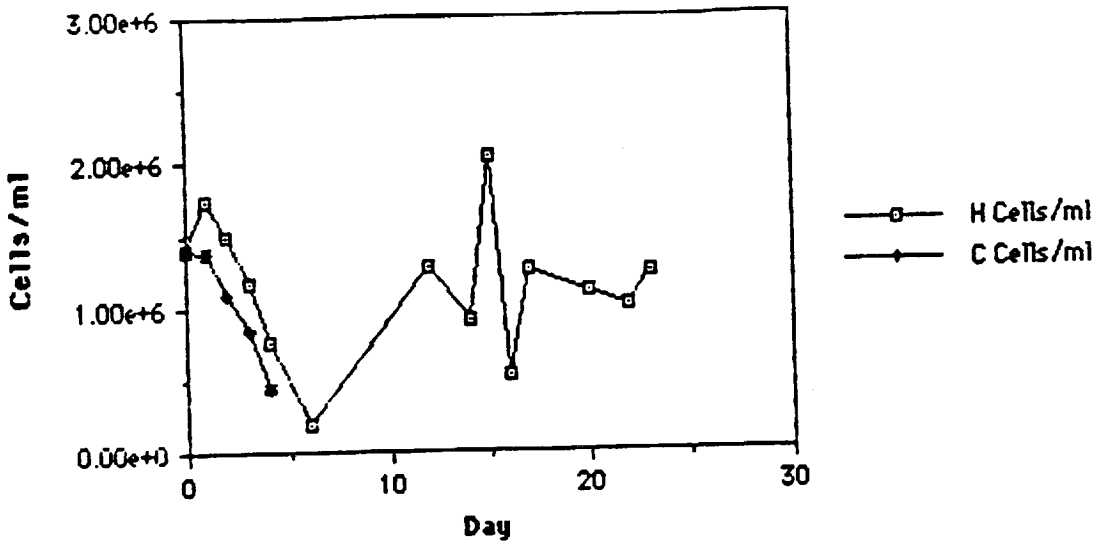
3.00e+6
2.00e+6
1.00e+6
0.00e+0
Cells/ml
0
10
20
30
Day
H Cells/ml
C Cells/ml

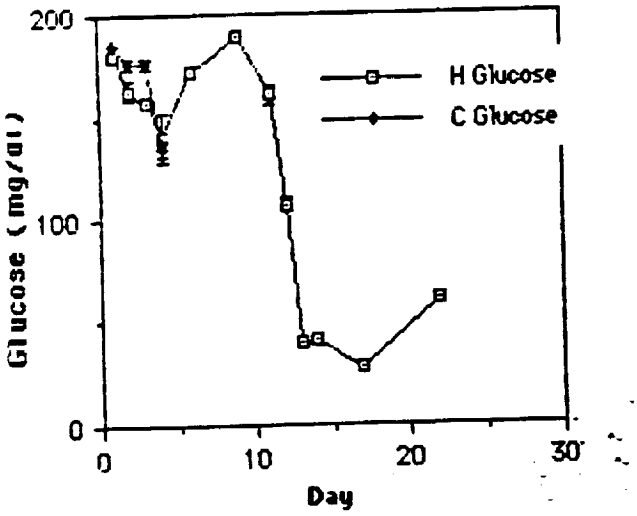
200
100
0
Glucose (mg/dl)
0
10
20
30
Day
H Glucose
C Glucose

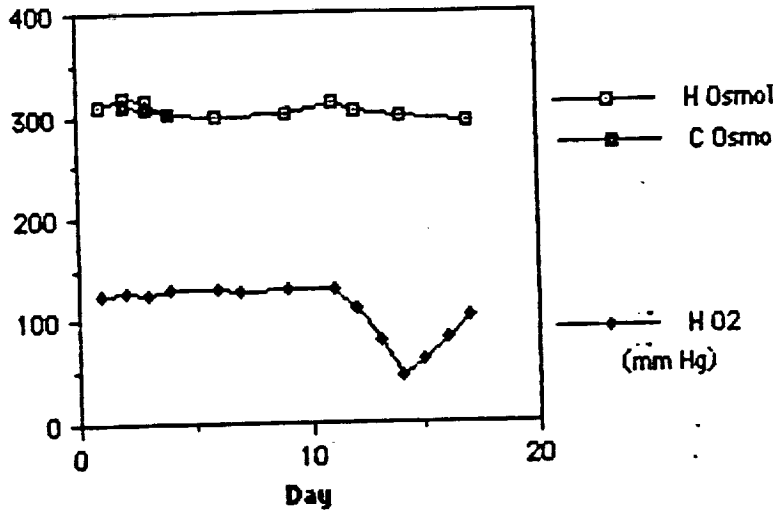
400
300
200
100
0
0
10
20
Day
H Osmol
C Osmo
H O2
(mm Hg)

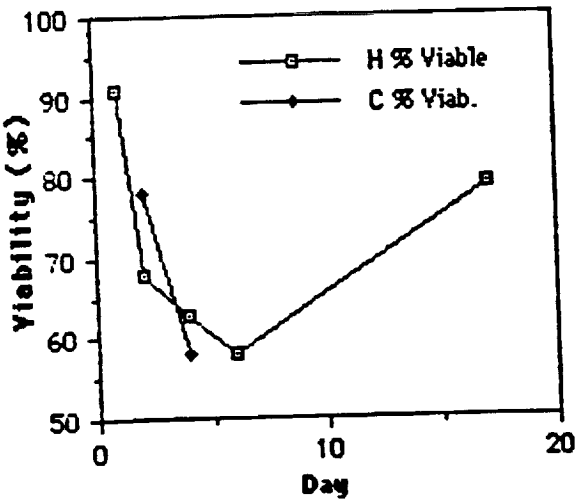
100
90
80
70
60
50
Viability (%)
0
10
20
Day
H % Viable
C % Viab.

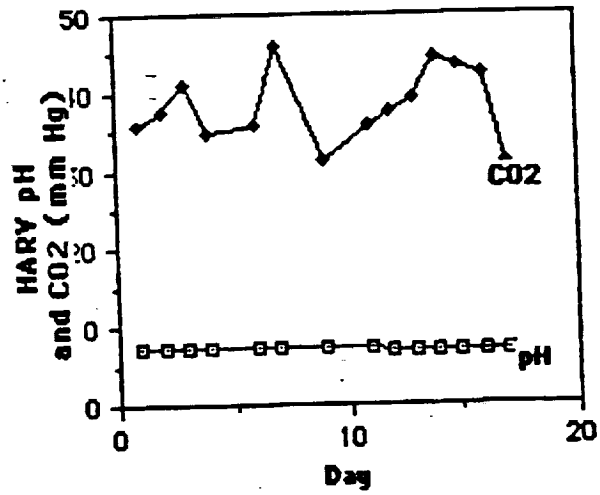
50
40
30
20
0
HARV pH
and CO2 (mm Hg)
0
10
20
Day
CO2
pH

Test # 2 Bone Marrow 6/28/89 Delrin-end
STLV (Trudeau mice)

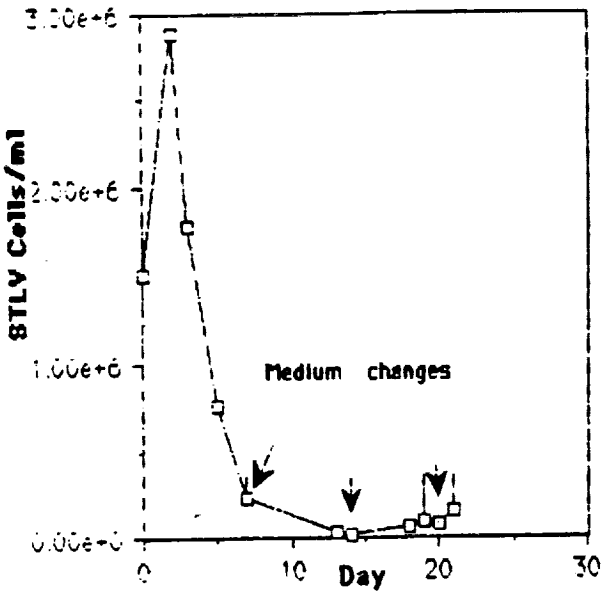


Selective Recovery of Cluster Type Cells

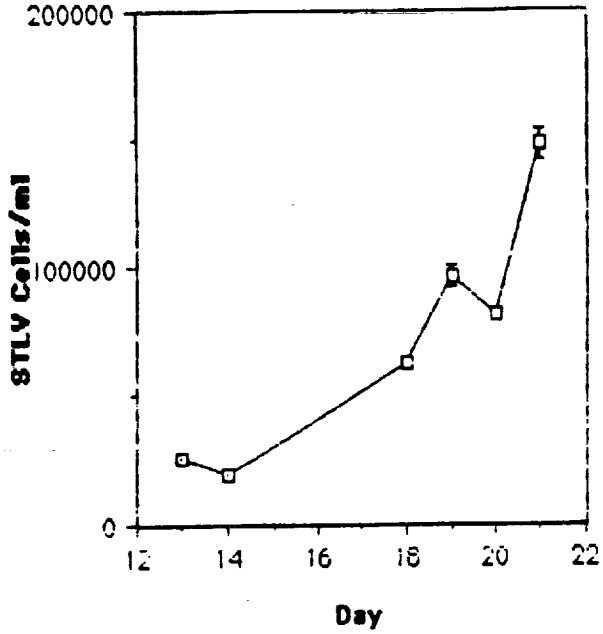


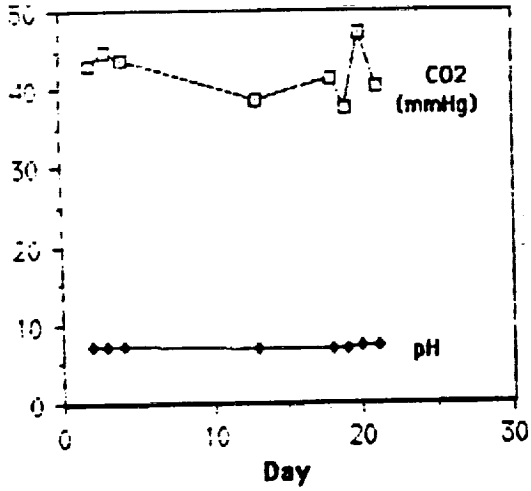


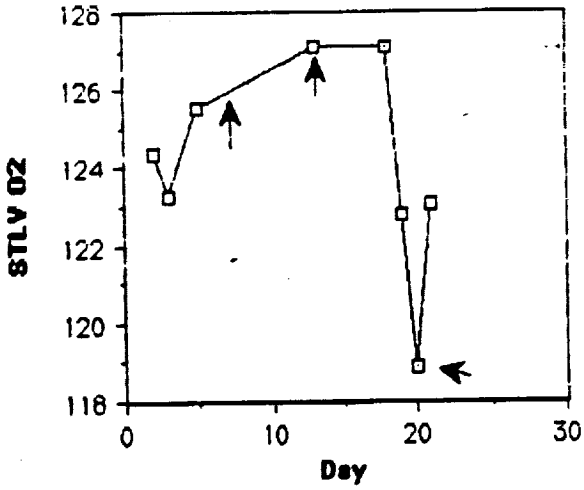


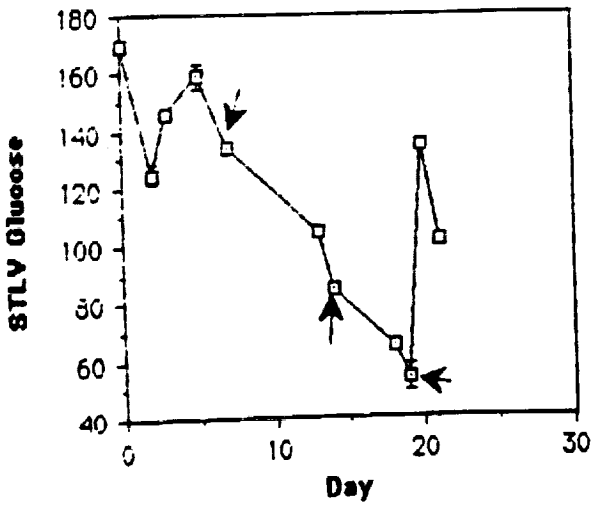


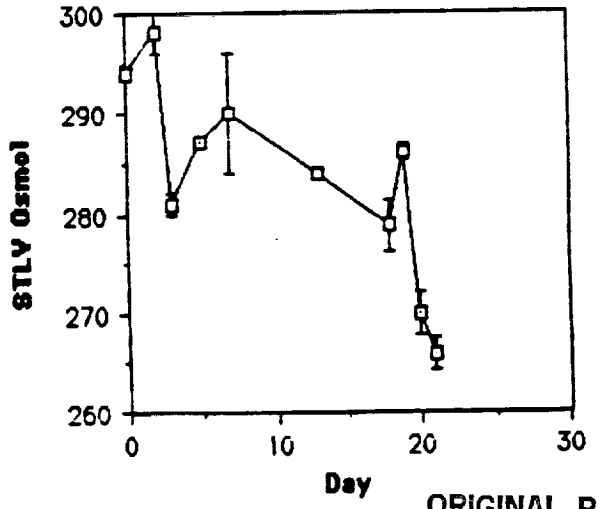

**Relationship of Cell Growth and Oxygen Use**

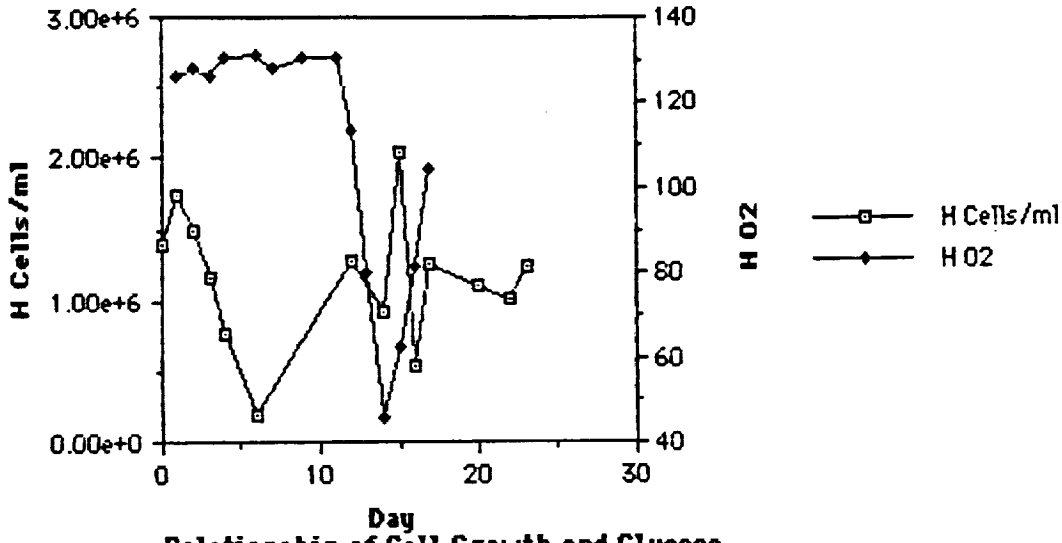


**Relationship of Cell Growth and Glucose Utilization**

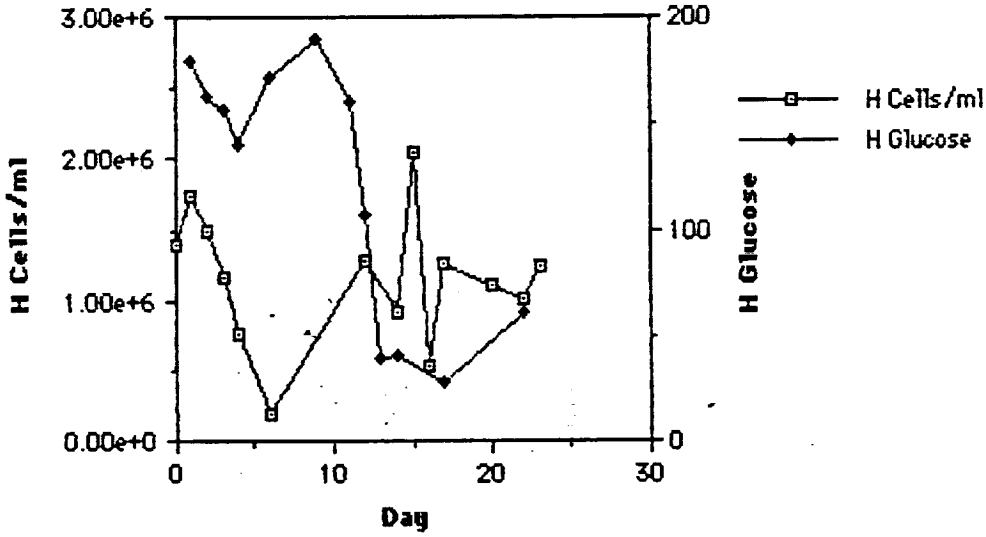


**Glucose and Oxygen Metabolism - HARY**

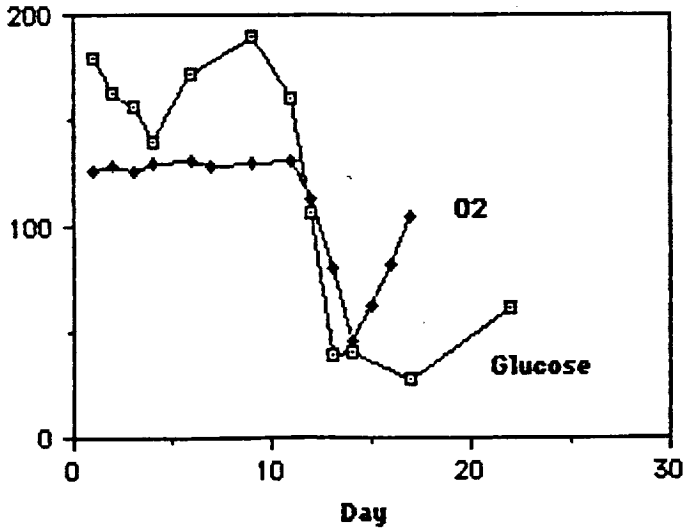

QUADRANT STATISTICS

EXTENDE
ANALYSI

LAW 14 0:50 20JUL89.00900E
831 GAM FITC
FALS -LRFL

PRINT

TOTAL= 8544


FALS 11
LRFL 10

LOWEST LEVEL
3

| QUAD | PERCENT | PEAK POS | PEAK HT | AREA |
|---|---|---|---|---|
| 1 | 9.89 | 8, 11 | 45 | 845 |
| 2 | 11.34 | 19, 21 | 13 | 969 |
| 3 | 9.34 | 0, 6 | 165 | 798 |
| 4 | 69.43 | 35, 0 | 383 | 5932 |

READY.ADJUST CURSOR

RETURN

31 days
DNA

ANALYZE DATA

LAN 14 3:29 28JUL89.86600C
B31 PI DNA
IGFL /IGFL

CONT

DISK STORE

SCALE 256

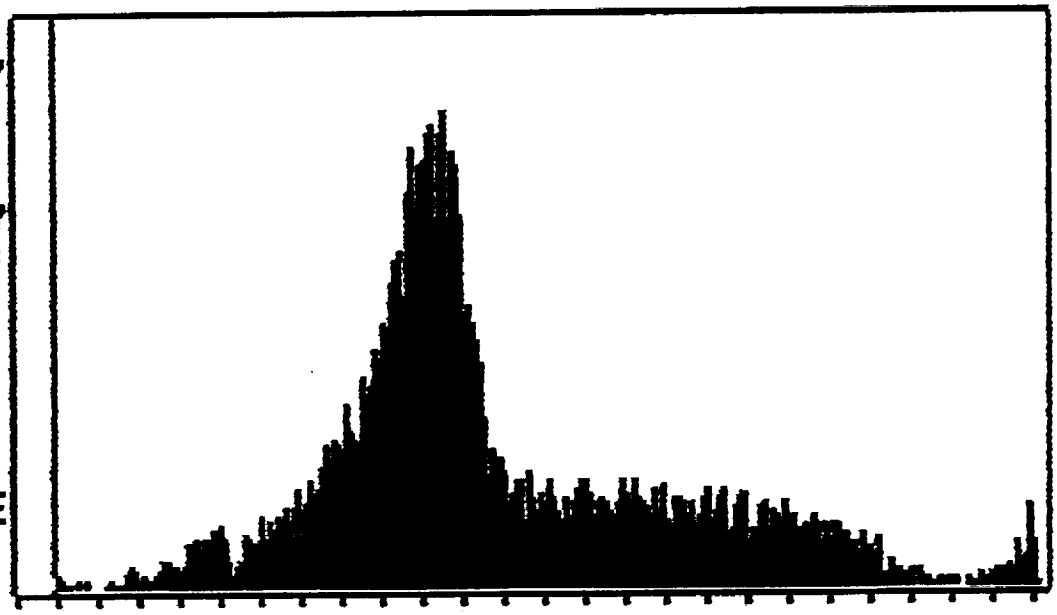

DISPLAY BITMAP: GATE

DISPLAY WINDOW: GATE

RESCALE

MEMORY DELETE

RESTAR

PLOT

IGFL GATE POSITION LOWER= 10 UPPER= 255

STATS

SEC
11
COUNT
10000

READY

DONE

TWO-HISTOGRAM COMPARISON

MERGE SCALE= 512 TOTAL= 10000
SCALE= 512 TOTAL= 10000

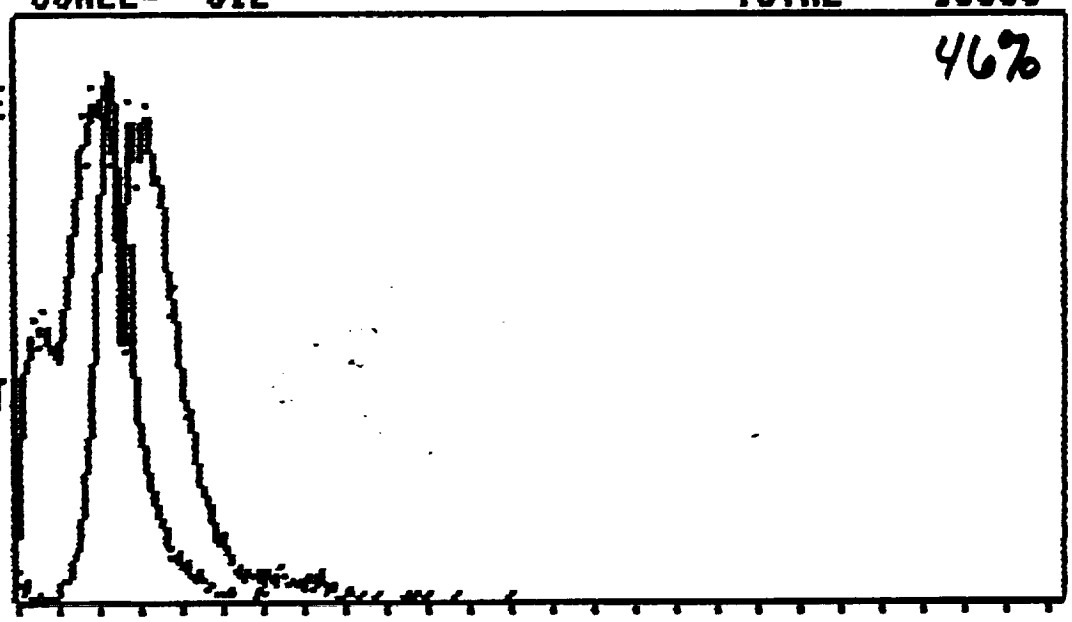


RESCALE

ADD

SUBTRCT

IMMUNO

KSTEST LAW 16 8: 1 24JUL89.83400C
B26 THY1 W/AB
LGFL /LRFL ,FALS

LAW 16 8: 0 24JUL89.83300C
B26 GARFITC W/AB
LGFL /LRFL ,FALS

RETURN

READY

TWO-HISTOGRAM COMPARISON

MERGE SCALE= 512 TOTAL= 10000
SCALE= 512 TOTAL= 10000

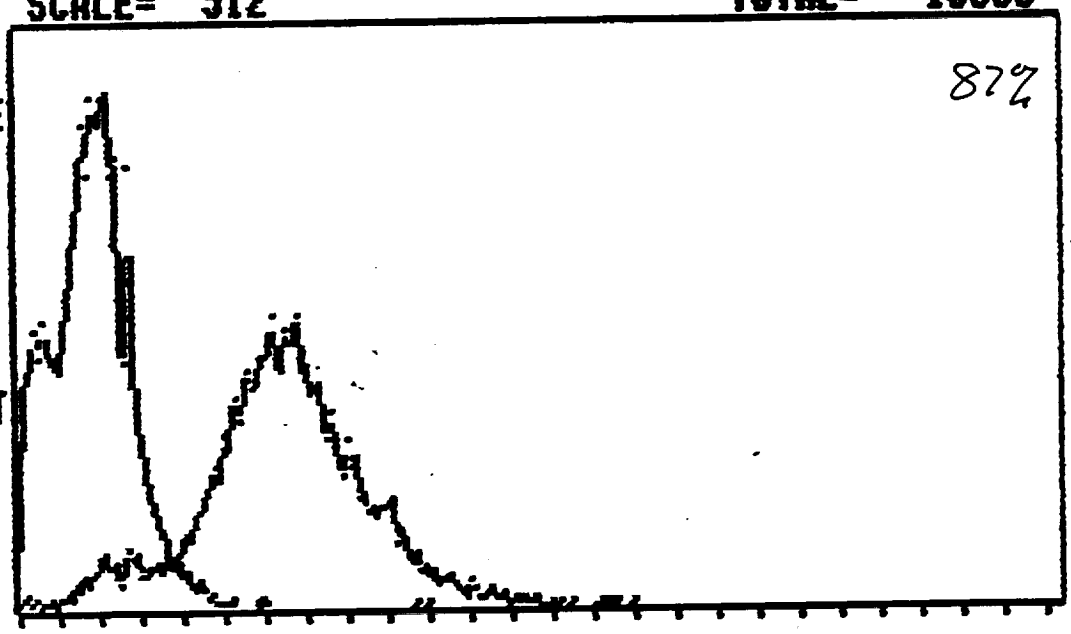


RESCALE

ADD

SUBTRCT

IMMUNO

KSTEST LAM 16 8: 5 24JUL89.03000C
B26 SCA W/AB
LGFL /LRFL ,FALS

LAM 16 8: 0 24JUL89.03300C
B26 GARFITC W/AB
LGFL /LRFL ,FALS

RETURN

READY

FcR.

TWO-HISTOGRAM COMPARISON

MERGE SCALE= 512 TOTAL= 10000
SCALE= 512 TOTAL= 10000

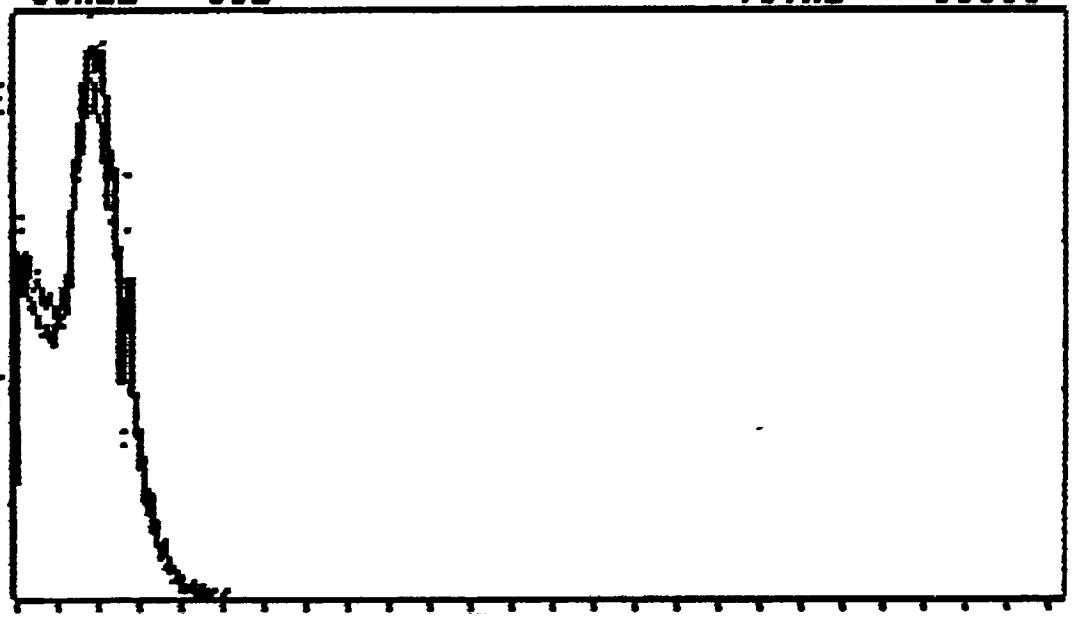

RESCALE

ADD

SUBTRCT

IMMUNO

KSTEST LAW 17 5:52 25JUL89.03300C
B27 2462
LGFL /LRFL ,FALS

LAW 17 5:48 25JUL89.03000C
B27 GAR FITC
LGFL /LRFL ,FALS

RETURN

READY

## DISCUSSION

Our objective in this summer research project was based on a number of premises. Cells of a fetal nature, e.g., bone marrow cells, would outlast differentiated cells if cell-cell contacts could be minimized. The in vitro separation would be discourage differentiation because of the lack of cytokine secretion by cells other than the original population. The environments encountered in in vivo hematopoiesis would be missing. It was for these reasons that we turned to the microgravity environment made available by the bioreactor vessels designed at the Johnson Space Center.

The work has yielded many of the results that we had sought. It also left us with numerous questions that we wish to pursue. We must now look at human bone marrow, but first we must identify and isolate an antigenic marker for the human stem cell. We would then obtain a monoclonal to recognize this compound.

We are eager to continue observations which we have made this summer with the murine thymus and proceed to the human thymus. A third population of cells we would want to observe are fetal liver cells.

## BIBLIOGRAPHY

Cogoli A., 1985. Lymphocyte reactivity during spaceflight. Immunology Today, 6:1.

Lorenzi, T. 1986. Effects of Hypergravity on "whole-blood" cultures of human lymphocytes. Aviat. Space Environ. Med. 57: 1131-5.

Spangrude, G.J., Heimfeld, S. and Weissman, IL., 1988. Puriafication and Characterization of Mouse Hematopoietic Stem Cells. SCIENCE, July , 1988.

Tschopp, P. 1984. Low gravity lowers immunity to disease. New Scientist. 102:36.

# THERMODYNAMIC AND FLUID MECHANIC ANALYSIS OF RAPID PRESSURIZATION IN A DEAD-END TUBE

Final Report

NASA/ASEE Summer Faculty Fellowship Program–1989

Johnson Space Center


| | |
|---|---|
| Prepared By: | Ian H. Leslie, Ph.D. |
| Academic Rank: | Assistant Professor |
| University & Department | New Mexico State University<br>Department of Mechanical Engineering<br>Las Cruces, New Mexico 88003 |

NASA/JSC/White Sands

| | |
|---|---|
| Directorate: | White Sands Test Facility |
| Division: | Laboratory Operations |
| JSC Colleague: | Frank Benz |
| Date Submitted: | October 30, 1989 |
| Contract Number: | NGT 44-001-800 |

## ABSTARACT

Three models have been applied to very rapid compression of oxygen in a dead-ended tube. Pressures as high as 41 MPa (6000 psi) leading to peak temperatures of 1400 K are predicted. These temperatures are well in excess of the autoignition temperature (750 K) of teflon, a frequently used material for lining hoses employed in oxygen service. These findings are in accord with experiments that have resulted in ignition and combustion of the teflon, leading to the combustion of the stainless steel braiding and catastrophic failure.

The system analyzed was representative of a capped off high-pressure oxygen line, which could be part of a larger system. Pressurization of the larger system would lead to compression in the dead-end line, and possible ignition of the teflon liner. The model consists of a large plenum containing oxygen at the desired pressure (500 to 6000 psi). The plenum is connected via a fast acting valve to a stainlees steel tube 2 cm inside diameter. Opening times are on the order of 15 ms. Downstream of the valve is an orifice sized to increase filling times to around 100 ms. The total length from the valve to the dead-end is 150 cm. The distance from the valve to the orifice is 95 cm.

The models describe the fluid mechanics and thermodynamics of the flow, and do not include any combustion phenomena. A purely thermodynamic model assumes filling to be complete upstream of the orifice before any gas passes through the orifice. This simplification is reasonable based on experiment and computer modeling. Results show that peak temperatures as high as 4800 K can result from recompression of the gas after expanding through the orifice.

An approximate transient model without an orifice was developed assuming an isentropic compression process. An analytical solution was obtained. Results indicated that fill times can be considerably shorter than valve opening times. Thus, even though manually opening a valve is slow compared to a fast acting valve, fill times can still be short. For a 100 cm long tube with a valve opening time of 100 ms, the fill time is about 30 ms.

The third model was a finite difference, 1-D transient compressible flow model. The code was obtained from Sandia Livermore and applied to the system. Results from the code show the recompression effect but predict much lower peak temperatures than the thermodynamic model. The difference is due mostly to the complete lack of mixing in the thermodynamic model. Pressure oscillations upstream of the orifice are predicted by this model as observed experimentally; however, damping is greater in the computer model.

## INTRODUCTION

Considerable effort has been made at the White Sands Test Facility (WSTF) to characterize and understand the phenomena associated with the rapid pressurization of flex hoses containing pure oxygen. Pressures in excess of $6000\,psig$, with pressurization rates as high as $600,000\,psi/s$ have been utilized. The primary concern involves the possibility of combustion. This can result from the high temperatures generated from the compression of the low pressure oxygen originally in the system, when exposed to a high pressure source. Valve opening times must be short ($\approx 0.1\,s$), but test have shown that opening times of this duration are within the ability of a person to achieve manually.

At present the mechanisms that lead to hose failure are believed to be pyrolysis of a portion of the teflon lining, followed by ignition of these pyrolysis products, followed in some cases by the ignition of the stainless steel braiding. Even in those cases which do not result in catastrophic failure, the teflon monomer and partially reacted species such as carbonyl fluoride ($COF_2$) have been observed. The later compound is highly toxic and could pose a serious health risk if the flex hose were part of a life support system.

To date, most of the effort at WSTF has been directed toward whether or not hoses met certain criteria regarding acceptable failure rates. However, in addition to these efforts a program [1] aimed at a more basic understanding of the phenomena of compression initiated combustion has been underway for about two years. These efforts have been primarily experimental in nature, and have provided the results mentioned above regarding the sequence of events that can lead to catastrophic failure. Current experimental efforts are directed to *in-situ* spectroscopic methods for measuring pressure and temperature in real time. These data will not only be valuable in themselves, but will provide input to, and verification of, flow models developed. The bulk of this report is concerned with various models, of varying degrees of complexity, for describing the compression process.

At the start of this summer program, modeling of the compression process itself had been based on a very simple picture of the system. Estimation of the maximum temperature near the dead end (assumed worst case) of a hose or tube was determined from the isentropic ideal gas relation between pressure and temperature. This relation is shown in Eq. 1.

$$\left(\frac{T_2}{T_1}\right) = \left(\frac{P_2}{P_1}\right)^{\frac{\gamma-1}{\gamma}} \tag{1}$$

Here $\gamma$ is the ratio of specific heats, assumed to be constant with respect to temperature.

The model assumes piston like compression of the low pressure gas by the high pressure gas. For a gas initially at ambient conditions and then pressurized to $6000\,psig$ a final temperature of 1370°C is theoretically possible. The limitations of this model are readily admitted. The assumed isentropy precludes friction, heat transfer, and mixing. A more realistic model could have great utility in providing predictions for configurations that cannot be conveniently obtained via experimentation, and in addition as a starting point for a model that includes combustion phenomena.

In the sections that follow several models are presented based on various assumptions. The order of presentation is essentially from the simplest to the most complex. A final section will give recommendations for further model development. It should be kept in mind that a flow model, no matter how sophisticated, will be incomplete without the chemistry of pyrolysis and combustion included. However, the phenomena involved are quite complicated in detail, and an initial effort that treats the flow as decoupled from the combustion is considered worthwhile and prudent.

## REAL GAS EFFECTS

The simplest improvement on the isentropic ideal gas model is to include real gas behavior. To assess the importance of real gas effects reference is made to a generalized compressibility chart. The critical temperature and pressure of oxygen are $158.4\,K$ and $5.08\,MPa$ respectively. Based on the ideal gas relation, compression from ambient to $6000\,psig$ ($\sim 41\,MPa$) will result in a gas temperature of 1370°C. The reduced temperature and pressure are 10.4 and 8.03 respectively. The compressibility factor Z is 1.08. This value suggests that that real gas effects should not be significant. However, the temperature effect on specific heats may still be important.

To determine the actual relation between temperature and pressure during isentropic compression a computer program was written. The real-gas model used was *van der Waals'* with constants 'a' and 'b' calculated using the critical point method. The expression to determine $T$ versus $P$ is given in Eq. 2.

$$\left(\frac{\partial T}{\partial P}\right)_s = \frac{T}{c_p}\left(\frac{\partial v}{\partial T}\right)_p \tag{2}$$

The results of the integration are shown in Fig. 1. Also shown in this figure is the curve based on Eq. 1. and a curve allowing for variation in specific heat with temperature, but assuming ideal gas behavior. This last relation was calculated from the expression

$$P = P_o\, exp\left[\frac{1}{R}\int_{T_o}^{T}\frac{c_p(T)}{T}dT\right] \tag{3}$$

where $P_o$ and $T_o$ are initial values, such as ambient conditions, and $c_p(T)$ is the constant pressure specific heat. The functional form of $c_p(T)$ was taken from reference [2].

Inspection of Fig. 1 reveals two important features. The first is that compressibility effects are not significant as anticipated. The second feature is that the temperature dependence of $c_p(T)$ is fairly important. For example, if ambient $O_2$ is compressed isentropically to $5000\,psig$, ($34.5\,MPa$) applying Eq. 1 predicts a temperature of 1295°C. If variable specific heat is accounted for this temperature drops to 1066°C. If both real gas behavior and variable specific heats are considered the predicted temperature is 1092°C. Each of the curves forms a straight or nearly straight line on a log-log plot. Thus, the two variable-property curves can be fit to functions of the form of Eq. 1. A least-squares method was used to find the appropriate exponent $n$ in Eq. 4.

$$\left(\frac{T}{T_o}\right) = \left(\frac{P}{P_o}\right)^n \tag{4}$$

The three values for $n$ and the correlation coefficient $r^2$ are listed below.

ideal gas with constant specific heats ($\gamma = 1.395$)
$n = 0.2829$ $\quad r^2 = 1.0000$

ideal gas with variable specific heats
$n = 0.2599$ $\quad r^2 = 0.9987$

real gas (*van der Waals*) with variable specific heats
$n = 0.2632$ $\quad r^2 = 0.9989$

The values on $n$ for the last two cases strickly apply to $T_o = 300\,K$ and $P_o = 100\,kPa$; however, small deviations from these values should cause little error.

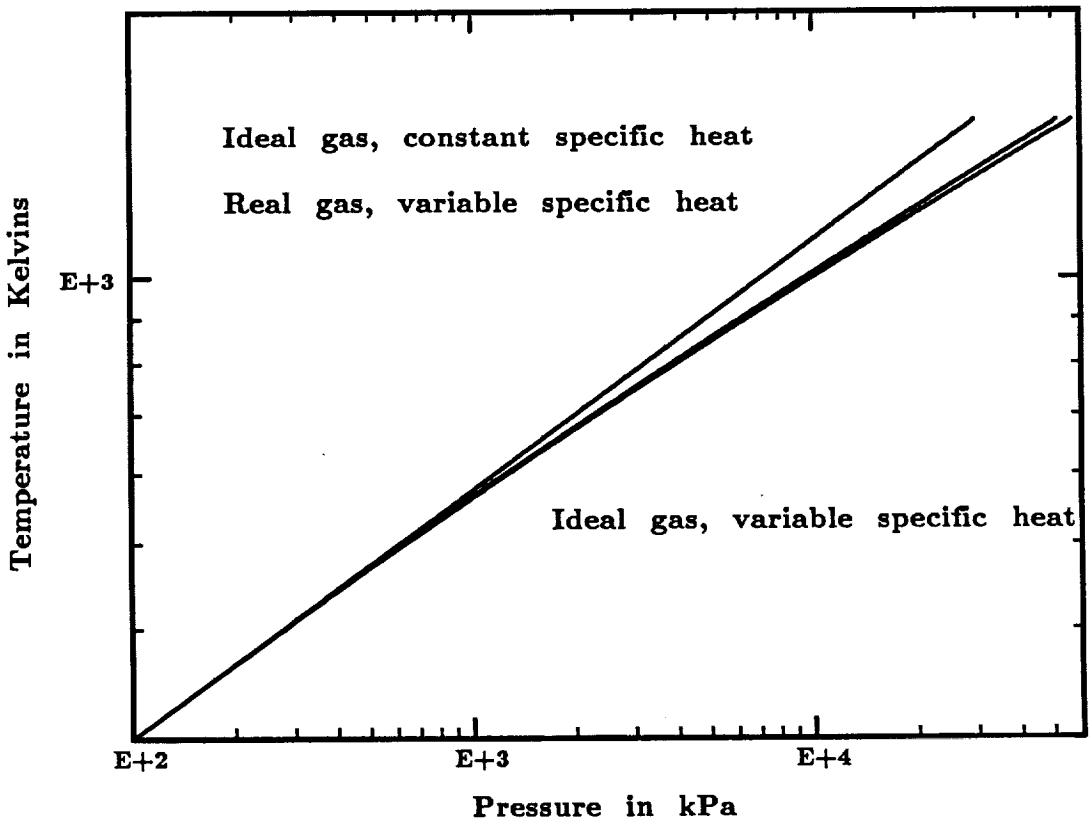


Figure 1.- Isentropic temperature-pressure relations.

## SIMPLE THERMODYNAMIC MODELS

Most of the experiments conducted at WSTF involving rapid pressurization of flex hoses or hard lines involve an orifice. The purpose of the orifice is to decrease the pressurization rate from those attainable by the fast acting valve. Valve opening times between 13 and 18 *ms* are typical; pressurization times would be of the same order. The orifice was sized so that pressurization times were on the order of 100 *ms*.

As a first approximation the orifice was accounted for in the following manner. The valve is assumed to open instantly, and high pressure plenum gas pressurizes the gas in the volume upstream of the orifice before any significant flow occurs through the orifice. Next, gas flows through the orifice with the pressure dropping to the local downstream pressure. Eventually the pressure is everywhere uniform and equal to the plenum pressure (assumed constant due to large volume). Additional assumptions include: ideal gas behavior, constant specific heats, no heat transfer, and no frictional losses. Pressure is assumed to be spatially uniform on each side of the orifice.

Even with all these assumptions and the simple nature of the model, several cases need to be considered. Two broad classes result from assuming piston like compression of the gas downstream of the orifice on the one hand, and complete mixing on the other. In both cases the gas originally upstream of the orifice is assumed to be compressed in a piston like manner. Two subcases result depending on whether or not the initially compressed gas is of sufficient quantity to compress the gas downstream of the orifice without any driver gas (gas originally in the plenum) passing through the orifice. The results are presented below for these cases.

Nomenclature:

$A$ subscript refers to gas originally between valve and orifice

$B$ subscript refers to gas originally downstream of orifice

$nm$ subscript refers to no mixing

$cm$ subscript designates complete mixing

$i$ initial conditions

$f$ final conditions

$P_f$ final pressure equal to plenum pressure

$P_i$ initial pressure (same for gases $A$ and $B$)

$\Re$ pressure ratio $P_f/P_i \geq 1$

$\gamma$ ratio of specific heats

$\vartheta_{A_i}$ volume between valve and orifice

$\vartheta_{B_i}$ volume downstream of orifice

$T_s$ isentropic temperature based on Eq. 1

The formulae for the various cases are presented based on whether or not driver gas passes through the orifice. With the various assumptions borne in mind, the limiting case for no flow through the orifice is determined from Eq. 5.

$$\left.\frac{\vartheta_{A_i}}{\vartheta_{B_i}}\right)_{critical} = \frac{\Re - 1}{\gamma \Re^{\frac{\gamma-1}{\gamma}}} \tag{5}$$

This result applies to both mixing and nonmixing of gases $A$ and $B$.

No Driver Gas Through Orifice And No Mixing

$$\left.\frac{T_B}{T_i}\right)_{nm} = \frac{T_s}{T_i} = \Re^{\frac{\gamma-1}{\gamma}} \qquad \text{Gas B} \tag{6}$$

$$\left.\frac{T_A}{T_s}\right)_{nm} = \frac{\gamma(\Re - \Re^{\frac{\gamma-1}{\gamma}})}{\Re - 1} \qquad \text{Gas A} \tag{7}$$

The volume of Gas B after compression can be found from Eq. 8.

$$\frac{\vartheta_{B_f}}{\vartheta_{B_i}} = \Re^{-1/\gamma} \tag{8}$$

Complete mixing downstream of orifice

$$\frac{T_{cm}}{T_s} = \frac{\gamma \Re}{\gamma \Re^{\frac{\gamma-1}{\gamma}} + \Re - 1} \tag{9}$$

Some Driver Gas Through Orifice And No Mixing

Before any Gas A passes through the orifice it is compressed to $P_f$. This state is referred to as state 1.

$$\frac{T_{A_1}}{T_i} = \Re^{\frac{\gamma-1}{\gamma}} \tag{10}$$

Due to the nature of the derivation a second intermediate state (state 2) is determined. This state occurs when all of Gas A has just passed through the orifice. Note that the temperatures are normalized to $T_s$ rather than $T_i$.

$$\left[1 + \frac{\vartheta_{A_i}}{\vartheta_{B_i}} \Re^{\frac{\gamma-1}{\gamma}} \left(\gamma - \frac{T_{A_2}}{T_s}\right)\right]^{\frac{1}{\gamma-1}} = 1 + \frac{\vartheta_{A_i}/\vartheta_{B_i}}{\Re^{\frac{1-\gamma}{\gamma}} \frac{T_s}{T_{A_2}} + \frac{\vartheta_{A_i}}{\vartheta_{B_i}} \left(\gamma \frac{T_s}{T_{A_2}} - 1\right)} \tag{11}$$

$$\frac{T_{B_2}}{T_s} = \Re^{\frac{1-\gamma}{\gamma}} + \frac{\vartheta_{A_i}}{\vartheta_{B_i}} \left(\gamma - \frac{T_{A_2}}{T_s}\right) \tag{12}$$

$$\frac{P_2}{P_i} = \Re \left(\frac{T_{B_2}}{T_s}\right)^{\frac{\gamma}{\gamma-1}} \tag{13}$$

The final state (state 3) is given by:

$$\frac{T_{A_3}}{T_s} = \frac{1}{\Re^{\frac{1-\gamma}{\gamma}} \frac{T_s}{T_{A_2}} - \frac{\vartheta_{A_i}}{\vartheta_{B_i}} \left(1 - \gamma \frac{T_s}{T_{A_2}}\right)} \tag{14}$$

$$\frac{T_{B_3}}{T_s}\Big) = 1 \tag{15}$$

The driver gas temperature is assumed to remain constant at $T_i$, except for that portion that passes through the orifice. The temperature of this portion is given by:

$$\frac{T_{D_3}}{T_i} = \frac{\gamma}{1 + \frac{\left(\frac{\vartheta_{A_i}}{\vartheta_{B_i}} \frac{T_{A_2}}{T_s} + \frac{T_{B_2}}{T_s}\right)\left(\frac{T_s}{T_{B_2}} - 1\right)}{\Re^{1/\gamma} - \frac{\vartheta_{A_i}}{\vartheta_{B_i}} \frac{T_{A_3}}{T_s} - \frac{T_{B_2}}{T_s}}} \tag{16}$$

In order to determine $T_{A_3}$ and $T_{D_3}$ (also $T_{B_2}$ and $P_2$) the values of $\vartheta_{A_i}/\vartheta_{B_i}$, $\Re$, and $\gamma$ must be known. With these values Eq. 11 is solved iteratively for $T_{A_2}/T_s)_{nm}$ and substituted into Eqs. 14 and 16.

Complete mixing

$$\frac{T_3}{T_i}\Big)_{cm} = \frac{\Re}{\frac{1}{\gamma}(\Re - 1) - \left(\frac{\vartheta_{A_i}}{\vartheta_{B_i}}\right)\left(\Re^{\frac{\gamma-1}{\gamma}} - 1\right) + 1} \tag{17}$$

Results for no driver gas through the orifice and no mixing were determined for the values are listed below.

$$T_i = 300\,K \qquad \Re = 300 \;\; (\sim 4400\,psig) \qquad \gamma = 1.395 \;\; (O_2 \text{ value})$$

The final temperature of Gas B is $1508\,K$ as is the temperature of Gas A when first compressed upstream of the orifice. However, the final temperature of Gas A that passes through the orifice is $2076\,K$ showing the recompression effect.

## TRANSIENT ISENTROPIC MODEL

An approximate model was developed for the filling of a tube or hose with only a valve in the system, no orifice was included. The model is applicable to moderate rates of filling such that $\frac{\partial P}{\partial x}$ is negligable. This condition will be satisfied when $t_f \ll t_a$. Here $t_f$ is the characteristic time to fill the hose, and $t_a$ is the wave relaxation time. The wave relaxation time is given by Faeth [3] as $L/a$, where $L$ is the length of the tube and $a$ is the velocity of sound. For a $1\,m$ tube and $a = 350\,m/s$, $t_a = 2.8\,ms$. From a practical standpoint the filling time should be considerably greater than twice this value. Thus $t_f$ should be at least $60\,ms$. For the fast acting valve this condition is not met. However, manual valve opening times are at least this long.

The model was further simplified by assuming the following:

1. isentropic compression downstream of valve
2. no axial mixing or diffusion
3. no heat transfer to tube wall
4. no chemical reactions
5. ideal gas model with constant specific heats
6. temperature of gas passing through valve is taken as $T_D$ (plenum temperature)

To obtain the results desired the conservation equations for energy and mass must be solved simultaneously. The momentum equation need not be solved because of the assumption of no spatial variation in pressure. In addition to the two conservation equations, the equation of state and the isentropic relation between temperature and pressure are employed. The appropriate equations are provided in Eqs. 18 through 21.

Energy
$$c_v \frac{\partial \rho T}{\partial t} = -c_p \frac{\partial \rho T V}{\partial x} \tag{18}$$

Mass
$$\frac{\partial \rho}{\partial t} = -\frac{\partial \rho V}{\partial x} \tag{19}$$

Equation of State
$$P = \rho R T \tag{20}$$

Process
$$\frac{DT}{Dt} = \frac{\gamma - 1}{\gamma} T_i P(\tau)^{\frac{1-\gamma}{\gamma}} \frac{1}{P^\gamma} \frac{DP}{Dt} \tag{21}$$

Equation 21, labeled as process, is the isentropic relation between pressure and temperature. The pressure designated $P(\tau)$ is the pressure at $t = \tau$, which is the time when the fluid element passed through the orifice. It is Eq. 21 which is used to determine temperature from pressure.

The solution is comprised of two time domains. The first is characterized by choked flow at the orifice. The second domain involves unchoked flow. The transition from one regime to the other may or may not occur while the valve is still opening. The most rapid pressure rise occurs when choked flow is present and the valve is fully open. This is so since the rate of pressure increase is directly proportional to the flow area of the valve. Formulae for mass flux and pressure rise rate were taken directly from Faeth [3]. Here the solution for $P(t)$ is given for a valve area that increases linearly with time.

$$A_v(t) = A_m \frac{t}{t_o} \tag{22}$$

Here $A_m$ is the maximum area of the valve and $t_o$ is the time to open. Note that $A_m$ is alway less than or equal to the area of the tube. The initial condition is $P = P_i$ and $T = T_D$ at $t = 0$. Thus,

for choked flow and $t \leq t_o$

$$\frac{P}{P_D} = \frac{P_i}{P_D} + \frac{\gamma B a_D A_m}{2\vartheta_{tube}} \frac{t^2}{t_o} \tag{23}$$

where $a_D$ is the sound speed at $T_D$, and $B$ is a function of $\gamma$ with a value near unity.

The condition for choking is

$$\frac{P}{P_D} \leq \left(\frac{2}{\gamma+1}\right)^{\frac{\gamma}{\gamma-1}} \tag{24}$$

Substitution of Eq. 24 into Eq. 23 permits the unchoking time $t_{uc}$ to be calculated, provide $t_{uc} \leq t_o$, the most likely case.

$$t_{uc} = \sqrt{\left[\left(\frac{2}{\gamma+1}\right)^{\frac{\gamma}{\gamma-1}} - \frac{P_i}{P_D}\right] \frac{2\vartheta_{tube}}{\gamma B a_D A_m} t_o} \tag{25}$$

The limiting case where $t_{uc} = t_o$ occurs when

$$t_o = t_o^* = \left[\left(\frac{2}{\gamma+1}\right)^{\frac{\gamma}{\gamma-1}} - \frac{P_i}{P_D}\right] \frac{2\vartheta_{tube}}{\gamma B a_D A_m} \tag{26}$$

Thus the unchoking time for $t_{uc} \leq t_o$ becomes

$$t_{uc} = \sqrt{t_o^* t_o} \tag{27}$$

For the purpose of an example air is chosen at ambient conditions. In addition, let $A_m = A_{tube}$ and the length of the tube be $1\,m$. For a pressure ratio $\Re = 10$, $t_o^* = 0.0030\,s$. For $\Re = 100$, $t_o^* = 0.0037\,s$. Inspection of Eq. 26 shows that as $\Re \to \infty$, $t_o^* \to 0.0038\,s$. These times are so short that it will almost alway be the case that unchoking will occur before the valve is fully open. For $t_{uc} < t < t_o$

$$\frac{P}{P_D} = \left\{1 - \left[\left(\frac{\gamma-1}{\gamma+1}\right)^{\frac{1}{2}} - \frac{\gamma-1}{\gamma}\frac{C}{4}(t^2 - t_{uc}^2)\right]^2\right\}^{\frac{\gamma}{\gamma-1}} \tag{28}$$

where the constant $C$ is given by

$$C = \frac{\gamma a_D A_m / t_o}{\vartheta} \left(\frac{2}{\gamma-1}\right)^{\frac{1}{2}}$$

For $t > t_o > t_{uc}$ the appropriate equation is

$$\frac{P}{P_D} = \left\{1 - \left[\left(1 - \left[\frac{P_o}{P_D}\right]^{\frac{\gamma-1}{\gamma}}\right)^{\frac{1}{2}} - \frac{\gamma-1}{\gamma}\frac{C}{2}(t - t_o)\right]^2\right\}^{\frac{\gamma}{\gamma-1}} \tag{29}$$

where $P_o/P_D$ is determined from Eq. 28 when $t = t_o$. Pressure versus time for the case described above with $\Re = 100$ and $t_o = 100\,ms$ is plotted in Fig. 2. The time for unchoking is $19.2\,ms$. It is interesting to note that the time to fill the tube is $30\,ms$, considerably less than the $100\,ms$ valve opening time.

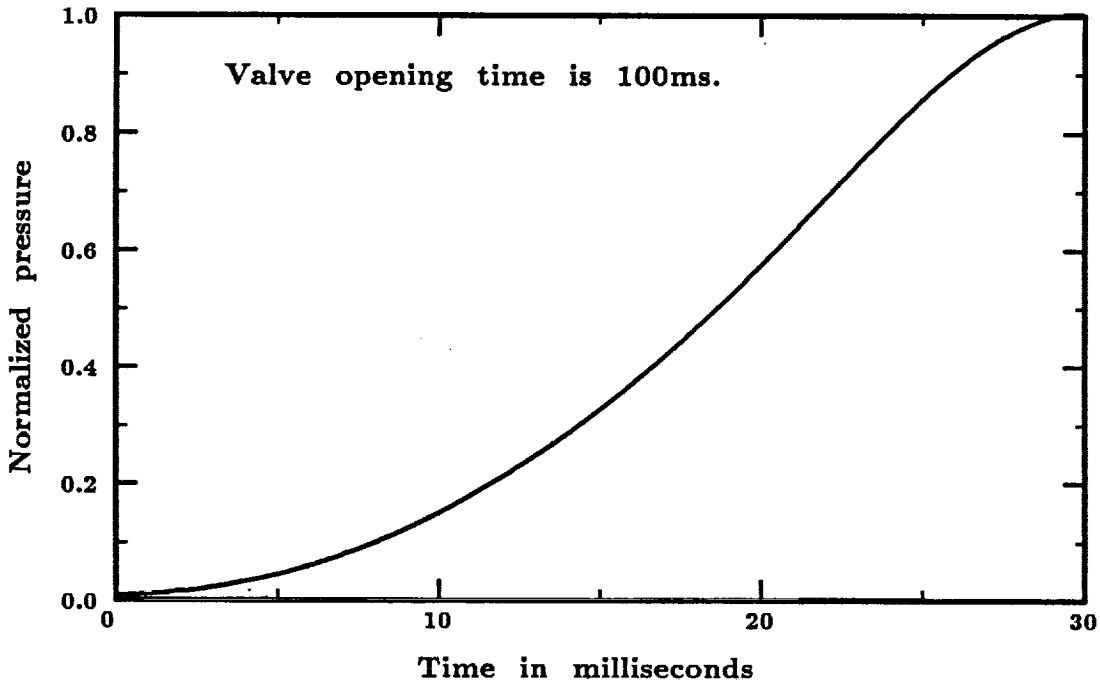


Figure 2.- Pressure rise from isentropic model

## COMPUTER RESULTS USING TOPAZ

In the words of the author of the computer code "**TOPAZ** is a *user friendly* computer code for modeling the one-dimensional-transient physics of multi species gas transfer in arbitrary arrangements of pipes, valves, vessels, and flow branches". The author is W. S. Winters of the Computational Mechanics Division, Sandia National Laboratories, Livermore, CA. Dr. Winters was most helpful and cooperative in making the source code available to me. For documentation on **TOPAZ** see [4,5,6,7].

Some experimental results for pressure were available at the start of this computational work. The exact physical setup appropriate for the data was not known, but data both upstream of the orifice and at the dead-end were available. Therefore, the general characteristics of the pressure transients were known. These characteristics included a very rapid and oscillatory pressure rise upstream of the orifice, and a much slower and well behaved pressure rise at the dead-end. The oscillations are believed to be due pressure waves traversing the distance between the high pressure plenum and the orifice. These oscillations were observed in the computed results as well.

The system modeled in **TOPAZ** was a $1\,m^3$ spherical high pressure plenum. Gas from the plenum flowed through five identical valves in parallel. Each valve when fully open is one-fifth the area of the main pipe. The first part of the main pipe was $95\,cm$ long and $2\,cm$ inside diameter. This pipe fed into an orifice $1\,cm$ long and $3\,mm$ in diameter. The orifice was followed by another $2\,cm$ diameter pipe $48\,cm$ long. Heat transfer was accounted for via the 'constant wall temperature' model.

Results are shown in Figs. 3 and 4. Figure 3 shows three pressure traces. Examination of the dead-end trace shows that the fill time is $\sim 90ms$. This fill time is somewhat less than the experimental results indicating that the orifice should be a little smaller. The other two traces are for locations just upstream of the orifice. The pressurization rates are much higher than at the dead-end, and show that the approximation (no gas passing through orifice while upstream is

pressurized) made in the thermodynamic analysis section was reasonable.

The control element (CE (control volume)) just upstream of the orifice experiences considerable pressure overshoot (factor of 1.8). The exact amount of the overshoot depends on how the system is modeled. Details such as the CE length both before and in the orifice can change the maximum value. However, the frequency of the oscillations and the time to decay to the final pressure are not significantly effected. This extreme overshoot only occurs in the CE just before the orifice independent of other changes. Further study is required to determine if this overshoot is real, or a manifistation of the numerical model.

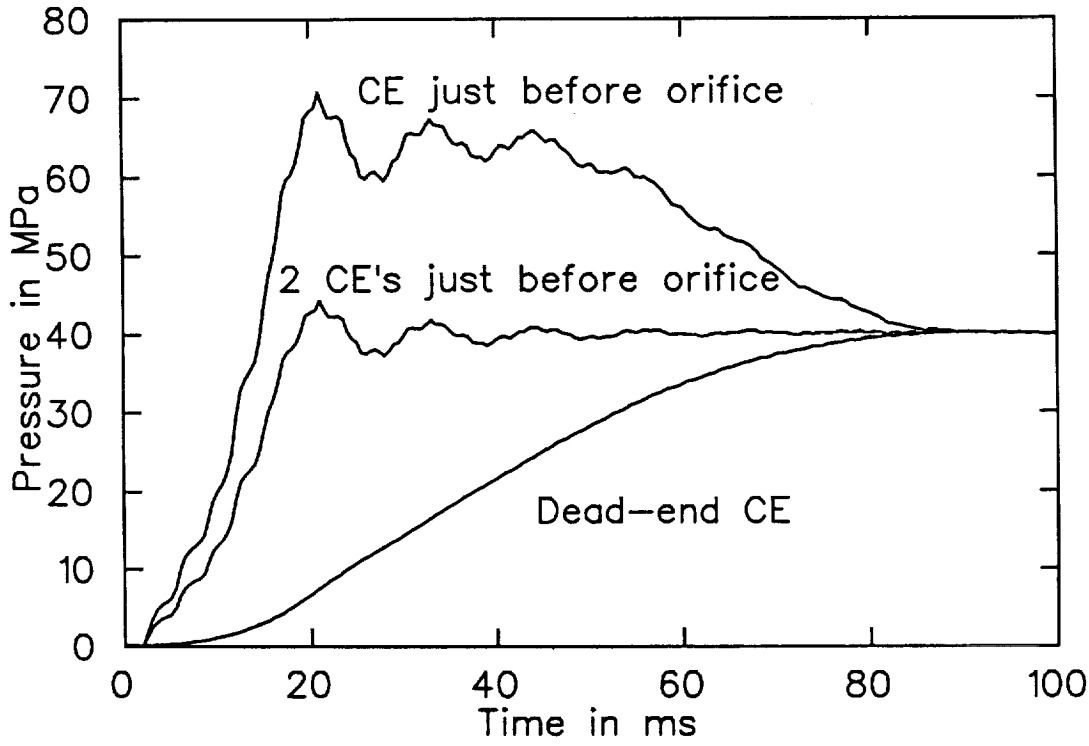


Figure 3.- Pressure rise in tube with $3\,mm$ orifice. Upper curves are just upstream of orifice, lower curve is at very end of tube.

Temperature traces at and near the dead-end are shown in Fig. 4. If the order of the curves at $100\,ms$ is examined, the highest temperature occurs at the dead-end with temperatures decreasing as one moves upstream. At least two significant features need to mentioned. The first feature is that the presence of the orifice results in a higher maximum temperatures. For a straight tube with no orifice, a maximum temperature of $\sim 980\,K$ was reached. With an orifice a maximum temperature near $1400\,K$ was reached. Thus, the recompression effect predicted earlier using thermodynamics only is confirmed; however, the effect is much smaller. The second feature is that the region that experience temperatures in excess of $750\,K$ (autoignition temperature of PTFE) is much larger than for a straight tube.

The placement of the orifice is important. If the orifice is located close to valve very little gas is initially pressurized and very little high temperature gas is recompressed. This means that pressurization rates can be controlled via an orifice with little unwanted recompression effects. On the other hand, a system in the field may contain restrictions some distance from the high pressure source and the dead-end and not be properly modeled unless the orifice is placed at the appropriate distance from the source.

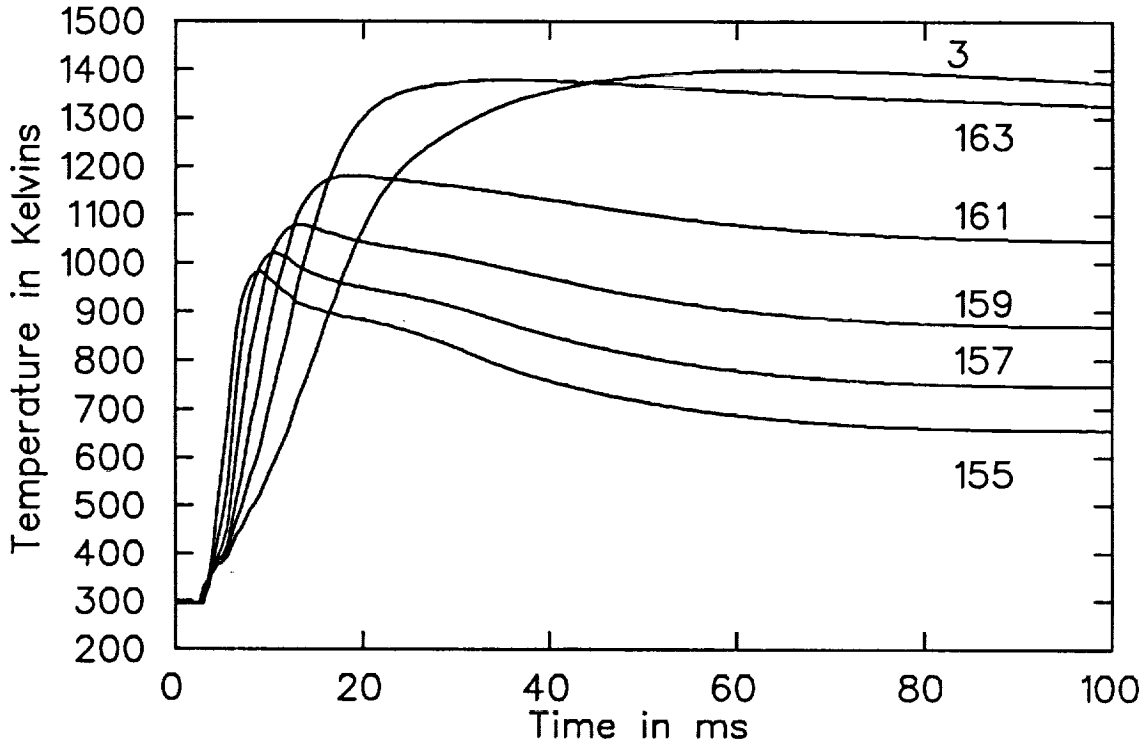


Figure 4.- Pressure rise in tube with $3\,mm$ orifice. Distance is referenced from dead-end, curve 3 (0-3cm), curve 163 (3-8cm), curve 161 (8-13cm), curve 159 (13-18cm), curve 157 (18-23cm), curve 155 (23-28cm).

## EXPERIMENTAL RESULTS

The available experimental results apply to a system somewhat different in detail to the system modeled by **TOPAZ**. The data are useful since they are "real" and because they show that **TOPAZ** is able to model the main features. The pressure data is considered most reliable because the response of the piezoelectric transducers is more than sufficient to capture any of the observed transients. The temperature data was obtained with a thin film thermocouple mounted at the dead-end. Only a very small portion of the tip was exposed and may have been within a thermal boundary layer after a very short time. There is also some question as to what the transient response characteristics are for the thin film thermocouple. A fairly sophisticated heat transfer analysis would be required to determine the *in situ* behavior.

Pressure traces are shown in Figs. 5 and 6 which were taken prior to the Summer of 1989. Mr. Dwight Janoff (now at JSC) made these data available, additional results are available. None of the traces was converted to pressure; however the reservoir pressure was $6000\,psig$. The relation between the vertical scale ($mV$) and pressure is fairly linear at early times. The apparent decrease in pressure observed beyond $0.2\,s$ is not real and is due to behavior of the piezoelectric transducer. Figure 5 shows the pressure rise at the dead-end. Fill times are about $150\,ms$. Figure 6 shows the pressure history just before the orifice. Note that the rise to peak pressure is very rapid ($\sim 20\,ms$). The oscillations are considered real and not due to the transducer. The **TOPAZ** results also show oscillations, but not as persistent as in the actual data. In both the experimental results and the computer predictions, the upstream pressure transients continue until the downstream pressure has reached its final value. The other significant difference between the data and the predictions is the degree of overshoot. The data indicates a factor of 1.3, versus 1.8 from **TOPAZ**.

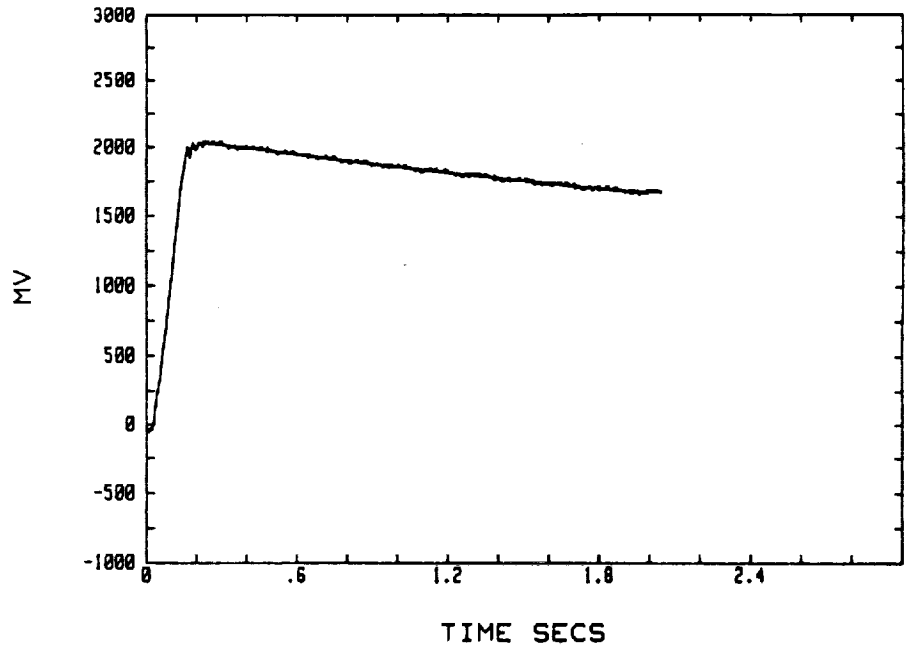


Figure 5.- Pressure trace at dead-end, orifice in place. Peak pressure was $\sim 6000 psi$.

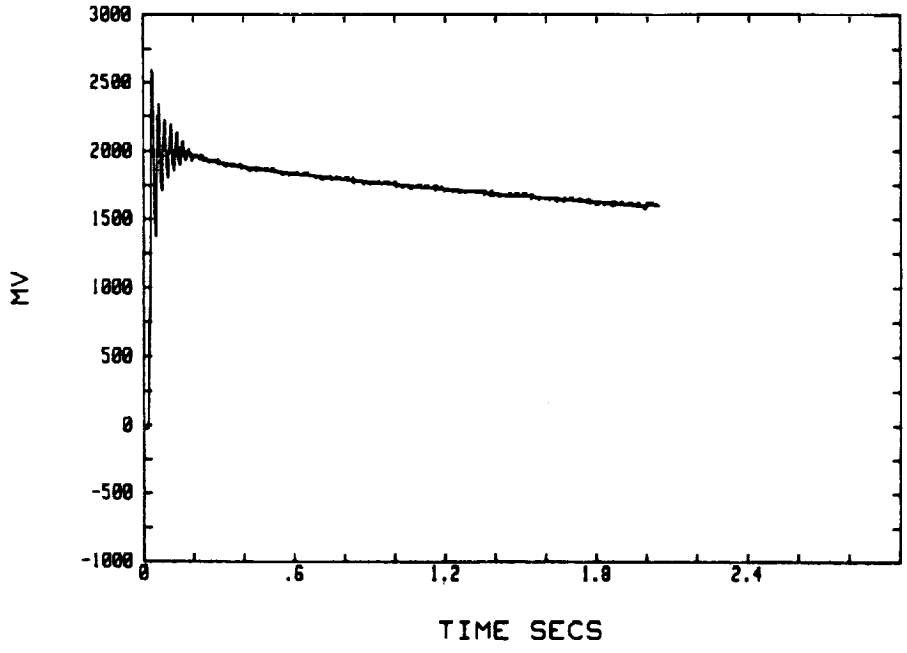


Figure 6.- Pressure trace just upsteram of orifice. Peak pressure was $\sim 6000 psi$.

## CONCLUSIONS

The highly transient nature of the rapid compression process requires that the compressible form of the Navier-Stokes equation be solved. At present the 1-D form of these equations provides useful results, although further assessment is required to determine what the limitations are. These limitations could include frictional modeling, heat transfer modeling, and valve modeling. Results based on the purely thermodynamic model are valuable to illustrate the effects of recompression and mixing versus non-mixing models, but are not quantitatively accurate. The approximate 1-D isentropic model is restricted to slow filling rates and no orifice, but allows very quick results to be obtained. In addition, this approximate model being in an analytical form allows the dependence of fill time on various parameters to be easily determined. One result from this model is that filling times are only partially dependent on valve opening times. In general the fill time is much less than the valve opening time if the opening is performed manually.

The computer results from the code **TOPAZ** reproduce the experimental results reasonably well. Some of the differences are due to the actual experimental system not being modeled exactly in the code. The dominant feature that shows up both experimentally and theoretically is damped pressure oscillations upstream of the orifice. The code also predicts a recompression effect due to the presence of an orifice. The net results of this are higher peak temperatures and a larger region above the autoignition temperature of teflon. Thus, if an actual oxygen system has an orifice (or a partially opened valve) in the piping, higher peak temperatures can be obtained than would be expected. In either case the peak temperatures are calculated to be less than temperatures based on adiabatic compression, although only somewhat less with the recompression effect accounted for.

**TOPAZ** results suggest that heat transfer is not a significant factor during the first 150 *ms* or so. These times are thought to be sufficiently long to allow ignition to take place. The major increase in temperature takes place at very early times. This is due to the dependence of temperature on pressure . The adiabatic model of Eq. 1 shows that temperature rises most rapidly at the low pressures. Thus, high temperatures can be reached in just a few 10's of millseconds.

## RECOMMENDATIONS

Several questions remain to be answered regarding the heating phase of the rapid compression (before significant pyrolysing or combustion). These questions are:

1. How do the various parameters of the problem effect final temperature?
2. Is the valve model used in **TOPAZ** 'good enough'?
3. What are the actual temperatures in the system?
4. Does the temperature drop very sharply right at the dead-end?
5. Is axial mixing significant?

To answer these questions the following recommendations are suggested:

1. continue calculations using **TOPAZ** to finish the parametric study of the problem,
2. apply existing 2-D codes to the problem to assess the accurateness of the 1-D code,
3. build an experimental system that is as simple as possible so that code predictions can be unambiguosly compared (all dimesions and parameters of the system must be known),
4. instrument the system for both pressure and temperature (either a 'hot-wire' method or optical technique needs to be used for temperature),
5. perform tests with nitrogen compressed by oxygen to assess mixing effects.

All code predictions require extensive amounts of CPU time. The VAX 8530 requires up to 65 hours to complete some runs. A 2-D code is expected to run longer. Although memory requirements are not great, the calculationally intensive nature of the compressible flow equations suggests using a super computer. Since both the 1-D and 2-D codes were originally written for a CRAY computer, it is suggested that this super computer be used.

## REFERENCES


1. Janoff,D., Bamford, L. D., Newton, B. E., and Bryan, C. J., "Ignition of PTFE-Lined Flexible Hoses by Rapid Pressurization with Oxygen", Symposium on Flammability and Sensitivity of Materials in Oxygen-Enriched Atmospheres: Fourth Volume, ASTM SPT 1040, Joel M. Stoltfus, Frank J. Benz, and Jack S. Stradling editors, American Society for Testing and Materials, Philadelphia, 1989.

2. Van Wylen, G. J. and Sonntag, R. E., Fundamentals of Classical Thermodynamics, 3rd Edition, SI Version, John Wiley & Sons, 1985.

3. Faeth, G. M., "Spontaneous Ignition during Charging Processes in Pneumatic and Hydraulic Systems", report to the United States Navy Bureau of Ships, Contract No. Nobs 78674, Index No. S-R001-0301, October 1963.

4. Winters, W. S., "Topaz - The Transient One-Dimensional Pipe Flow Analyzer: User's Manual", Sandia Report SAND85-8215.UC-32, July 1985.

5. Winters, W. S., "Topaz - The Transient One-Dimensional Pipe Flow Analyzer: An Update on Code Improvements and Increased Capabilities", Sandia Report SAND87-8225.UC-32, September 1987.

6. Winters, W. S., "Topaz - The Transient One-Dimensional Pipe Flow Analyzer: Code Validation and Sample Problems", Sandia Report SAND85-8236.UC-32, Reprinted February 1988.

7. Winters, W. S., "Topaz - The Transient One-Dimensional Pipe Flow Analyzer: Equations and Numerics", Sandia Report SAND85-8248.UC-32, Reprinted August 1988.

# A comparison of two neural network schemes for navigation

Final Report
NASA/ASEE Summer Faculty Fellowship Program 1989
Johnson Space Center


| | |
|---|---|
| Prepared by: | Paul W Munro, PhD |
| Academic Rank: | Assistant Professor |
| University & Department: | Department of Information Science<br>University of Pittsburgh<br>Pittsburgh PA 15260 |
| Electronic Mail: | munro@idis.lis.pittsburgh.edu |


**NASA/JSC**

| | |
|---|---|
| Directorate: | Mission Support |
| Division: | Mission Planning and Analysis |
| Branch: | Artificial Intelligence |
| JSC Colleague: | James Villarreal |
| Date: | July 27, 1989 |
| Contract Number: | NGT 44-001-800 |

## Abstract

Neural networks have been applied to tasks in several areas of artificial intelligence, including vision, speech, and language. Relatively little work has been done in the area of problem solving. Two approaches to path-finding are presented, both using neural network techniques. Both techniques require a training period. Training under the back propagation (BPL) method was accomplished by presenting representations of [current position, goal position] pairs as input and appropriate actions as output. The Hebbian/interactive activation (HIA) method uses the Hebbian rule to associate points that are nearby. A path to a goal is found by activating a representation of the *goal* in the network and processing until the current position is activated above some threshold level. BPL, using back-propagation learning, failed to learn, except in a very trivial fashion, that is equivalent to table lookup techniques. HIA, performed much better, and required storage of fewer weights. In drawing a comparison, it is important to note that back propagation techniques depend critically upon the forms of representation used, and can be sensitive to parameters in the simulations; hence the BPL technique may yet yield strong results.

# Introduction

*Description of the problem.*

A *map* is given, which is a represention of landmarks and allowed paths and/or obstacles in the relevant region of space. Given an arbitrary pair of points, **I** (initial) and **G** (goal), the problem is to compute a sequence of actions which will bring the subject from **I** to **G**. Several approaches to this classic problem have been put forward (see for example, Brooks, 1983). These tend to rely upon explicit geometrical computations on polygonal representations of obstacles. In contrast, any geometrical considerations in the neural network approaches described below are *implicit*; that is, they are emergent artifacts of the learning processes. Two principles for processing and training of neural networks are briefly described in this section. More detailed treatments can be found in the references.

*Back-propagation learning*

Back propagation (Rumelhart, Hinton, & Williams, 1986) is a general algorithmic framework for training a feed-forward network of semi-linear units by randomly selecting pairs of input-output patterns from a training set and incrementally adjusting the network parameters, such that the network produces the appropriate output for a given input. The parameters of the network are usually, but not necessarily, restricted to the weights on the links (edges, in graph theoretic terminology) between the units (nodes). Initially, the parameters are set to random values. With each presentation of an input-output pair, the network produces a response to the input, which is compared to the desired output; the back-propagation learning (BPL) algorithm specifies a method for adjusting the network parameters, such that the discrepancy between the response and the desired output is reduced. The procedure is based on a gradient descent of the parmeter vector across an error measure. Like other gradient descent techniques, BPL is not guaranteed to find the global minimum; instead, it often gets stuck in local minima, which may nevertheless result in acceptable performance by the network. As originally conceived, BPL was limited to static patterns; however there has been recent progress in processing time-varying inputs. (e.g. Jordan, 1987; Elman, 1988).

*Hebbian/Interacive Activation*

An interactive activation network (McClelland & Rumelhart, 1981) consists of a population of "neuron-like" elements, each representing an identifiable concept, in most implementations. The

nodes are connected with positive weights, if their concepts are positively associated, and with negative weights if they are negatively associated. Normally, the weights are "hard-wired"; that is, the weights are preset and do not modify. However Hebb's postulate (1949) can be realized as a differential equation for learning in such networks, as has been done in other models, such as the Brain State in the Box (BSB) model of Anderson (1977).

## A BPL approach to navigation: Method and results

The back propagation algorithm is typically applied to categorization problems, by learning an input-output mapping, where the inputs are exemplars and the outputs are categories. Jordan (1987) showed how a network could be trained to learn sequences, by partitioning the input into a represention labelling the sequence and a representation of one element of the sequence, and the output as a representation of the successor element in the sequence. Below, a similar scheme is applied to the navigation problem. The input is partitioned into a representation of the current state and a representation of the desired (goal) state. The output drives some sort of effector which changes the current state. The network architecture is shown in Figure 1. The current state and goal states are represented as patterns of activation across sets of input units. Each of the input units is connected to each of the "hidden" units (hidden, because they do not interact with the environment external to the network) in the next layer. Each of the hidden units is connected to each of the output units. The connection matrices are symbolized by the bold arrows in Figure 1.

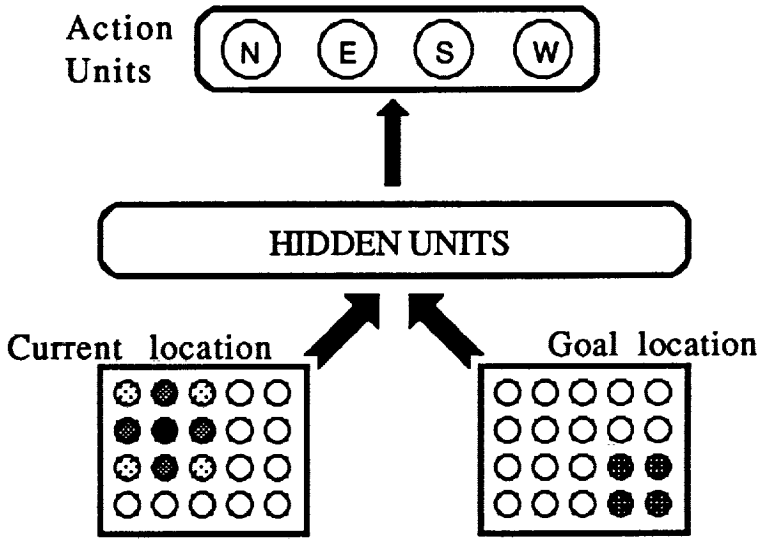


**Figure 1.** Basic route-finding network. Input units specify current and goal locations. The network generates an appropriate action as the output. The current location is updated according to the interaction of the action with the physics of the environment.

Attempts were made to train such a network on a very simple environment, consisting of a 5 by 5 grid of cells, each accessable by a single step from its 4 (N, E, S, and W) neighbors. With a small set of training data, the network was able to learn the steps in that set perfectly. However, if the set became too large, performance would suffer. The performance of the network (with the addition of a second layer of hidden units) is shown in Figure 2. For each of the 25 possible goals, a five by five matrix of arrows depicts the motion taken by the network. A circle indicates where the position is identical to the goal; thus for each matrix the circle is the target. Note that while the trend is generally correct, the network makes errors that lead to dead ends (edges) or limitless oscillations (for example, when two arrows point toward each other).

```
O^<<^   <O<<^   <^O>^   >^>O^   >>>>O
><<<<   >^<<<   >>^<<   >>>^^   >>>>^
^^<<<   ^^^<<   >^^^<   >>^^^   >>>^^
^^^<<   ^^^^<   ^^^^^   >^^^^   >>^^^
^^^^^   ^^^^^   ^^^^^   >^^^^   >>^^^

<<<<<   <<<<^   v^v<^   >>>>^   >>>>^
O<<<<   >O<<<   >>O<<   >>>O^   >>>>O
^<<<<   >^<<<   >>^<<   >>>^<   >>>><
^^<<<   ^^^<<   >^^^<   >>^^^   >>>^^
<^^<<   ^^^^^   >^^^^   >>^^^   >>^^>

<<<<<   v<vv<   v>vv^   v>vv^   >>>>^
<<<<<   vv<<<   >>v<<   >>>v<   >>>>>
O<<<<   >O<<<   >>O<<   >>>O<   >>>>O
<<<<<   ^^<<<   >>^<<   >>>^^   >>>>^
<<<<<   v^^<^   v>^^^   >>^^^   >>^^>

v<<v<   vvvv<   vvvv<   v>vvv   v>vv>
vv<<<   vvv<<   >vvv<   >>vvv   >>>vv
v<<<<   >v<<<   >>v<<   >>>v<   >>>>v
O<<<<   >O<<<   >>O<<   >>>O<   >>>>O
<<<<<   v<<<<   >>^^>   v>^v>   >>>v>

vvvv<   vvvv<   vvvvv   vvvvv   v>vvv
vvv<<   vvvv<   vvvvv   >vvvv   >>vvv
vv<<<   vvv<<   >vvv<   >>vvv   >>>vv
<<<<<   vv<<<   >>v<<   >>>v<   >>>>v
O<<<<   vO<<v   v>O>v   >>>O>   v>>vO
```

**Figure 2.** The results from a fully connected BPL network. See text for description.

It was generally found that learning was much better when the patterns were presented to the network independently of the previous pattern. In the initial investigations, a particular goal was held constant while the network was trained on a sequence of steps leading to the goal, after which the goal was shifted to a random location. However, under such a training schedule, the

goal position can remain constant too long, such that the weights from the current position representation "forget" what they learned with respect to other goals.

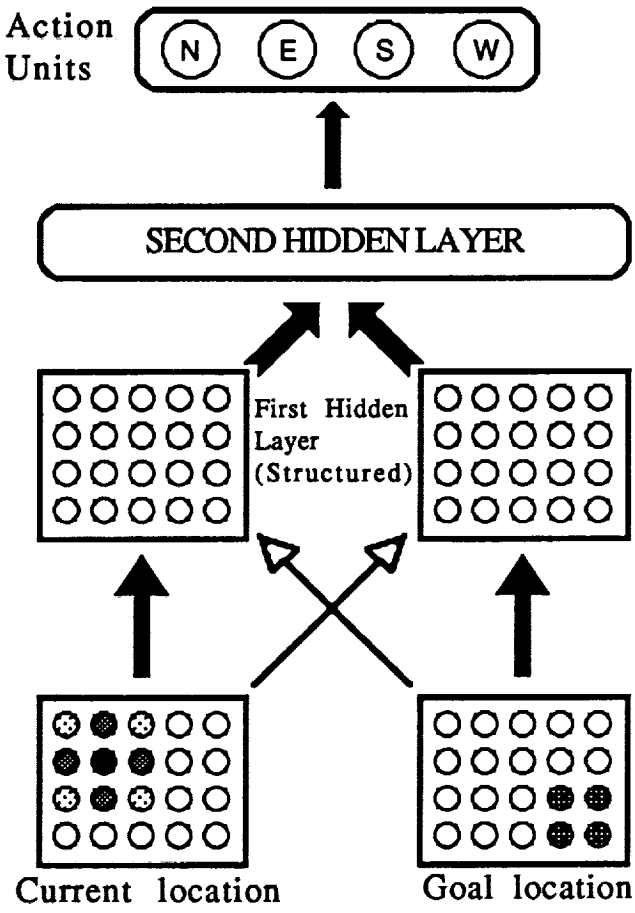


**Figure 3.** In this network, two sets of units have been inserted between the input layer and the hidden unit layer. One has a set of one-to-one connections with the GOAL input units and is fully connected to the CURRENT input units, and the other is connected in a complementary fashion. This "structured" hidden layer facilitates learning, but leads to poor generalization.

To remedy this, a more complex architecture was introduced (see Figure 3), by inserting another layer of hidden units into the previous structure between the input layer and the hidden layer. This new hidden layer consists of two sets of units. One set has one unit corresponding to each unit in the goal location input layer and receives input from that unit alone among the goal location input units; all of the units in that set receive input from *all* units in the current location input set. That is, that set in the first hidden layer receives one-to-one connections (thin arrow) from the goal location input set and is fully connected to the current location input set (thick arrow). The other hidden set has a complementary set of connections. The one-to-one

connections were *gates*, or *multiplicative connections*; that is, unless input was received from one of these connections the hidden unit did not respond.

With this architecture, the network was able to learn the 5 by 5 environment perfectly, as shown in Figure 4. However, in this case learning is quite brittle. The network is now nothing more than a lookup table, since it has specific weights corresponding to every input combination. Thus, there is no generalization of information from one learning trial to any other situation.

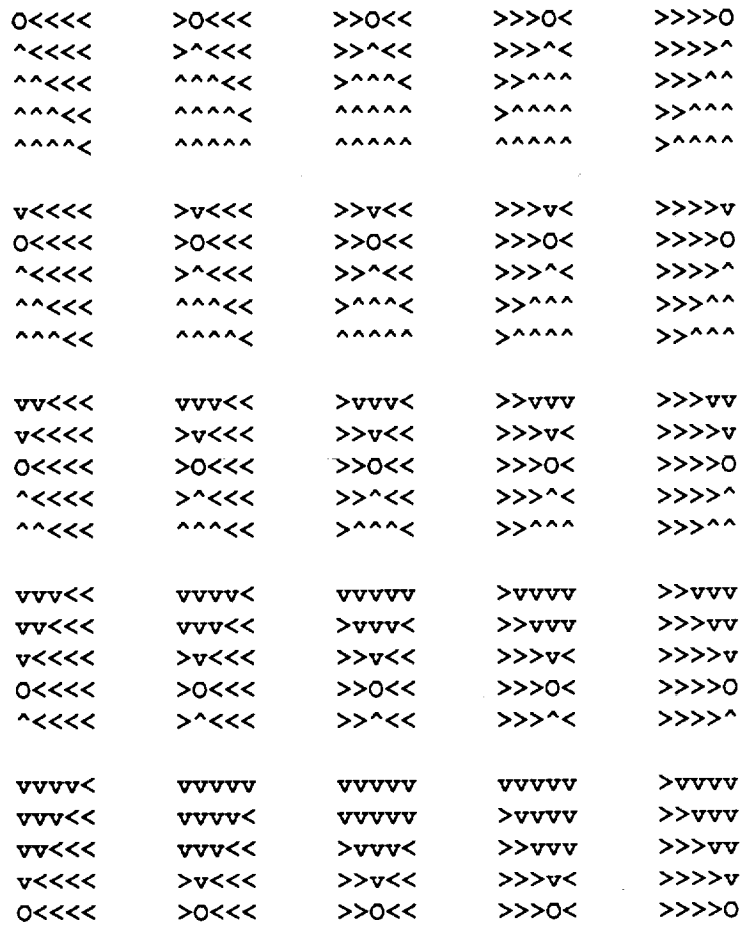


**Figure 4.** The results from a partially connected BPL network. See text for description.

## A Hebbian/Interactive activation approach to navigation: Method and results

In this network, the environment was represented similarly to the above input representation, in that there is a unit for every landmark in the environment. Again, in consideration of designing the computer simulation, a rectangular grid was used. However, the architecture was quite different. In this network, all units were connected (initially) to all other units. Simulations

using this model were performed in more complex environments; here, not every grid element was connected to its four neighbors. Instead environments, such as that shown in Figure 5, were used.

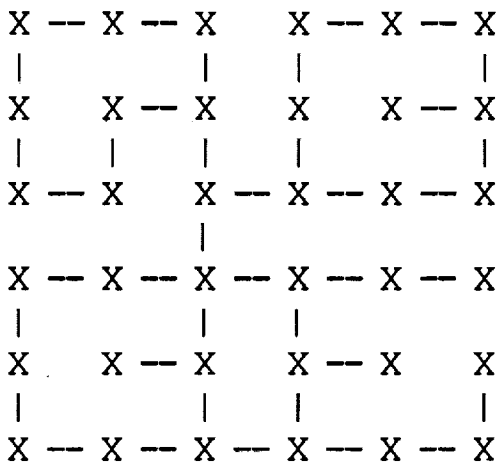

**Figure 5.** An example of a maze environment, such as was used in the HIA simulations.

Training was accomplished by an exploratory "wandering" process through the maze. Each cycle of the simulation began with taking a random step from the current position to a neighbor (neighbors in this case were defined by the links in the maze), with no backtracking unless necessary. Upon arrival at a node, the corresponding unit in the activation network was activated. Activatation in each unit would decay by a fraction $\alpha$, with each cycle of the simulation. The weights bewteen units would increase in proportion to the product of the activity in the two units, and decay by another factor $\beta$. Appropriate choice of $\alpha$ and $\beta$ led to a situation in which the weights between adjacent units were much stronger than the weights bewteen units two or more steps removed. Hence, these were all set to zero, and the neural net became isomorphic to the maze. This network was used to compute paths between arbitrary points in the maze by the following three stage procedure:

[1] The unit, *g*, corresponding to the goal is stimulated continuously at a high level, K, and activation spreads through the network via repeated iteration of matrix multiplication and simultaneous exponential decay, until the unit, *c*, corresponding to the current position is activated to a criterion level $\theta$:

$$A_j(t) = \sum_k W_{jk} A_k(t) - \eta A_j(t) \quad \text{for } j \neq g$$

$$A_g(t) = K \text{ until } A_c > \theta$$

[2] The resulting pattern of activation A is then multiplied, element by element, by the pattern of the squares of the weights connecting $c$ to the other units, $\mathbf{W_c}$.

[3] The current position is then updated, by moving to the unit with the greatest resulting product:

$$c(t+1) = \text{index j that gives a maximum for } W^2_{c(t)j} A_j$$

Steps [2] and [3] are repeated until the goal is reached.

This method was found to work quite well over a set of different mazes, usually finding the shortest path. In cases where the shortest path was not found, the result was close to the optimum.

## Discussion

While BPL was found to be inadequate for solving relatively simple problems, it should be recognized that it frequently requires considerable time and effort (and educated guesswork) to apply it successfully to a particular problem. The pattern representations must be carefully considered. Also, the network architecture and even such parameters as the learning rate and the momemtum (see Rumelhart, Hinton, and Williams, 1986 for a detailed description) can be critical in determining the success of a particular simulation. Thus, while the results reported above are discouraging, it is too soon to dismiss this approach.

The second technique, HIA, performed much better. The algorithm for finding a path is not especially novel; it is essentially equivalent to searching though a graph for the shortest path. The novelty is in the Hebbian modification technique used to construct the graph via temporally correlated activitations. This is somewhat sensitive to the parameters $\alpha$ and $\beta$. Further work is required for a general solution using this approach.

Other future plans include using more sophisticated representations for location, using multiple maps of the environment, such as maps for various types of transportation (e.g., walking vs. driving), or maps covering various scales (e.g., city maps vs. world maps). Recent work (Munro & Hirtle, 1989) has shown how the interactive activation model can account for a variety of documented psychological data, which indicates interactions between internal representations

of different maps in free recall of geographical information. Conceivably, a hybrid technique, involving both the BPL and HIA methods will be used. Such a combination would probably use HIA for the high level planning and BPL to issue the action commands to the drive mechanism.

## References


Anderson, J. A., Silverstein, J. W., Ritz, S. A., and Jones, R. S. (1977) Distinctive features, categorical perception, and probability learning: Some applications of a neural model. *Psychological Review,* **84**:413-451.

Brooks, R. (1983) Solving the find-path problem by good representation of free space. *IEEE Transactions on Systems, Man, and Cybernetics*, **SMC 13:** 190-197.

Elman, J. L. (1988) Finding structure in time. CRL TR 8801. Center for Research in Language. University of California at San Diego.

Hebb, D. O. (1949) *The Organization of Behavior*, New York: Wiley.

Jordan, M. I. (1987) Attractor dynamics and parallelism in a connectionist sequential machine. *Proceedings of the Eighth Annual Conference of the Cognitive Science Society,* 531-546.

McClelland, J. L. and Rumelhart, D. E. (1981) An interactive activation model of context effects in letter perception: Part I. An account of basic findings. *Psychological Review,* **88**:375-407.

Munro, P. and Hirtle, S. C. (1989) An interactive activation model for priming of geographical information. *Proceedings of the Eleventh Annual Conference of the Cognitive Science Society,* [Accepted for presentation]

Rumelhart, D. E., Hinton, G. E., & Williams, R. J. (1986) Learning internal representations by error propagation. In: *Parallel distributed processing: Explorations in the microstructure of cognition.* D. E. Rumelhart and J. L. McClelland, eds. Cambridge, MA: MIT

# EVALUATING SPC TECHNIQUES AND COMPUTING THE UNCERTAINTY OF FORCE CALIBRATIONS

Final Report

NASA/ASEE Summer Faculty Fellowship Program--1989

Johnson Space Center


| | |
|---|---|
| Prepared by: | Sharon E. Navard, Ph.D. |
| Academic Rank: | Assistant Professor |
| University & Department: | Virginia Commonwealth University<br>Department of Mathematical Sciences<br>Richmond, Virginia 23284-2014 |


| | |
|---|---|
| NASA/JSC | |
| Directorate: | Safety, Reliability and Quality Assurance |
| Division: | Quality Assurance and Engineering |
| Branch: | Flight Systems Quality Engineering |
| JSC Colleague: | Otho T. Dickerson |
| Date Submitted: | August 11, 1989 |
| Contract Number: | NGT 44-001-800 |

## ABSTRACT

In recent years there has been a push within NASA to use statistical techniques to improve the quality of production. Two areas where statistics is used is in establishing product and process quality control of flight hardware and in evaluating the uncertainty of calibration of instruments. The Flight Systems Quality Engineering branch is responsible for developing and assuring the quality of all flight hardware; the statistical process control methods employed are reviewed and evaluated in the first section of this report. The Measurement Standards and Calibration Laboratory performs the calibration of all instruments used on-site at JSC as well as those used by all off-site contractors. These calibrations must be performed in such a way as to be traceable to national standards maintained by the National Institute of Standards and Technology, and they must meet a four-to-one ratio of the instrument specifications to calibrating standard uncertainty. In some instances this ratio is not met, and in these cases it is desirable to compute the exact uncertainty of the calibration and determine ways of reducing it. A particular example where this problem is encountered is with a machine which does automatic calibrations of force. The second section of this report describes in detail the process of force calibration using the United Force Machine, identifies the sources of error and quantifies them when possible, and makes suggestions for improvement.

## INTRODUCTION

Historically, quality assurance at NASA has not relied heavily on statistical techniques because of the nature of the work done. The equipment developed for space flight was so specialized that very few like items were manufactured and thus one hundred percent inspection was possible. However, since the advent of the Space Transportation System with its reusable orbiter, and particularly since the 51-L accident, there has been a push within NASA to apply trend analysis techniques to maintain tighter control on the quality of flight hardware. The first section of this report covers our examination of the statistical process control (SPC) techniques which were being used by the Quality Assurance and Engineering Division and our suggestions for improvement.

A particular area of Quality Assurance which is prone to a variety of statistical problems is the Measurement Standards and Calibration Lab (MSCL). The MSCL is responsible for calibrating all of the instruments used on-site as well as those of all off-site contractors. These calibrations must be performed in such a way as to be traceable back to national standards, to control the measurement process error, and to meet a four-to-one ratio of the uncertainties of calibrated item to calibrating standard. In some cases, the laboratory has been unable to achieve the last two criteria. The second section of this report presents our efforts to calculate the uncertainty associated with calibrations done by a United Force Machine.

## STATISTICAL PROCESS CONTROL

Quality control is maintained on each of ten divisions by the use of separate control charts for each division. The data is obtained as follows. When any type of test is to be performed, a Test Preparation Sheet (TPS) must be filed. One TPS can cover an item as simple as a single screw or as complex as an entire satellite. After the test, any irregularities must be reported with a Discrepancy Report (DR). These DR's fall into three categories--Type I (damage or potential damage to hardware, persons, or both), Type II (deterioration of performance), and Type III (incidental). It is possible to have more than one DR for one TPS. Data consists of the number of TPS's and DR's per division since January 1986, with the DR's being classified as Type I, Type II, or Type III since January 1989.

The type of control chart which was being used was the p-chart with constant control limits, as described in Feigenbaum (1984), pp. 432 - 435. The p-chart is used for plotting the fraction of defective units out of n total units; constant control limits are used when the sample size n remains the same for each inspection period. This is not appropriate for this situation. The p-chart, which is based on the

normal approximation to the binomial distribution, assumes that the same number n of independent, identical units is being observed each period, and each unit is being classified as either defective or nondefective. In fact, the number of TPS's filed per month changes, the TPS's are not identical, and it is possible to get more than one defective per unit.

A more appropriate type of chart to use for this situation is the u-chart with variable control limits, as described in Duncan (1965), pp. 376 - 378. Using variable control limits will account for the fact that the number of TPS's filed per month does not remain constant. Furthermore, the u-chart, which is based on the Poisson rather than the binomial distribution, plots the fraction of defectives per (identical) unit rather than the proportion of defective (identical) units. U-charts with variable control limits are now being employed.

The fact that the TPS's are not identical means that even u-charts are not correct for this situation. The information gleaned from these charts could be improved by weighting the TPS's according to their complexity--for example, by the number of inspections actually done for each TPS. Unfortunately, this information has not been entered into the data base. The charts could also be improved by weighting the DR's according to their criticality; this type of weighting is discussed in Besterfield (1987), pp. 171 - 174. At present, not enough historical data is available to set control limits based on weighted DR's, but these weights will be implemented when sufficient data has been recorded.

## COMPUTING THE UNCERTAINTY OF FORCE CALIBRATIONS

### The Measurement Standards and Calibration Laboratory

The Measurement Standards and Calibration Laboratory is composed of three departments: Reference Standards Laboratory/Metrology Engineering, which maintains the standards; Instrument Calibration & Repair Services, which does the customer instrument calibrations and repairs, and Metrology Information & Management Services, which supplies technical and information support. The MSCL is responsible for calibrating and repairing all of the instruments used on-site at JSC, as well as all instruments used by off-site contractors. It services over eighty customers, performing an average of 18,500 calibrations and 1500 instrument repairs per year. The calibrations require and average of 2.26 manhours per item, with an average turn around time of 5.4 working days per instrument.

Each of these calibrations must be performed using a standard which is traceable back to the national standards maintained by the National Institute of Standards and Technology (NIST), formerly the National Bureau of Standards. Furthermore, a check standard should

be maintained--that is, repeated observations on an artifact, or differences in artifacts, under all environmental and operational conditions under which calibrations will be performed. The purpose of the check standard is twofold. It gives an estimate of the random error of the measurement process itself, which is a component of the uncertainty, and it also allows one to use control charts to monitor the stability of the measurement process. For more information on check standards, see Croarkin (1984). Finally, the ratio of the specifications of the customer test item to the uncertainty of the calibrating standard must be at least four-to-one. For example, if the specification of an instrument is accuracy to within 1%, the uncertainty of the standard used to calibrate it cannot exceed 0.25%.

The MSCL uses standards calibrated by the NIST to assure traceability. However, for many of the calibrations done, no check standard is maintained, often due to time and financial constraints. When no check standard is available, it becomes impossible to use control charts to monitor the measurement process stability. It is also not possible to estimate the random error and, therefore, the uncertainty of the calibrated item. In cases where it is impossible to compute an exact value, the uncertainty of a calibrated item is arbitrarily assigned a value four times the uncertainty of the standard used to calibrate it. However, when this is done, in some instances the MSCL's standards no longer meet the four-to-one ratio. Thus it is desirable to have a means of computing the exact uncertainty.

## Calibration of Force Measuring Devices

Considered here are two types of devices which can be used to measure force: proving rings and load cells. A proving ring is a metal ring equipped with a micrometer which measures the actual deflection of the ring when a force, either tension or compression, is applied. A load cell is a device which outputs an electric current when a force is applied. The particular situation examined here is the use of a United Force Machine to do automatic calibrations of customers' load cells.

In order to maintain traceability to national standards, all calibrations begin with a primary standard which was calibrated by the NIST. For force calibrations, the primary standard is a proving ring which the NIST calibrates using dead weights of known mass. Thirty data points are used--two repetitions each of fifteen known loads or three repetitions of ten known loads--and ordinary least-squares is used to fit the deflection (D) as a quadratic function of the load (L):

$$D = A + BL + CL^2.$$

Ordinary least-squares is appropriate for this situation because it can be assumed that the exact values of the load are known without error.

These calibrations are done at 23° C. The uncertainty associated with the calibration is taken to be 2.4s, where s is the estimate of the standard deviation of the residuals, $\sigma_\varepsilon 2$.

The laboratory does not use the primary standards to calibrate customers' instruments. Rather, they are used to calibrate the laboratory's secondary standards, which are then used for customer calibrations. For the MSCL force calibrations, the secondary standard is a load cell. This standard load cell is calibrated by the United Force Machine, using the primary standard to determine the values of the loads applied. Because the ambient temperature may not be 23° C, a temperature correction must be made to the deflection values of the proving ring. The loads (L) as measured by the proving ring and corresponding responses (R) of the load cell (in MV/V) are used to obtain the least-squares fit

$$L = A + BR + CR^2.$$

Least-squares is not entirely appropriate at this step because the responses as well as the loads are measured with error. The uncertainty of this calibration is taken to be four times the uncertainty reported by the NIST for the proving ring.

Once the standard load cell is calibrated, it is then used to determine the values of the loads to calibrate customers' load cells. The process is similar to the previous step except that no temperature adjustment is made, and the reported calibration equation is linear, that is,

$$L = A + BR.$$

The residuals, or deviations of each data point from the line, are computed, and if none of the residuals exceeds the specified accuracy of the load cell, it is said to be calibrated. However, if the specified accuracy of the calibrated load cell is not a least four times as great as the uncertainty of the standard load cell, the calibration does not meet the ratio. When this occurs, the MSCL is required to give a full report of the calibration procedure to the customer and inform him that the ratio was not met.

Because of the increasing precision of customer load cells, it is becoming more frequent for the MSCL to do force calibrations which do not meet the four-to-one ratio. For this reason, it is of interest to compute the actual uncertainty associated with the standard load cell, rather than using four times the uncertainty of the proving ring. Unfortunately, it will be impossible to compute the random error component of the uncertainty because at present no check standard is being maintained on the United Force Machine. However, other sources of error can be identified and possibly reduced. The following

sections describe in more detail the sources of systematic error inherent in the calibration of the standard load cell.

Inverse Regression versus Classical Calibration

The first problem encountered in using the primary standard to calibrate the standard load cell is obtaining values of the load from the deflection of the proving ring. The equation supplied by the NIST gives the deflection of the ring as a function of the load, yet the ring must be used to obtain the values of the load as a function of the deflection. This is known as the calibration problem, and there are two approaches to solving it.

The classical method of calibration is to use the given equation, $D = A + BL + CL^2$, and simply solve it for L as a function of D. Since it is a quadratic equation, there will be two solutions; the correct one is the one which lies in the calibration range of the proving ring. Denote the classical estimator of load by $L_C$. Then

$$L_C = [-B + \sqrt{B^2 - 4C(A - D)}] / 2C.$$

The standard error of the classical estimator of L is different from $\sigma_\varepsilon^2$, the quantity currently being used by the MSCL; it will, in fact, be larger because the least-squares equation is being used in the opposite direction than the one in which the errors were minimized. Not much work has been done on determining estimates of $\sigma_C$, the standard error of the classical calibration estimator, when the response is quadratic.

The second approach to the calibration problem, known as inverse regression, is to take the original data points supplied by the NIST and use least-squares to fit the load as a quadratic function of the deflection. Denote the inverse regression estimator of load by $L_{IR}$. Then

$$L_{IR} = \alpha + \beta D + \gamma D^2,$$

where $\alpha$, $\beta$, and $\gamma$ are the parameter estimates obtained using ordinary least-squares. As in the case of the classical estimator, little work has been done in obtaining estimates of $\sigma_{IR}$, the standard error of the inverse regression estimator, when the response is quadratic. It will not be simply the standard error of the residuals because one of the major assumptions of least-squares has been violated: it is the dependent variable, rather than the independent variable, which has been measured without error. Inverse regression is the technique currently being employed by the MSCL.

A serious question at this point is to ask which of the two methods is "better." This is a question which has been addressed

extensively in the literature, although generally only a linear response is considered. The first author to address the issue was Eisenhart (1939), who concluded that the classical method is the only reasonable one to use for two reasons. First, the classical method minimizes the actual observed errors, while the inverse regression method minimizes the "errors" in a variable that was measured without error. Second, the classical method is asymptotically unbiased, whereas the inverse regression estimator is asymptotically biased.

This seemed to be the final word on the subject until Krutchkoff (1967) reopened the question with a simulation paper which indicated that the inverse regression estimator has uniformly smaller mean squared error (MSE) than the classical estimator, and is therefore superior based on that criterion. In an ensuing letter, Krutchkoff (1968) pointed out that the classical estimator will in fact have infinite MSE if the linear slope term (or in our case, the quadratic term, C) is allowed to be zero, and that truncating the estimator will introduce a bias. Then, in Krutchkoff (1969), he demonstrated that as the number of observations at each L value increases, the MSE of the classical estimator decreases faster than that of the inverse estimator and can in fact get smaller. The classical estimator also gave a smaller MSE when there was an ignored quadratic term.

At this point more authors began to address the question. Williams (1969) demonstrated that not only the classical estimator, but *any* unbiased estimator will have infinite MSE and therefore MSE is not a good criterion to use to compare the estimators. Berkson (1969) claimed that classical estimator is consistent, whereas the inverse estimator is inconsistent, and the inverse estimator should thus never be used. Martinelle (1970) derived analytic results which basically agreed with Krutchkoff's simulation results. Halperin (1970) compared the two estimators using Pitman closeness, concluding that the classical estimator is generally better. Hoadley (1970) approached the problem from a Bayesian point of view and demonstrated that the inverse estimator is actually Bayes with respect to a particularly informative prior. For additional information on the calibration problem, consult the bibliography.

Further research is required to determine which of the two methods is better for use in force calibrations. Currently, inverse regression is being used. Table 1. demonstrates the differences in the estimates of load obtained using the two methods for determining compression loads for the 100,000 pound proving ring. It can be seen that the percent difference in the two estimators is not very large, especially for the larger loads.

TABLE 1.- ESTIMATES OF LOAD USING THE CLASSICAL AND INVERSE REGRESSION ESTIMATORS

| | Load | |
|---|---|---|
| Deflection | Classical Method | Inverse Regression |
| 0 | -10.695 | 0.624 |
| 100 | 9919.771 | 9926.369 |
| 200 | 19826.557 | 19829.628 |
| 300 | 29709.660 | 29710.400 |
| 400 | 39569.465 | 39568.686 |
| 500 | 49405.969 | 49404.485 |
| 600 | 59219.176 | 59217.798 |
| 700 | 69009.461 | 69008.624 |
| 800 | 78777.219 | 78776.963 |
| 900 | 88522.055 | 88522.816 |
| 1000 | 98244.352 | 98246.182 |

Propagation of Temperature Errors

Another problem encountered when using the primary standard to calibrate the standard load cell is the effect of differences in temperature. The proving ring was calibrated at 23° C, and if it is used at a different temperature, then the deflection readings must be adjusted according to the equation

$$d_{23} = d_t[1 + k(t - 23)],$$

where $d_{23}$ is the deflection at 23° C, t is the current temperature, $d_t$ is the observed deflection, and k is the expansion coefficient of the ring. For the proving rings used by the MSCL, k = -.00027.

Unfortunately, the thermometer being used to determine the temperature of the proving ring is only accurate to within ± .95° F ≅ .53 ° C. For a temperature error of .53° C, the percent error in the deflection, denoted $\%_D$, is computed as

$$\%_D = |\text{Actual } d_{23} - \text{Computed } d_{23}| \ / \ \text{Actual } d_{23},$$

and is approximately .00015, or .015% for temperatures near 23° C.

To determine the effect of this deflection error on the values of the load, the error must be propagated through the expression

$$L = F(D) = \alpha + \beta D + \gamma D^2.$$

The general propagation of errors formula as given in Ku (1966) is

$$\text{Var}(L) = [dF/dD]^2 \, \text{Var}(D).$$

An estimate of Var(D) is required in order to use this formula. One may be obtained by noting that the percent error in deflection is the ratio of the error in the deflection to the deflection; but the error in deflection can be expressed as the uncertainty, which is generally a multiple r of the standard deviation of deflection, $\sigma_D$. (The NIST uses r = 2.4.) Thus

$$\%_D = (\text{error in } D)/D \cong \text{uncertainty}/D \cong r\sigma_D/D,$$

and

$$\text{Var}(D) \cong [D\%_D/r]^2.$$

Using this estimate of Var(D) in the propagation of error formula yields an estimate of the standard deviation of load values due only to the .53° C error in temperature, $\sigma_{L(t)}$:

$$\sigma_{L(t)} \cong D\%_D[\beta + 2\gamma D]/r.$$

Thus the percent uncertainty of load values due to this error in temperature, $\%_{L(t)}$, is

$$\%_{L(t)} \cong r\sigma_{L(t)}/(\text{maximum load}) \times 100\%.$$

For the 1000 and 100,000 pound proving rings, this error ranged from .015% to .017%. These values are approximately equal to the percent uncertainties associated with the calibration of the proving rings themselves. Therefore the error due to inaccuracy of the temperature readings is a significant contributor to the total uncertainty of the standard load cell.

The Errors-in-Variables Model

When the proving ring is used to determine values of the load in order to calibrate the standard load cell, there is error associated with these load values as well as with the response values of the load cell. Therefore, when the MSCL uses least-squares to fit the equation $L = A + BR + CR^2$, this is not an example of inverse regression, but is rather what is known as an errors-in-variables (EV) model. EV models result when both of the variables are measured with error, and in this situation even determining consistent estimators of the regression parameters when one of the error variances or their ratio is unknown

is an open problem. See Gunst and Lakshminarayanan (1984) for more details on the EV model.

More research is required in order to determine the best estimates of the parameters of the EV model and their associated standard errors. Also, since the MSCL is currently using least-squares to estimate the regression parameters, an estimate of the standard error of load estimates thus obtained, $\sigma_{EV}$, is also a quantity which needs to be determined in order to compute the uncertainty of the standard load cell.

To compute the uncertainty associated with the standard load cell, it is necessary to combine the systematic and random errors. While it is still a source of contention as to how exactly this should be done, the general consensus seems to be that independent systematic errors can be added in quadrature, while correlated systematic errors and random errors should be added linearly. Thus the uncertainty of the standard load cell, $\text{uncertainty}_{SLC}$, can be estimated as

$$\text{uncertainty}_{SLC} = 2.4[\sqrt{\sigma_{IR}^2 + \sigma_{L(t)}^2} + \sigma_{EV} + \sigma_{RE}],$$

where $\sigma_{RE}$ is the random error of the measurement process, as determined by the check standard.

### Calibrating the Customer's Load Cell

The problems encountered when calibrating customers' load cells are similar to those of calibrating the standard load cell. Once again, there is error in the values of the load determined by the standard load cell, as well as in the response of the customer's load cell, so this is also a case of an EV model. There is also an uncompensated systematic error due to a drift in the response of load cells at different temperatures. Thus the uncertainty associated with the calibration will be a sum of the uncertainties of the standard load cell, the temperature drift, the EV model, and the random error of the measurement process.

## DISCUSSION

### Improving Use of the United Force Machine

Under current practices, a customer's load cell can be properly calibrated only if its specifications are more than sixteen times the uncertainty of the proving ring used to calibrate it. This is because the MSCL takes the uncertainty of the standard load cell to be four times that of the proving ring calibrated by the NIST, and the uncertainty of the customer's load cell to be four times that of the standard load cell.

If the actual uncertainty were computed, it may or may not be smaller. However, it will not be possible to compute the uncertainty until some of its component values are determined.

The most important step for the MSCL to take at this time is to institute a check standard for the United Force Machine. This will supply an estimate of the random error of the measurement process, which is actually added twice into the overall uncertainty. It will also enable the stability of the measurement process itself to be monitored through the use of control charts, thus allowing a faster identification of any problems with the process which may arise.

The uncertainty of the calibrations can be reduced by obtaining more accurate measurements of the temperature of the proving rings during calibration of the standard load cells. When considering more precise measurements of the temperature, however, one is faced with the problem of the temperature varying on different parts of the ring, due to stress on the ring or changes in the ambient temperature. This problem could be reduced if the proving rings could be stored and used in a temperature-controlled environment. Using proving rings with a smaller expansion coefficient would also reduce the error due to inaccurate temperature readings.

The systematic error due to the temperature drift of the load cells could be reduced by obtaining an accurate determination of the drift from the manufacturer, if such is available, and incorporating the temperature correction into the software. If this is done, the error in temperature readings will become a factor, but this error should be smaller than the full drift error.

## Applications to Other Areas of the MSCL

The discussion here has centered on automatic force calibrations using the United Force Machine. However, some of the same principles can be applied to other calibration processes. In particular, the use of check standards should be made on as many of the processes as possible, especially those which are subject to large variations and those where mistakes are most likely to be made. Not only will this provide an estimate of the random error, but it will also facilitate the identification of operator errors, changes in the values of the reference standards, effects due to unusual environmental fluctuations, etc.

A tighter control on the environment is also something which should be sought. Many of the calibrations done in the MSCL are affected by changes in temperature, pressure, humidity, etc. In some cases these effects are compensated for, but even in these instances errors in the readings can have significant effects on the final results. The more stable the environment is, the more accurate the calibrations will be.

## REFERENCES


Berkson, Joseph: Estimation of a Linear Function for a Calibration Line; Consideration of a Recent Proposal. *Technometrics*, vol. 11, no. 4, Nov. 1969, pp. 649-660.

Besterfield, Dale H.: *Quality Control*, 2nd Ed. Prentice-Hall, 1987.

Croarkin, Carroll: Measurement Assurance Programs Part II: Development and Implementation. National Bureau of Standards Special Publication 676-II, Apr. 1984.

Duncan, Acheson J.: *Quality Control and Industrial Statistics*, 3rd Ed. Richard D. Irwin, Inc., 1965.

Eisenhart, C.: The interpretation of Certain Regression Methods and Their Use in Biological and Industrial Research. *Annals of Mathematical Statistics*, vol. 10, no. 2, June 1939, pp. 162-186.

Feigenbaum, Armand V.: *Total Quality Control*, 3rd Ed. McGraw-Hill, Inc., 1984.

Gunst, Richard F., and Mani Y. Lakshminarayanan: Estimation of Parameters in Linear Structural Relationships: Sensitivity to the Choice of the Ratio of Error Variances. *Biometrika*, vol. 71, 1984, pp. 569-573.

Halperin, Max: On Inverse Estimation in Linear Regression. *Technometrics*, vol. 12, no. 4, Nov. 1970, pp. 727-736.

Hoadley, Bruce: A Bayesian Look at Inverse Linear Regression. *Journal of the American Statistical Association*, vol. 12, no. 4, Nov. 1970, pp. 356-369.

Krutchkoff, R. G.: Classical and Inverse Regression Methods of Calibration. *Technometrics*, vol. 9, no. 3, Aug. 1967, pp. 425-439.

Krutchkoff, R. G.: Letter to the Editor. *Technometrics*, vol. 10, no. 2, May 1968, pp. 430-431.

Krutchkoff, R. G.: Classical and Inverse Regression Methods of Calibration in Extrapolation. *Technometrics*, vol. 11, no. 3, Aug. 1969, pp. 605-608.

Ku, Harry H.: Notes on the Use of Propagation of Error Formulas. *Journal of Research of the National Bureau of Standards--C. Engineering and Instrumentation*, vol. 70C, no. 4, Oct. - Dec. 1966.

Martinelle, Sten: On the Choice of Regression in Linear Calibration. Comments on a paper by R. G. Krutchkoff. *Technometrics*, vol. 12, no. 1, Feb 1970, pp. 157-161.

Williams, E. J.: A Note on Regression Methods in Calibration. *Technometrics*, vol. 11, no. 1, Feb. 1969, pp. 189-192.

## BIBLIOGRAPHY


Brown, G. H.: An Optimization Criterion for Linear Inverse Estimation. *Technometrics*, vol. 21, no. 4, Nov. 1979, pp. 575-579.

Hunter, William G., and Lamboy, Warren F.: A Bayesian Analysis of the Linear Calibration Problem. *Technometrics*, vol. 23, no. 4, Nov. 1981, pp. 323-328.

Kalotay, A. J.: Structural Solution to the Linear Calibration Problem. *Technometrics*, vol. 13, no. 4, Nov. 1971, pp. 761-769.

Krutchkoff, R. G.: Letter to the Editor. *Technometrics*, vol. 12, no. 2, May 1970, pp. 433-434.

Ku, Harry H., ed.: *Precision Measurement and Calibration--Selected Papers on Statistical Concepts and Procedures.* National Bureau of Standards Special Publication 300, vol. 1, Feb. 1969.

McKeon, James John: Statistical Calibration Theory. Ph. D. Thesis, Old Dominion University, 1985.

Minder, Ch. E., and Whitney, J. B.: A Likelihood Analysis of the Linear Calibration Problem. *Technometrics*, vol. 17, no. 24, Nov. 1975, pp. 463-471.

Perng, S. K., and Tong, Y. L.: Optimal Allocation of Observations in Inverse Linear Regression. *Annals of Statistics*, vol. 5, no.1, 1977, pp. 191-196.

Scheffe, Henry: A Statistical Theory of Calibration. *Annals of Statistics*, vol. 1, no.1, 1973, pp. 1-37.

Shukla, G. K.: On the Problem of Calibration. *Technometrics*, vol. 14, no. 3, Aug. 1972, pp. 547-553.

# CONSERVATION OF BODY CALCIUM BY INCREASED DIETARY INTAKE OF POTASSIUM: A POTENTIAL MEASURE TO REDUCE THE OSTEOPOROSIS PROCESS DURING PROLONGED EXPOSURE TO MICROGRAVITY

Final Report

NASA/ASEE Summer Faculty Fellowship Program--1989

Johnson Space Center


| | |
|---|---|
| Prepared By: | Bohdan R. Nechay, D.V.M. |
| Academic Rank: | Professor |
| University & Department: | University of Texas Medical Branch<br>Department of Pharmacology & Toxicology<br>Galveston, Texas 77550 |
| NASA/JSC | |
| Directorate:<br>Division: | Space and Life Sciences<br>Medical Sciences |
| Branch: | Biomedical Laboratories |
| JSC Colleague: | Nitza M. Cintron, Ph.D. |
| Date Submitted: | August 28, 1989 |
| Contract Number: | NGT 44-001-800 |




C-2

## ABSTRACT

During the 1988 NASA Summer Faculty Fellowship Program, I proposed that the loss of skeletal calcium upon prolonged exposure to microgravity could be explained, in part, by a renal maladjustment characterized by an increased urinary excretion of calcium. We theorized that because the conservation of body fluids and electrolytes depends upon the energy of adenosine triphosphate and enzymes that control the use of its energy for renal ion transport, an induction of renal sodium and potassium-dependent adenosine triphosphatase (Na + K ATPase) by oral loading with potassium would increase the reabsorption of sodium directly and that of calcium indirectly, leading to improved hydration and to reduced calcium loss.

Preliminary studies showed the following. Rats drinking water containing 0.2 M potassium chloride for six to 13 days excreted in urine 22 $\mu$Eq of calcium and 135 $\mu$Eq of sodium per 100 grams of body weight per day. The corresponding values for control rats drinking tap water were 43 $\mu$Eq and 269 $\mu$Eq respectively. Renal Na + K ATPase activity in potassium loaded rats was higher than in controls. Thus, oral potassium loading resulted in increased Na + K ATPase activity and diminished urinary excretion of calcium and of sodium as predicted by our hypothesis.

An extension of these studies to humans has the potential of resulting in development of harmless, non-invasive, drug-free, convenient measures to reduce bone loss and other electrolyte and fluid problems in space travelers exposed to prolonged periods of microgravity.

## INTRODUCTION

During Skylab flights, astronauts experienced an increased excretion of body calcium in urine (1). Last year, we proposed that the loss of calcium could be attributed to the reduced renal tubular reabsorption of the mineral (2). This resulted in urinary excretion of 0.29 gm of calcium per day during flight, up from 0.16 gm per day control rate. The net total calcium loss attributable to the kidney during the Skylab flights of 60 to 85 days equaled 7.8 gm to 11.05 gm respectively. The crewmen had an adequate average dietary intake of 0.73 gm calcium per day but went into negative calcium balance because fecal calcium excretion also increased (1,3). The calcium-wasting by the kidney is further demonstrated by the lack of renal conservation of calcium in the face of the increased fecal calcium losses.

To place the magnitude of the calcium loss in perspective, it is essential to realize that all extracellular body fluids contain only about 1 gm of calcium, cells contain 5 gm, and bone contains a total of 1,200 gm (4). Thus, any sizeable calcium loss, like that which occurred during the Skylab flights, must come eventually from bone. Calcium homeostasis involves continuous mineral turnover in bone, absorption from food and reabsorption by the kidney. Overall calcium metabolism is primarily set to maintain a constant calcium concentration in extracellular fluid, even at the expense of bone density. Absorption from the gut is controlled by vitamin D, bone resorption and renal reabsorption are promoted by parathyroid hormone and inhibited by calcitonin (4,5).

Based on the above considerations, options for prevention of calcium loss are: 1) increase intake and/or decrease losses of calcium from the gut; 2) decrease calcium loss from bone; and 3) decrease calcium loss from the kidney. Relative to option 1, stable and adequate calcium intake during Skylab flights did not prevent negative calcium balance (1,3). In fact, there was an increased amount of calcium lost in feces (3). Enhancement of calcium absorption from food deserves further study.

Decreased egress of calcium from bone appears to be under most intensive investigation at present as a solution to bone demineralization during space flight. In our opinion, producing a halt to bone resorption without increased absorption from the gut and reduced loss via the kidneys would lead to a reduced intracellular and extracellular calcium concentration. Since calcium is required for muscular contraction and nerve conduction, inadequate calcium levels may lead to increased weakness and atrophy, already a problem during space flight (6). Diminished supply of calcium to the heart could lead to impairment of cardiac output and to irregularities of heart rhythm (arrhythmias) that could result in sudden death.

Relative to the third option, reversal of the acquired defect in tubular reabsorption of calcium would be a desirable solution to the excessive calcium loss during space flight. Because renal calcium reabsorption is in part dependent upon the transport of sodium, we propose that an induction of renal sodium and potassium-dependent adenosinetriphosphatase (Na + K ATPase), an enzyme system that allows the use of adenosine triphosphate (ATP) for ion transport (7), would improve tubular reabsorption of sodium directly and that of calcium secondarily. In addition to calcium conservation, this maneuver would improve reabsorption of sodium, chloride and water, all of which are also excessively lost during space flight. Practical methods for induction of renal Na + K ATPase deserve further investigation in an attempt to prevent osteoporosis and fluid and electrolyte loss associated with space travel. The magnitude of renal-related calcium losses, coupled with the fact that Skylab astronauts had adequate calcium intake and excessive fecal calcium losses, make it wise to consider ways in which renal losses of calcium can be curtailed.

## METHODS

Chronic dietary administration of potassium salts appears to be a harmless method of inducing renal Na + K ATPase activity (8,9). After several trials, we devised the following protocol to study the effects of oral potassium loading on urinary calcium excretion in rats. Sprague-Dawley female

rats, 200 - 250 grams, were divided into four groups. Each group of two rats was kept in a separate holding cage. Food, Purina's Formulate 5008, was offered ad libitum. Drinking fluids were as follows: Group 1: 0.2 M potassium chloride; group 2: 0.3 M potassium chloride; group 3: 0.2 M sodium chloride; group 4: tap water. After six days of this regimen, one rat from each group was placed in an individual Nalge Metabolism Cage (Fisher Scientific) for a 24 hour urine collection. No food or fluid was given on that day. Urinary calcium, potassium and sodium were measured by atomic absorption spectrophotometry. The experiment was repeated seven days later with the remaining rats. Promptly after each experiment, kidneys were removed under pentobarbital (60 mg/kg i.p.) anesthesia for determination of Na + K ATPase activity using methods described previously (10). Briefly, whole kidney tissue homogenates were prepared 1:10 in a sucrose solution containing Tris (hydroxymethyl)-aminomethane, disodium edtate, and sodium deoxycholate. Enzyme activity was measured by the rate of release of inorganic phosphate (Pi) from exogenous ATP during 20 minutes of incubation at 37 degrees C. The incubation mixture contained the enzyme source (subdiluted kidney homogenate, 100 mM NaCl, 3 mM MgCl2, 3 mM ATP, and 40 mM HEPES (N-2-hydroxyethylpiperazine-N'-2-ethanesulphonic acid) buffer at pH 7.4. Enzyme activity inhibited by $2 \times 10^{-3}$ Mouabain represented Na + K ATPase activity.

## RESULTS

These preliminary results (Table) are based on data from two rats per group. The outstanding observation is that six and 13 days of potassium loading via drinking water resulted in about one half as much urinary calcium excretion than that of control animals loaded with sodium or tap water. Potassium-induced calcium conservation was accompanied by selectively higher renal Na + K ATPase specific activity, ie., sensitive to ouabain, than that found in control groups. Ouabain-insensitive ATPase specific activity was essentially the same in all groups.

## DISCUSSION

There is sufficient knowledge of renal handling of calcium (4) to formulate rational experiments aimed at reducing urinary excretion of calcium when and if indicated. Briefly, the protein-unbound portion of blood calcium is filtered through the glomeruli. Normally, over 98% of this calcium is reabsorbed by the renal tubules and the remaining fraction is excreted in the urine. To some degree, the tubular reabsorption of calcium is dependent upon the reabsorption of sodium which, to a large extent, utilizes the ubiquitous Na and K pump driven by the Na + K ATPase system. Accordingly, inhibition of renal Na + K ATPase by digitalis glycosides results not only in natriuresis but also in increased excretion of calcium (7). We have modified the method of Epstein's group (8,9) to induce renal Na + K ATPase activity by an increased dietary offering of potassium to rats. Predictably, our experiments resulted in renal conservation of sodium and calcium.

The same phenomena are probably operational in humans. Pak's data (11) in patients treated for months with potassium citrate for nephrolithiasis suggest renal conservation of calcium, but the study was not specifically designed to bring out this feature.

In Skylab astronauts, urinary potassium excretion, and thus dietary intake, was on the order of three grams (1) or even 1.5 grams (3). These amounts correspond to the average dietary potassium intake of the general population in Western countries.

Louis Tobian, a pioneer in investigating the link between low potassium intake and high blood pressure diseases, suggested that people increase their average daily intake of potassium to six grams (12). We suggest that a similar regimen would be reflected in renal conservation of calcium as well.

Renal calcium conservation may be relevant to the prevention of osteoporosis. There is a growing awareness that osteoporosis has a dietary component whereby high salt intake contributes to the loss of calcium (13, 14). We would like to expand upon these emerging views by proposing that osteoporosis is exacerbated by low dietary intake of potassium.

## REFERENCES


1. Leach, C.S. & Rambaut, P.C. Biomedical responses of the skylab crewmen: an overview. In Biomedical Results from Skylab, R.S. Johnston and L.F. Dietlein (Eds.), National Aeronautics and Space Administration, Washington, D.C., pp. 204-216, 1977.

2. Nechay, B.R. Maladjustment of Kidneys to microgratiry: Design of measures to reduce the loss of calcium. Final Report, NASA/ASEE Summer Faculty Fellowship Program, Johnson Space Center Library, Houston Texas, 1988.

3. Whedon, G.D., Lutwak, L., Rambaut, P.C., Whittle, M.W., Smith, M.C., Reid, J., Leach, C., Stadler, D.R., & Sanford, D.D. Mineral and nitrogen metabolic studies, experiment M071. In Biomedical Results from Skylab, R.S. Johnston and L.F. Dietlein (Eds.), National Aeronautics and Space Administration, Washington, D.C., pp. 164-174, 1977.

4. Sutton, R.A.L. & Dirks, J.H. Calcium and magnesium: Renal handling and disorders of metabolism. In The Kidney, Vol. 1, B.M. Brenner and F.C. Rector, Jr. (Eds.), W. B. Saunders Co., Philadelphia, Pa., pp. 551-618, 1986.

5. Coburn, J.W. & Slatopolsky, E. Vitamin D, parathyroid hormone and renal osteodystrophy. In The Kidney, Vol. 2, B.M. Brenner and F.C. Rector, Jr. (Eds.), W. B. Saunders Co., Philadelphia, Pa., pp. 1657-1729, 1986.

6. Thornton, W.E. & Rummel, J.A. Muscular deconditioning and its prevention in space flight. In Biomedical Results from Skylab, R.S. Johnston and L.F. Dietlein (Eds.), National Aeronautics and Space Administration, Washington, D.C., pp. 191-197, 1977.

7. Nechay, B.R. Biochemical basis of diuretic action. J. Clin. Pharmacol. 17:626-641, 1977.

8. Silva, P., Hayslett, J.P., & Epstein, F.H. The role of Na-K-activated adenosine triphosphatase in potassium adaptation. Stimulation of enzymatic activity by potassium loading. J. Clin. Invest. 52:2665-2671, 1973.

9. Finkelstein, F.O. & Hayslett, J. P. Role of medullary Na-K-ATPase in renal potassium adaptation. Am. J. Physiol. 229:524-528, 1975.

10. Nechay, B.R. & Contreras, R.R. In vivo effect of ethacrynic acid on renal adenosine triphosphatase in dog and rat. J. Pharmacol. Exp. Ther. 183:127-126, 1972.

11. Pak, C.Y.C. & Fuller, C. Idiopathic hypocitraturic calcium-oxalate nephrolithiasis successfully treated with potassium citrate. Ann. Int. Med. 104:33-37, 1986.

12. Dienhart, P. The Cave Man Diet, Update, Univ. of Minn. 12 (9):4, 1985.

13. Goldfarb, S. Dietary factors in the causation of negative calcium balance in osteoporosis. In A CPC Series: Cases in Metabolic Bone Disease, The Rogosin Institute at the New York Hospital-Cornell Medical Center, 3 (4), 1989.

14. Langford, H.G. The passive role of calcium in hypertension: A position statement as of August 20, 1985. Can. J. Physiol. Pharmacol. 64:808-811, 1986.

TABLE

Effects of potassium chloride or sodium chloride added to drinking water on urinary calcium, potassium and sodium excretion and renal Na + K ATPase activity in rats.

| GROUP 1 | | GROUP 2 | | GROUP 3 | | GROUP 4 | | GROUP 1 | GROUP 2 | GROUP 3 | GROUP 4 |
|---|---|---|---|---|---|---|---|---|---|---|---|
| Salts added to drinking water, M. | | | | | | | | | | | |
| KCl 0.2 | | KCl 0.3 | | NaCl 0.2 | | 0 | | KCl 0.2 | KCl 0.3 | NaCl 0.2 | 0 |
| Rat #1 | Rat #2 | Rat #1 | Rat #2 | Rat #1 | Rat #2 | Rat #1 | Rat #2 | Mean, Rats #1 & #2 | | | |
| (Rats #1 treated for 6 days, Rats #2 treated for 13 days) | | | | | | | | | | | |
| Mean daily fluid consumption, ml/100 g body weight | | | | | | | | | | | |
| 15.9 | 13.7 | 24.0 | 15.4 | 29.3 | 27.0 | 11.1 | 9.7 | 14.8 | 19.7 | 28.2 | 10.4 |
| No food or fluids on day of 24 hour urine collection (day 7 for Rats #1, day 14 for Rats #2) | | | | | | | | | | | |
| Urine flow, ml/100 g/24 h | | | | | | | | | | | |
| 1.7 | 1.6 | 3.0 | 2.0 | 4.1 | 3.0 | 4.5 | 2.5 | 1.7 | 2.5 | 3.6 | 3.5 |
| Calcium, µEq/100 g/24 h | | | | | | | | | | | |
| 22 | 22 | 30 | 18 | 44 | 34 | 50 | 36 | 22 | 24 | 39 | 43 |
| Potassium, µEq/100 g/24 h | | | | | | | | | | | |
| 458 | 425 | 792 | 556 | 420 | 422 | 456 | 416 | 442 | 674 | 421 | 436 |
| Sodium, µEq/100 g/24 h | | | | | | | | | | | |
| 137 | 133 | 179 | 144 | 416 | 382 | 343 | 194 | 135 | 162 | 399 | 262 |
| Na + K ATPase Activity in Whole Kidney Homogenates µmol Pi/mg protein/hr | | | | | | | | | | | |
| | | | | | | | | 10 | 12 | 7 | 9 |
| Ouabain-insensitive ATPase activity µmol Pi/mg protein/hr | | | | | | | | | | | |
| | | | | | | | | 14 | 14 | 13 | 14 |

# A COMPARISON OF SELECT IMAGE-COMPRESSION ALGORITHMS FOR AN ELECTRONIC STILL CAMERA

Final Report

NASA/ASEE Summer Faculty Fellowship Program -- 1989

Johnson Space Center


| | |
|---|---|
| Prepared By: | Rosalee Nerheim, Ph.D. |
| Academic Rank: | Assistant Professor |
| University & Department | DePaul University<br>Department of Computer Science<br>243 S. Wabash<br>Chicago, IL 60604 |
| NASA/JSC | |
| Directorate: | Space and Life Sciences |
| Division: | Man-Systems |
| Branch: | Flight Systems |
| JSC Colleague: | H. D. Yeates |
| Date Submitted: | August 25, 1989 |
| Contract Number: | NGT 44-001-800 |

ABSTRACT

This effort is a study of image-compression algorithms for an electronic still camera. An electronic still camera can record and transmit high-quality images without the use of film, because images are stored digitally in computer memory. However, high-resolution images contain an enormous amount of information, and will strain the camera's data-storage system. Image compression will allow more images to be stored in the camera's memory. For the electronic still camera, a compression algorithm that produces a reconstructed image of high fidelity is most important. Efficiency of the algorithm is the second priority. High fidelity and efficiency are more important than a high compression ratio. Several algorithms were chosen for this study and judged on fidelity, efficiency and compression ratio. The transform method appears to be the best choice. At present, the method is compressing images to a ratio of 5.3:1 and producing high-fidelity reconstructed images.

## INTRODUCTION

This study of image-compression algorithms is part of the High-Resolution Still Camera Project under the direction of Don Yeates at Johson Space Center.[1] The Electronic Still Camera (ESC) project will provide for the capture and transmission of high-quality images without the use of film. The image quality will be markedly superior to video, and will approach the quality of 35mm film. The camera will have the same general shape and handling as a 35mm camera.

The camera will be of great use on Space Station. The period between Shuttle visits to Space Station will be 90-180 days. If pictures were recorded on conventional film, people on the ground would have to wait three to six months to see the images. Space Station crewmembers using the ESC will be able to send high-quality images to earth in near real-time. Space Station uses of the ESC will include crew health, in-flight maintenance, experiment monitoring, damage assessment and public relations.

Instead of film in a film canister, the ESC uses computer memory (RAM) in a removable cartridge to store an image. To take a picture, the user clicks the shutter. Light entering the camera is converted into numbers and stored in the memory. To see a picture, the user removes the cartridge and inserts it into a computer. The picture can be viewed on a high-resolution monitor or sent to earth to be analyzed and printed.

It takes an enormous amount of memory to store a single image. Each pixel (spot) of an image is represented by three 8-bit numbers, one each for red, green and blue. The final version of the ESC will record images that are 2048 x 2048 pixels. Because each pixel needs three bytes of storage, one image requires 12Mbytes.

Because the ESC body needs to resemble a 35mm camera body, there is not room in the cartridge for much more than 12Mbytes. In other words, there is room for only one image on the cartridge. This is analogous to having a film canister that contains one exposure of film. This is unsatisfactory from a human factors point of view.

## IMAGE COMPRESSION

An image-compression algorithm stores an image using less memory. If each image needs less memory, then more images can be stored in a memory cartridge.

The image-compression process takes an image as input, and produces a compressed image that occupies less space. In the ESC, the compression will take place inside the camera and the compressed images are stored in the memory cartridge. After taking pictures, the user transfers the compressed images from the cartridge to a computer. The images are expanded to their

original size and are called reconstructed images. The user can view the reconstructed images on the high-resolution monitor. (See figure 1.)

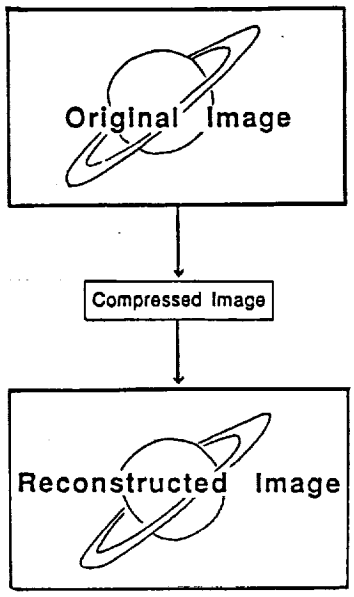


Figure 1: The compression process

Performance criteria for image-compression algorithms

Each image-compression algorithm is a tradeoff among the following criteria:

1. fidelity
2. efficiency
3. compression ratio

Fidelity refers to how well the reconstructed image resembles the original image. There are quantitative measures of fidelity, including signal-to-noise and mean-squared-error, but these do not always give an accurate measure of fidelity. Two images with the same mean-squared-error can have radically different fidelities when viewed by the human eye.

Efficiency has three aspects -- speed, space and parallelism. Speed is a measure of the length of time the algorithm takes to finish the compression. Space is a measure of the amount of auxiliary storage the algorithm needs to compress an image. Parallelism is a measure of how well an algorithm can be

decomposed into parts that can be executed simultaneously. A slower algorithm with a greater degree of parallelism can be more interesting than a faster algorithm with a low degree of parallelism.

Compression ratio is a ratio of the size of an original image to the size of the compressed image. This is a measure of how many images can be stored on the ESC memory cartridge.

The ESC requires the highest possible fidelity. The people receiving pictures from the camera will want images of the highest quality. Efficiency is second in importance. The compression must take place quickly so the user will not have to wait a long time between shots. Further, the algorithm cannot need a lot of extra space because memory is at a premium. Fidelity and efficiency are more important than an extremely high compression ratio.

Algorithms chosen for study

Image compression algorithms fall into two categories -- lossless and loss-y.[2] Lossless algorithms lose no information when compressing an image. The reconstructed images are exact duplicates of the original images. When using a loss-y algorithm, some information is lost in the compression process. The reconstructed image will differ from the original. The differences may or may not be visible to the human eye.

For purposes of this study, I chose some algorithms from each category:

Lossless
- Run-length coding[3]
- Frequency-based coding[4]

Loss-y
- Block-truncation coding[5]
- Transform coding[6]

I based the choices primarily on efficiency. Some other algorithms, such as contour encoding[7] and the predictive methods[8], are rather time-consuming. Others, like the Laplacian pyramid method[9], require a large amount of auxiliary storage. Others sacrifice fidelity for a high compression ratio.[10]

Of the lossless schemes, run-length encoding is the simplest and the fastest. The frequency-based schemes include Huffman, S-codes. These are a little slower, but provide a higher compression ratio.

Of the loss-y schemes, the block-truncation encoding method is superior in terms of speed and parallelism. It also needs little auxiliary space. The block-truncation scheme uses a moment-preserving quantizer. An image is divided into n x n pixel blocks. Each pixel in the block is quantized to one of two levels x and y such that the block's sample mean and variance are preserved. To perform the compression, a new n x n bitplane is created. A binary 1 in the bitplane indicates that the corresponding pixel in the original block was

above the sample mean, and a binary 0 indicates that correspoding pixel was below the sample mean. To preserve the sample mean and variance, all the pixels above average are quantized to

$$x = \mu - \sigma(q/p)^{0.5}$$

All pixels below average are quantized to

$$y = \mu + \sigma(p/q)^{0.5}$$

where $\mu$ is the sample mean, $\sigma$ the standard deviation, and q and p are the number of pixels above and below the sample mean, respectively. A compressed block consists of the n x n bitplane, and the values of x and y.

The transform methods need more space and run more slowly. The transform method in this study used a Fourier transform on a 8 x 8 tile of pixels. First, the tile of pixels was converted from RGB to YIQ. The Fourier transform was performed only on the Y-component, because most of the image's bandwidth is located there.[11]

Compression was achieved by retaining the dc coefficient and the l highest-energy ac coefficients in the block. The retained coefficients were truncated to m bits. Coefficients $c_{ij}$ for a block were quantized within a single block. A second method involves generating all $c_{ij}(k)$ coefficients, where (i,j) is the position in the block, and k is the block number. After it has generated and stored all the coefficients for an entire image, the second method quantizes coefficient $c_{ij}(k)$ over all blocks k. The latter method gives a better compression ratio, but takes too much space.

The I- and Q-components are handled differently. For each block, the average I-component value is computed and stored. The Q-component is handled similarly.

The following information is stored in a compressed block

1. 8 x 8 bitplane
   A binary 1 at location (i,j) implies that the corresponding coefficient $c_{ij}$ was retained.
2. sample mean of the retained coefficients
3. standard deviation of the retained coefficients
4. the retained coefficients
5. an average I-value
6. an average Q-value

A range of compression ratios can be achieved by varying the number of retained coefficients, and the number of bits used to quantize the coefficients.

Comparison method

Because all chosen algorithms have acceptable efficiency, comparisons among the algorithms were based on fidelity and compression ratio. Four images were chosen for the study. These included a face shot, a view of the Shuttle payload bay, a shot of the remote manipulator arm with the earth in the background, and a picture of an experiment located on the Shuttle middeck. These images are representative of the images that will be needed by the Space Station applications.

For the lossless compression algorithms, whose fidelity is perfect, the images were compressed and the compression ratio recorded. The test of the loss-y algorithms was more involved. For a given compression ratio, each image was compressed twice, once using the block-truncation method, and once using the transform method. The images reconstructed from the two methods were compared side-by-side.

Results

The lossless algorithms were superior in fidelity, but their compression ratios were very low. The ratios of the four images ranges from 1.7:1 to 2.1:1. We decided that the compression ratios were adversely affected by noise introduced by the device used to scan the images. However, even if the images were noise free, the compression ratio produced by a lossless algorithm is not constant. The compression ratio of any lossless algorithm is bounded above by the amount of entropy in the picture. Entropy is a measure of information content. If an image has high entropy (if the image complexity is high), the compression ratio will be lower than if the image had lower entropy.

The block-truncation method was disappointing. To get a reconstructed image of acceptable fidelity, the method produced a compression ratio of 1.8.

The transform method produced reconstructed images that had few artifacts, and the compression ratio was 5.3. As the compression ratio was increased to 8.5, the fidelity did not deteriorate significantly. Figure 2 shows an original image and an image that has been compressed and reconstructed using the transform method. The compression ratio is 5.3.

Future Work

The transform method is the most promising. To improve the method's performance, a cosine transform will be substituted for the fourier transform because the cosine transform concentrates more energy into fewer coefficients.

The compression ratio would increase significantly if each compressed block did not contain the 8 x 8 bitplane that gives the location of the retained coefficients. Elimination of the bitplane would mean that the pattern of the coefficient retention would have to be fixed. This requires a study of the distribution of the high-energy coefficients within a block. Another possibility is to have a few (say four) fixed patterns of coefficient retention.

Each block would contain a number indicating which pattern of coefficient retention was used in that block.

Another way to increase the compression ratio and/or increase image fidelity is to quantize the coefficients more carefully. In the present method, each coefficient is quantized to a fixed number of bits. In a future method, a coefficient could be quantized to some number of bits chosen from a range, depending on the position and energy of the coefficient.

With these improvements, the transform method should be able to produce high fidelity reconstructed images with a compression ratio of 10:1.

## CONCLUSIONS

The ESC could have two compression modes: on and off. Normally, the compression would be turned on, and a user of the ESC could store ten images on a memory cartridge. If, however, a researcher wants every bit of an original image, the user of the ESC could turn off the compression, and store the one image on a memory cartridge. Even though the lossless algorithms produce reconstructed images with flawless fidelity, the compression ratios are too unpredicatable for use in the ESC. The transform method will compress the images with reasonable efficiency, produce images of high fidelity, and guarantee an acceptable compression ratio.

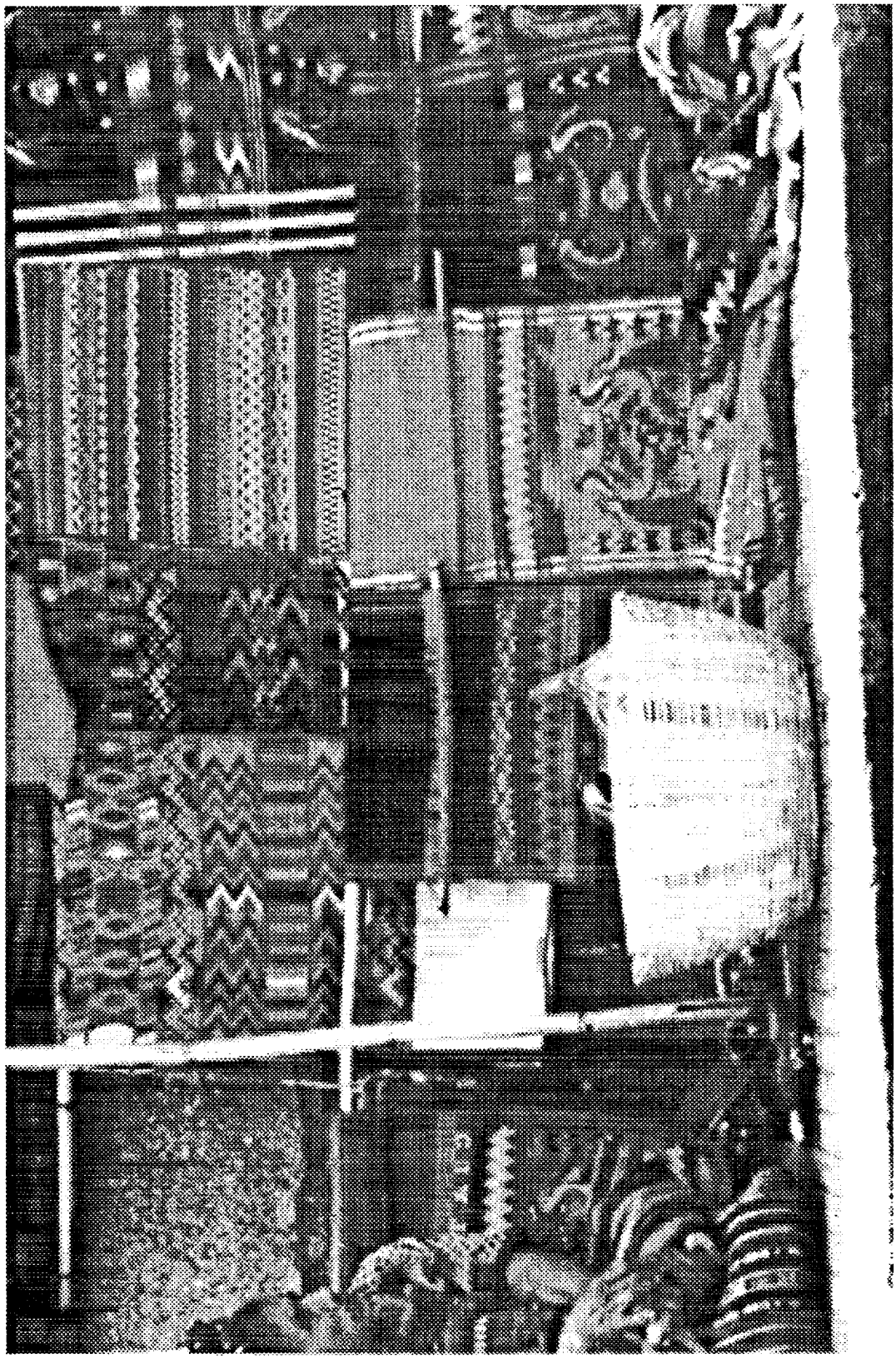

Figure 2a: Original Image

ORIGINAL PAGE
BLACK AND WHITE PHOTOGRAPH



ORIGINAL PAGE IS
OF POOR QUALITY

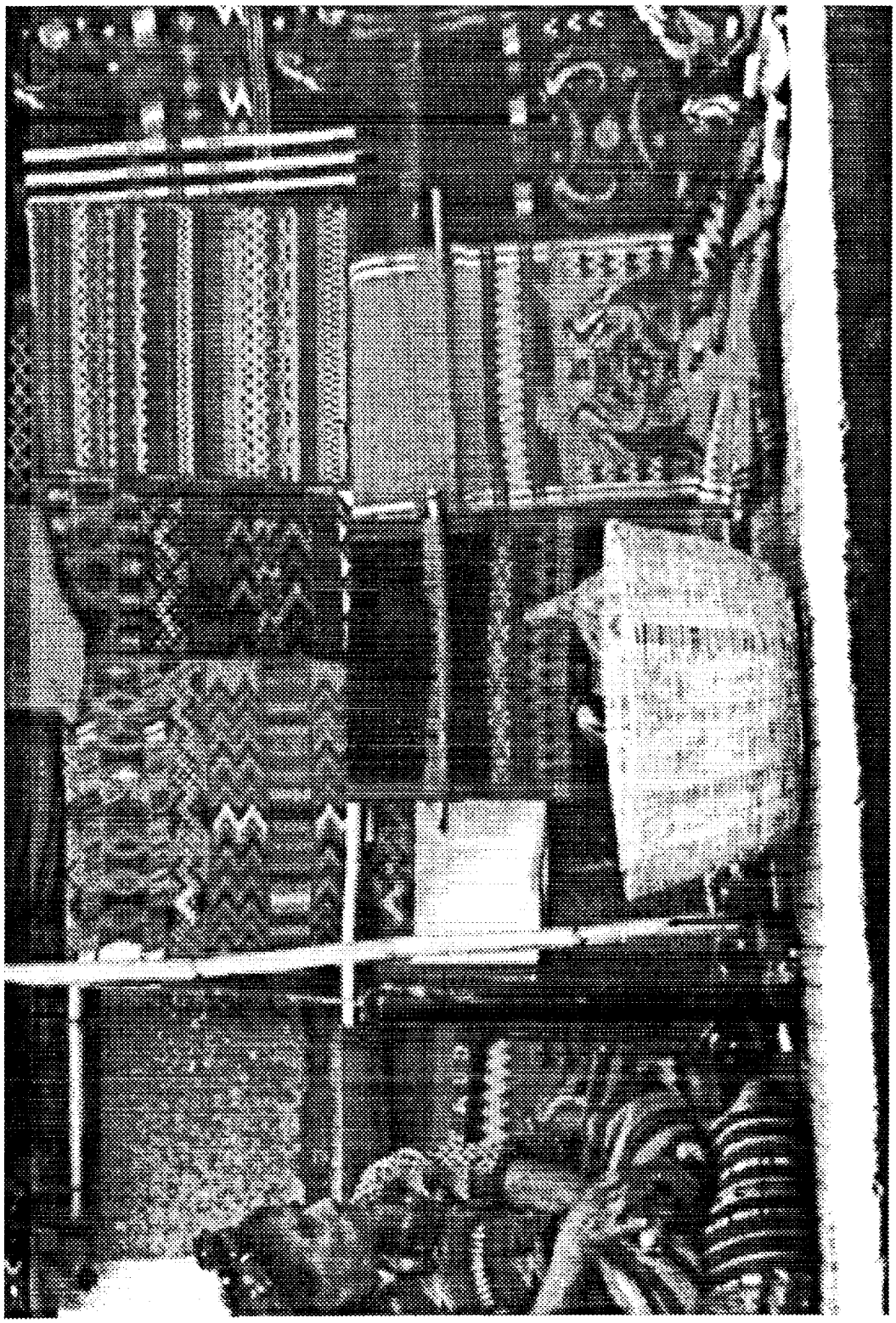

Figure 2b: Reconstructed Image Using Transform Method

[1] Don Yeates, Douglas Holland, Rao Linga and Rosalee Nerheim, "High-Resolution Electronic Still Camera (HRESC)" talk given at NASA Johnson Space Center, Man-Systems Division, Flight Equipment Branch, August 23, 1989.

[2] Johannes G. Moik, *Digital Processing of Remotely Sensed Images*.. NASA SP-431 Washington, DC: NASA Scientific and Technical Information Branch, 1980. pp. 294-295.

[3] Thomas Lynch, *Data Compression: Techniques and Applications*. New York: Van Nostrand Reinhold, 1985. pp. 144-155.

[4] Azriel Rosenfeld and Avinash Kak, *Digital Image Processing*. New York: Academic Press, 1976. pp. 181-193.

[5] E. J. Delp and O. R. Mitchell, "Image Truncation Using Block Truncation Coding." *IEEE Transactions on Communications* **COM-27** 1979, pp. 1335-1342.

[6] Ali Habibi and Paul Wintz, "Image Coding by Linear Transformation and Block Quantization." *IEEE Transactions on Communications* **COM-19** 1971, pp. 50-62.

[7] Rafael Gonzalez and Paul Wintz, *Digital Image Processing* 2nd. ed. Reading Massachusetts: Addison-Wesley, 1987, pp. 275-287.

[8] Anil K. Jain, Paul M. Farrelle, and V. Ralph Algazi, "Image Data Compression" pp. 173-187. In *Digital Image Processing Techniques* Michael Eckstrom, ed. New York: Academic Press, 1984.

[9] Peter Burt and Edward Adelson, "The Laplacian Pyramid as a Compact Image Code." *IEEE Transactions on Communications* **COM-31** 1983, pp. 532-540.

[10] Murat Kunt, Michel Benard, and Riccardo Leonardi, "Recent Results in High-Compression Image Coding." *IEEE Transactions on Circuits and Systems* **CAS-34** 1987, pp. 1306-1335.

[11] Stevan Eidson, "Applications of a DSP Semiconductor for Still-Frame Transform Image Compression." *Zoran Technical Note*. Santa Clara, California: Zoran Corporation, 1986.

# THE USE OF UNDERWATER DYNAMOMETRY TO EVALUATE TWO SPACE SUITS

Final Report

NASA/ASEE Summer Faculty Fellowship Program--1989

Johnson Space Center


| | |
|---|---|
| **Prepared By:** | **W. G. Squires Ph.D** |
| Academic Rank: | Professor |
| University & Department: | Texas Lutheran College<br>Department of Biology<br>Sequin, Texas |
| NASA/JSC | |
| Directorate: | Space and Life Sciences |
| Division: | Man Systems |
| Branch: | Crew Station |
| JSC Collegue: | **Mike Greenisen Ph.D.** |
| Date Submitted: | August 9, 1989 |
| Contract Number: | NGT 44-001-800 |

## ABSTRACT

Four Astronauts were instrumented and donned one of three EVA suits. The currently in use shuttle suit (STS), the Mark III (MK3), and the AX5. The STS was used as the comparison suit because of approved status. Each subject performed ten different exercise in each suit in three different manners(static,dynamic and fatigue) in two different environments,WETF and KC-135( KC-135 not completed as of this report). Data were recorded from a flight qualified underwater dynamometer(Cybex power head) with a TEAC multichannel recorder/tape and downloaded into the VAX computer system for anaylsis. Also direct hard copy strip chart recordings were made for backup comparisons. Data were anaylized using the ANOVA procedure and results were graphed and reported without intrepretation to the NASA/JSC ABL manager.

## INTRODUCTION

The proctective garment that the astronaut will wear during EVA activities has long been and continues to be a major concern for the manned space program. The shuttle suit (STS) has been up to this point the workhorse of the program. With the advent of the space station and the required extended EVA activity involved, new designs with unique changes have been sought. Thus two new prototype suits have been developed the Mark III (MK3), and the AX5.

## PURPOSE

The purpose of this study was to investigate the capabilities of the three suits while performing ten different activities in three different modes under two different conditions. (appendix#1).

## METHODS

Four male astronauts were assigned to perform ten different exercises in three different modes under two different environmental conditions. Subjects donned one of the suits entered the WETF and were transported by the safety divers to the dynamometer station. On the command of the test director the subject initiated the activity in the sequence of the protocol. The static exercise was done first, followed by the dynamic, then the fatigue. There was a mandatory rest of ten minutes between exercises. Data was collected on a TEAC recorder and then later downloaded to the Vax system for later anaylsis. A simultaneous hard copy recording was made on all subjects on all trials. Data was collected and anaylized using the double blind procedure to reduce experimenter bias.

## RESULTS

All data was double checked by two independent investigators and entered into a Macintosh II computer data base. Data was anaylized using ANOVA for independent samples (suits). Anaylsis was run on each exercise and each mode (static, dynamic, and fatigue). Mean forces and standard errors were graphically developed. All results were presented confidently to the manager of the ABL lab for intrepretation and dissemination.

# ADVANCE SUIT TEST PROGRAM FILENAMES

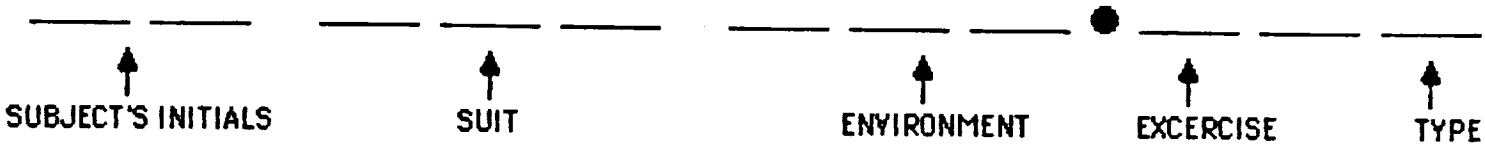


## SUBJECT

- DH
- SC
- JH
- JR

## SUIT

- SHUTTLE SUIT → STS
- MARK III → MK3
- AX5 → AX5

## ENVIRONMENT

- WETF → WET
- KC-135 → KC

## EXERCISE

- SHOULDER ADDUCTION → 1
- EVA RATCHET WRENCH CRANK → 2
- SHOULDER ROTATION-MED. INT. → 3
- ELBOW FLEXION → 4
- ELBOW EXTENSION → 5
- SHOULDER FLEXION → 6
- EVA RATCHET WRENCH PUSH → 7
- EVA RATCHET WRENCH PULL → 8
- SHOULDER ROTATION- Y-AXIS → 9
- SHOULDER ADDUCTION-FLEXION → 0

## TYPE

- STATIC → 1
- DYNAMIC → 2
- FATIGUE → 3

ORIGINAL PAGE IS
OF POOR QUALITY

This information pertains to the following two pages of Cybex exercises.

The reference system used for defining the range of motion for each exercise is as shown - looking down the dynamometer shaft from the crewmember exercise station

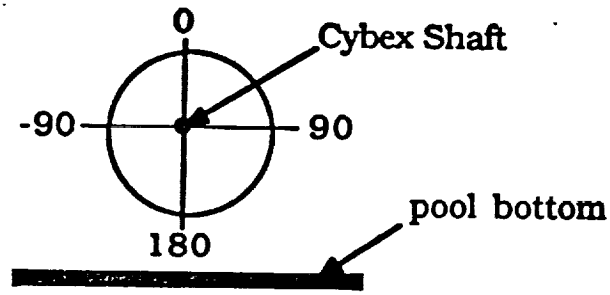


| Exercise | Static Position | Dynamic Range of Motion |
|---|---|---|
| Shoulder Adduction | 60° | 45° to 135° |
| EVA Ratchet Wrench Crank | 75° | 45° to 135° |
| Shoulder Rotation - Med. Int. | -45° | 0° to -110° |
| Elbow Flexion | -105° | 180° to -45° |
| Elbow Extension | -75° | -45° to 180° |
| Shoulder Flexion | -80° | -45° to -135° |
| EVA Ratchet Wrench Push | 15° | 45° to -45° |
| EVA Ratchet Wrench Pull | -15° | -45° to 45° |
| Shoulder Rotation - Y Axis | -45° | 0° to -90° |

# FINITE ELEMENT FORMULATIONS FOR COMPRESSIBLE FLOWS

Final Report

NASA/ASEE Summer Faculty Fellowship Program 1989

Johnson Space Center


| | |
|---|---|
| Prepared by: | Tayfun E. Tezduyar |
| Academic Rank: | Associate Professor |
| University and Department: | University of Minnesota<br>Aerospace Engineering and Mechanics<br>Minneapolis, Minnesota 55455 |
| NASA/JSC | |
| Directorate: | Engineering |
| Division: | Advanced Programs |
| Branch: | Aerosciences |
| JSC Colleague: | Chien Li, Ph.D. |
| Date Submitted: | August 14, 1989 |
| Contract Number: | NGT 44-001-800 |

## ABSTRACT

We have started our studies related to the development and application of computational methods for compressible flows. Particular attention is given to proper numerical treatment of sharp layers occuring in such problems and to general mesh generation capabilities for intricate computational geometries. Mainly finite element methods enhanced with several state-of-the-art techniques (such as the streamline-upwind/Petrov-Galerkin, discontinuity capturing, adaptive implicit-explicit, and grouped element-by-element approximate factorization schemes) will be employed.

## INTRODUCTION

The physics and dynamics of the problems involving compressible flows in aerospace applications are not yet fully understood. Particularly, better understanding of dynamical, thermal and chemical aspects of the renetry conditions is needed. Prediction of aerodynamic and heating loads is very important for designing space vehicles. The conditions such as altitude and speed under which such maneuvering is to be performed makes the simulation by ground test facilities impossible Therefore, computational predictions based on the solution of appropriate governing equations become very important and imperative.

The main objective of this project is to investigate the development and application of computational tools for aerospace problems with special reference to compressible flows. These tools need to be not only accurate and reliable but also efficient and easy to apply to complicated geometries. Unrestricted geometric generality of a numerical analysis tool will become more and more important and indispensible as research in this area targets more and more flow simulations for computational geometries which give realistic representations of the actual configurations. To this end we plan to base our efforts on the finite element method (FEM) which is widely acknowledged to be the most geometrically flexible computational fluid dynamics (CFD) tool available.

Among the difficulties associated with the numerical simulation of compressible flows is the treatment of shocks and sharp layers. For hypersonic flows the magnitude of such sharp variations in the flow field becomes very large and this makes the computation even more challenging. We plan to use streamline-upwind/Petrov-Galerkin (SUPG) formulations which are well-known to result in stable and accurate results for convection-dominated problems in the presence of discontinuites and sharp layers at moderately high wave numbers. The SUPG method essentially introduces a disspative effect in the direction of the flow (or in the direction of the characteristic vector). For very strog discontinuities and sharp layers (i.e. very high wave numbers) we plan to use the discontinuity capturing (DC) method which introduces a dissipative effect in the direction of the vector normal to the discontinuity front. This approach produced very satisfactory results for the model problems studied. Furthermore, with our adaptive implicit-explicit (AIE) method we will be able to have an implicit refinement around sharp layers. This will not only increase the efficiency of the computations substantially, but also, and the most importantly, will result in stable and accurate results near sharp layers.

## PROBLEM STATEMENT

Let $\Omega$ be an open region $\Re^{nsd}$, where $n_{sd}$ is the number of space dimensions. The boundary of $\Omega$ is denoted by $\Gamma$. Spatial coordinates are denoted by $\mathbf{x} \in \Omega$.

Assuming real gas behavior with equilibrium chemistry, mass, momentum and energy balance equations are given as follows:

$$\frac{\partial \rho}{\partial t} + \nabla \bullet (\mathbf{u}\,\rho) = 0 \qquad \text{(mass balance)} \tag{1}$$

$$\frac{\partial}{\partial t}(\rho \mathbf{u}) + \nabla \bullet (\mathbf{u}\,\rho\,\mathbf{u} - \sigma) = 0 \qquad \text{(momentum balance)} \tag{2}$$

$$\frac{\partial}{\partial t}(\rho e) + \nabla \bullet (\mathbf{u}\,\rho\, e - \sigma \mathbf{u} + \mathbf{q}) = 0 \qquad \text{(energy balance)} \tag{3}$$

where $\rho$, $\mathbf{u}$, $\sigma$, $\mathbf{q}$ and $e$ are the density, velocity vector, stress tensor, heat flux vector and total specific energy, respectively.

Assuming Newtonian fluids which obey the Fourier's law of heat conduction we can express the constitutive relations as follows:

$$\sigma = -p\,\mathbf{I} + \tau \tag{4}$$

$$\tau = \lambda (\nabla \bullet \mathbf{u})\,\mathbf{I} + \mu (\nabla \mathbf{u} + (\nabla \mathbf{u})^T) \tag{5}$$

$$\mathbf{q} = -\kappa \nabla T \tag{6}$$

In the above expressions p is the pressure, $\tau$ is the viscous stress tensor, $\lambda$ and $\mu$ are the two coefficients of viscosity, T is the temperature, and $\kappa$ is the conductivity.

The total energy e can be written as

$$e = i + (1/2)\ \|u\|^2 \tag{7}$$

where i is the specific internal energy. We assume that for real gases, pressure and temperature data is available in a form which can be expressed as follows:

$$p = p(\rho, i) \tag{8}$$

$$T = T(\rho, i) \tag{9}$$

Remark

In a more compact vector form, equations(1) - (3) can be written as follows:

$$\frac{\partial U}{\partial t} + \nabla \bullet F(U) = 0 \tag{10}$$

where $U(x,t)$ is the vector of unknown variables and $F(U)$ is the flux vector.

We assume that associated with (10) the following boundary and initial conditions are given:

$$B\,U = G \qquad \text{on } \Gamma \tag{11}$$

$$U(x,0) = U_0(x) \qquad \text{on } \Omega \tag{12}$$

where $B(U)$ is a boundary operator and $G$ and $U_0(x)$ are given functions.

## THE FINITE ELEMENT FORMULATION

Consider a discretization of $\Omega$ into element subdomains $\Omega^e$, e = 1,2,..., $n_{el}$ where $n_{el}$ is the number of elements. Let $\Gamma^e$ denote the boundary of $\Omega^e$. We assume

$$\bar{\Omega} = \bigcup_{e=1}^{n_{el}} \bar{\Omega}^e \tag{13}$$

$$\varnothing = \bigcap_{e=1}^{n_{el}} \Omega^e \tag{14}$$

Throughout, we shall assume that trial solutions, **U**, satisfy **BU** = **G** on $\Gamma$ and weighting functions, **W** , satisfy **BW** = **0** on $\Gamma$.

The weak(variational) form of (10) -(12) is given as follows:

$$\int_{\Omega} \mathbf{W} \bullet \left( \partial \mathbf{U}/\partial t + \nabla \bullet \mathbf{F} \right) d\Omega = 0 \tag{15}$$

$$\int_{\Omega} \mathbf{W} \bullet \left( \mathbf{U}(x,0) - \mathbf{U}_0(x) \right) d\Omega = 0 \tag{16}$$

Remark

If the weighting functions are selected from the same set of functions as the trial solutions then (15) is a regular (Bubnov-) Galerkin formulation; else, it is a Petrov-Galerkin formulation. The significance of the Petrov-Galerkin formulation will be explained in the sequel.

Spatial discretization of (15-16) is carried out by expanding **U** and **W** in terms of a set of finite element basis functions corresponding to (13-14). For example the expression for **U** might take the form

$$U(x,t) = \sum_{B} N_B(x)\ U_B(t) \tag{17}$$

where B is the nodal index, $N_B$ is the finite element basis function associated with node B, and $U_B$ is the nodal value of U.

The spatial discretization leads to a set of semi-discrete, ordinary differential equations:

$$\mathbf{M}\ \dot{\mathbf{V}} + \mathbf{N}\ (\mathbf{V}) = \mathbf{F} \tag{18}$$

with the initial condition:

$$\mathbf{V}(0) = \mathbf{V_0} \tag{19}$$

where V is the vector of nodal values of U, $\mathbf{V_0}$ is its given initial value, M is a generalized "inertia" matrix, N is a nonlinear vector function of V, and F is a "force" vector. A superposed dot denotes time differentiation.

Given the initial condition (19), equation (18) can be integrated by an appropriate temporal discretization scheme.

## CONCLUSIONS

We have started with our development efforts and preliminary computations for finite element formulations applied to compressible flows.We are particularly interested in the proper numerical treatment of sharp layers occuring in such problems We also target the most general mesh generation capabilities for intricate computational geometries. Our methods will be enhanced with several state-of-the-art techniques such as the streamline-upwind/Petrov-Galerkin, discontinuity capturing, adaptive implicit-explicit, and grouped element-by-element approximate factorization schemes. Our preliminary computations show that these methods are stable, have minimal numerical dissipation, and are very reliable.

# OPTICAL RATE SENSOR ALGORITHMS

Final Report

NASA/ASEE Summer Faculty Fellowship Program - 1989

Johnson Space Center


| | |
|---|---|
| Prepared by: | Jo A. Uhde-Lacovara, Ph.D. |
| Academic Rank: | Assistant Professor |
| University and Department: | Stevens Institute of Technology<br>Dept. of Electrical Engineering<br>and Computer Science<br>Hoboken, NJ 07030 |
| NASA/JSC | |
| Directorate: | Engineering |
| Division: | Avionics Systems |
| Branch: | Guidance, Navigation,<br>and Control Systems |
| JSC Colleague: | J. R. Thibodeau III |
| Date Submitted: | August 11, 1989 |
| Contract Number: | 44-001-800 |

## ABSTRACT

Optical sensors,in particular CCD arrays, will be used on Space Station to track stars in order to provide inertial attitude reference. Algorithms are presented to derive attitude rate from the optical sensors.The first algorithm is a recursive differentiator. A variance reduction factor (VRF) of 0.0228 was achieved with a rise time of 10 samples. A VRF of 0.2522 gives a rise time of 4 samples. The second algorithm is based on the direct manipulation of the pixel intensity outputs of the sensor. In 1-dimensional simulations, the derived rate was within 0.07% of the actual rate in the presence of additive Gaussian noise with a SNR of 60 dB.

## INTRODUCTION

Optical sensors will be of great use on Space Station as part of the on-board guidance, navigation, and control system. These sensors can be used to track stars to provide inertial attitude reference. The information may also be used by astronomical experiments to allow reference to a known star catalog to provide precise pointing of instruments. Optical sensors can be used on Space Station to keep track of other nearby objects such as incoming orbiters. Co-orbitting platforms may also use optical sensors for their GN&C needs.

Because optical sensors will provide attitude information to Space Station, it would be useful if attitude rate could be derived from these sensors. An optical rate sensor is currently being developed in the Avionic Systems Division at Johnson Space Center. The sensor will look at stars to obtain both attitude information and to derive attitude rate. A Videk Megapixel camera is supported by a Compac Deskpro 386 for data capture and processing. The Videk camera uses a Kodak charge coupled device (CCD) array. This array is made up of 1320 horizontal by 1035 vertical pixels. The pixels are 6.8 microns square and the array is full fill. The camera is capable of 7 still frames per second and has a grey scale of 256 levels.

## RATE PROCESSING ALGORITHMS

### Centroiding/Differentiator Approach

The centroids of the star images are obtained for each camera frame. The centroids are in field coordinates which can later be translated to inertial attitude. To obtain rate, the centroids are processed by a discrete time differentiator Previous analysis of this problem showed that a nonrecursive differentiator with low systematic errors to meet Space Station requirements had the following parameters:

100 Hertz sample rate decimated to 10 Hertz
Input bandlimited to 0.5 Hertz
Filter order of 127
Linear frequency response to 0.01 Hertz [1]

This nonrecursive differentiator has several drawbacks; the filter order is

high and, therefore, the delay in obtaining a an estimate of the derivative for a particular sample point is excessive. Also, the useful frequency range is severely limited compared to the sampling frequency.

In reworking the centroiding/differentiator approach, consideration was given to the type of data processed. Space Station orbital pitch rate is relatively constant at 240 degrees per hour. We want to track small, slow variations to this basic rate while smoothing out high frequency noise. A heuristic design approach was taken in which a nonrecursive differentiator was modified with feedback from the previous outputs. This new, recursive design provides noise reduction and small time delays.

The difference equation for a first order, nonrecursive, backward difference differentiator is given below:

$$y(n) = x(n) - x(n - 1)$$

This difference equation is modified to provide feedback as follows:

$$y(n) = K(x(n) - x(n - 1)) + (1 - K)(y(n - 1))$$

A second order, nonrecursive difference equation is modified in a similar manner:

$$y(n) = K(x(n) - x(n - 2))/2 + (1 - K)(y(n - 1) + y(n - 2))/2$$

K is a constant chosen to be between 0 and 1. Values of K close to 1 give greater weight to the inputs; this gives a steady state frequency response closer to the ideal. Values of K close to 0 give greater weight to the previous outputs; this gives more high frequency noise attenuation.

Recursive Differentiator Results

A set of 10,000 random numbers with a Gaussian distribution were processed by the recursive differentiators. The variance of the output was computed, giving the variance reduction factor. It should be noted that the first order, nonrecursive differentiator causes the variance to increase by a factor of two

[2]. Another set of inputs consisting of 100 samples with a constant rate of 1.0, followed by 100 samples with a constant rate of 2.0 was applied to the recursive differentiators. The rise time, in samples, from time of change in the input to the time that the output reaches 90% of its final value was found. The above results are summarized in Table 1 and in Figures 1 and 2. The solid line represents the ideal response; the dotted, dashed and dot-dash curves are for K equal 0.75, 0.50, and 0.25 respectively. Satisfactory results are obtained for a first order recursive differentiator, obviating the need for a second order filter with the added time delay and computational expense of a second order filter.

## Image Processing Approach

In the image processing approach, the rate is derived by looking directly at the variation of intensity of the pixel outputs. The output of a CCD array is the two-dimensional, spatially sampled version of the transfer function of a pixel convolved with the input image field [3]. A specialized image field was used where all of the energy of the source is concentrated in the area of a single pixel. If the pixel is moved across the array at a constant rate, an intensity profile for a pixel $I_p(t)$ as a continuous function of time, is given below, and shown in Figure 3, where R is the rate in $t^{-1}$.

$$I_p(t) = \begin{cases} I_{max}Rt & 0 < t < 1/R \\ I_{max}(2 - Rt) & 1/R < t < 2/R \\ 0 & \text{elsewhere} \end{cases}$$

Note that the slope of the above curve is $I_{max}R$. The rate cannot be obtained directly from the slope, but must be normalized by the maximum intensity of the image. The system is discrete not only spatially, but also in time since images are processed on a frame by frame basis. Figure 4 shows a set of intensity profiles for 5 adjacent pixels with the image moving at a rate of 0.2930 pixels per frame and a maximum intensity of 1.0000.

Image Processing Rate Algorithm

In the absence of noise, the algorithm used to derive rate directly from variations in pixel intensities is given as follows:

1) Obtain the frame to frame intensity differences for the pixels of interest.
2) Make a histogram of the absolute values of these differences.
3) Find the difference magnitude with the highest frequency of occurrence. This value gives the raw rate which must be normalized.
4) Find the sums of intensities of adjacent pixels taken two at a time for a given frame. Form a collection of these intensity sums for several frames.
5) Make a histogram of these sums. The sum with the highest frequency of occurrence is $I_{max}$.
6) Take the raw rate found in step 3) and divide by the maximum intensity, $I_{max}$, found in step 5). The result is the derived rate.

In the presence of noise, modifications must be made to steps 3) and 5) above. When the histograms are formed in each of these cases, the peak is found, and the the weighted average of that peak and nearby values is computed in order to derive rate in step 6).

Examples

Three examples are presented below with and without noise:

1) The rate is R1 = 0.2930 pixels per frame. The maximum intensity is $I_{max} = 1.0000$.
2) The rate is R1 = 0.2930 pixels per frame. The maximum intensity is $I_{max} = 0.8410$.
3) The rate is R2 = 0.2464 pixels per frame. The maximum intensity is $I_{max} = 1.0000$.

The noise was additive Gaussian random noise with a standard deviation of 0.001. This corresponds to the dark current noise of the CCD camera. The bins for the histograms have a resolution of 0.004 and range from 0.0 to 1.0. This is to approximately correspond with the 256 grey levels. The cumulative sums and differences for 5 pixels were used for a total of 9 frames for each pixel.

The results of these simulations are summarized in Table 2.

## CONCLUSIONS

Two algorithms have been developed for obtaining rate information from optical sensors. Both approaches depend on having the camera frames accurately time-tagged. The recursive differentiator gives rapid rise times and significant variance reduction. The usefulness of the approach depends on how accurately the image centroids can be obtained.

The image processing approach has been shown to give good results for the one-dimensional simulations performed. An interesting finding is that noise, of the magnitude expected to be generated by the camera, can actually improve the accuracy of the results. This is because the noise distributes values across several bins in the histogram. The weighted average of the noisy histogram peaks gives sub-bin resolution. The accuracy of the computed rate can be improved by having a greater number of grey levels. A twofold improvement in grey levels can presently be obtained by cooling the CCD array.

The modifications to the algorithm to make it applicable to the two-dimensional case are straight forward. Modifications to allow for an image which is not exactly of one pixel width are also straight forward. Open issues involve optimizing for frame rate, processing time, array size, pixel size, number of grey levels, number of pixels and frames to be processed at one time, and noise performance. The algorithm will soon be applied to data obtained in laboratory simulations of a star moving at a constant rate.

## REFERENCES


[1] Uhde-Lacovara, J., "Analysis of the Continuous Stellar Tracking Attitude Reference (CSTAR) Attitude Rate Processor", NASA/ASEE Summer Faculty Fellowship Program, 1986, Volume 2 (N87-25884 19-85).

[2] Hamming, R., Digital Filters, Second Edition, Prentice-Hall, Englewood Cliffs, New Jersey, 1983.

[3] Nordbryhn, A., "Sampling and Aliasing Problems with Imaging Arrays", Society of Photo-optical Instrumentation Engineers (SPIE) Proceedings, Volume 467, pp 116-121.

**TABLE 1**

| DIFFERENTIATOR ORDER | K | VRF | RISE TIME (samples) |
|---|---|---|---|
| 1 | 0.75 | 0.9059 | 3 |
| 1 | 0.50 | 0.3351 | 4 |
| 1 | 0.25 | 0.0717 | 7 |
| 2 | 0.75 | 0.2522 | 4 |
| 2 | 0.50 | 0.1006 | 5 |
| 2 | 0.25 | 0.0228 | 10 |

**TABLE 2**

| EXAMPLE | NOISE | ACTUAL RATE | $I_{max}$ | ¦DIFFERENCE¦ | INTENSITY SUMS | DERIVED RATE |
|---|---|---|---|---|---|---|
| 1 | NO | 0.2930 | 1.0000 | 0.2920 | 1.0000 | 0.2920 |
| | YES | | | 0.2928 | 1.0000 | 0.2928 |
| 2 | NO | 0.2930 | 0.8410 | 0.2480 | 0.8400 | 0.2952 |
| | YES | | | 0.2464 | 0.8409 | 0.2930 |
| 3 | NO | 0.2464 | 1.0000 | 0.2480 | 1.0000 | 0.2480 |
| | YES | | | 0.2463 | 0.9998 | 0.2463 |

## FIGURE 1

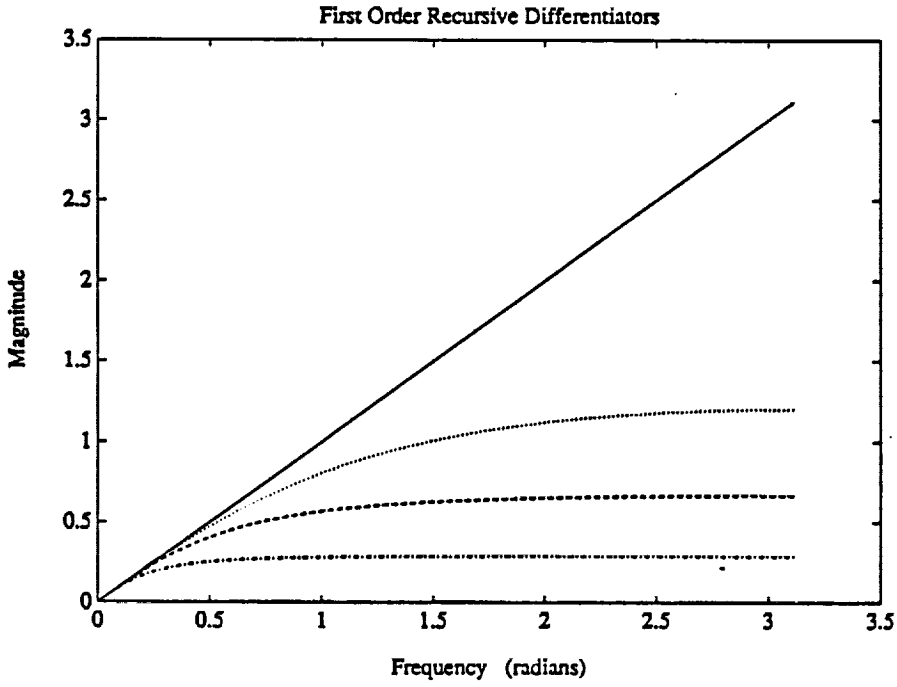


## FIGURE 2

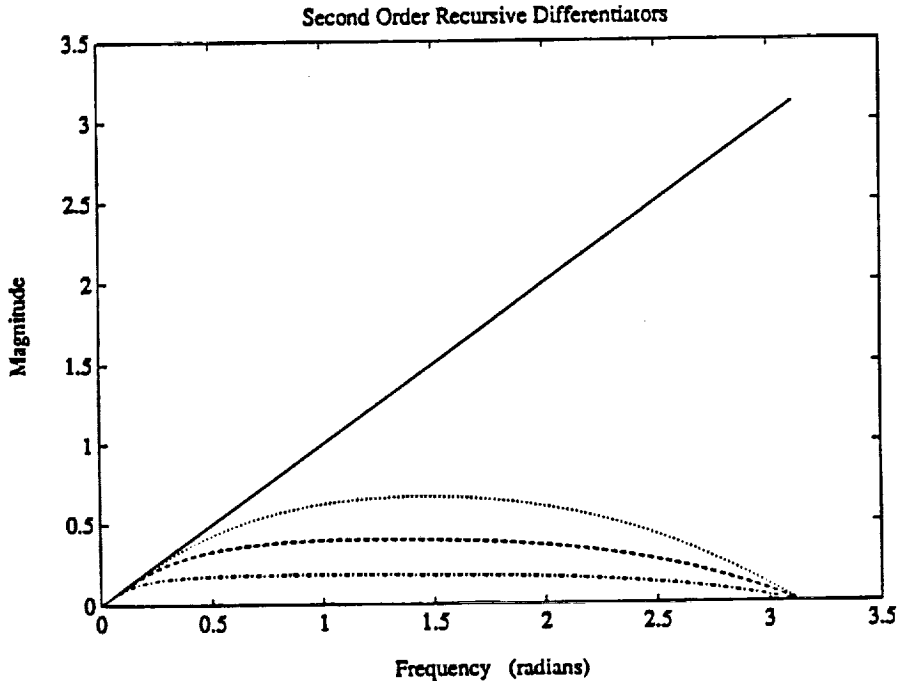

## FIGURE 3

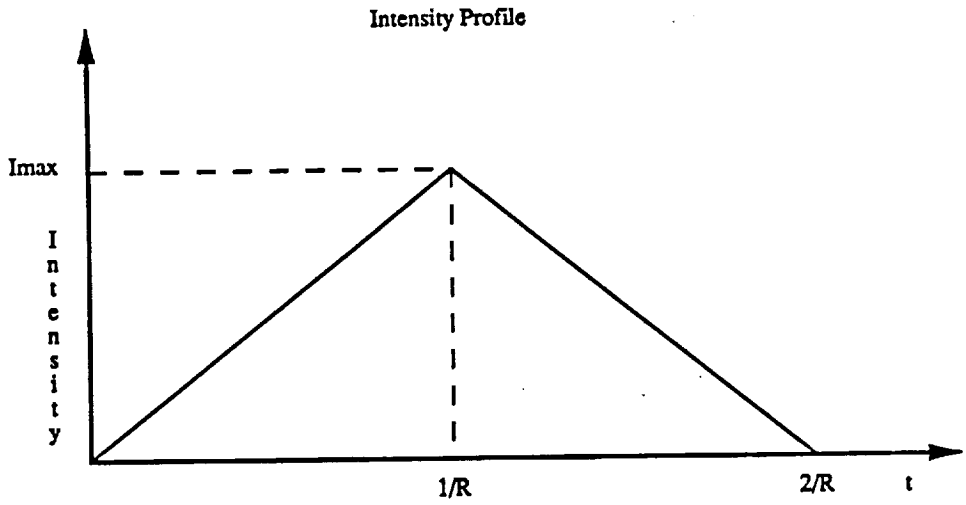


## FIGURE 4

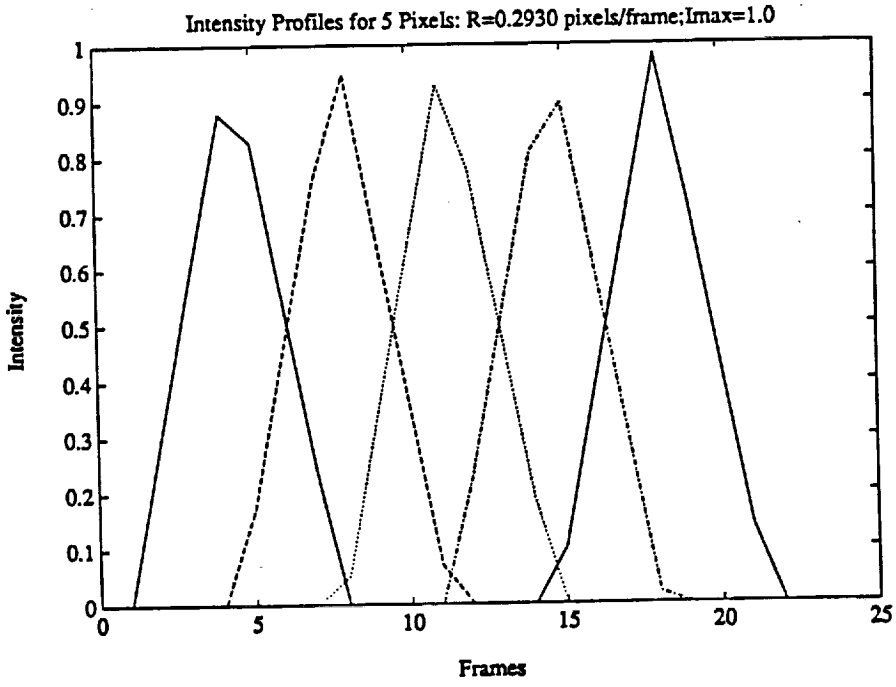

# WEIGHT AND COST FORECASTING FOR ADVANCED MANNED SPACE VEHICLES

Final Report

NASA/ASEE Summer Faculty Fellowship Program--1989


| | |
|---|---|
| Prepared by: | Raymond Williams, Ph.D |
| Academic Rank: | Associate Professor |
| University & Department: | Mississippi Valley State<br>Computer Science and<br>Mathematics Department<br>Itta Bena, Mississippi 38941 |
| NASA/JSC | |
| Directorate: | New Initiatives Office |
| Division: | Advanced Projects |
| Definition Office | |
| JSC Colleague: | Jared R. Woodfill |
| Date Submitted: | August 11, 1989 |
| Contract: | NGT 44-001-800 |

ABSTRACT

The study develops a mass and cost estimating computerized methology for predicting advanced manned space vehicle weights and costs. The user friendly methology designated MERCER (Mass Estimating Relationship/Cost Estimating Relationship) organizes the predictive process according to major vehicle subsystem levels. Design, devlopment, test, evaluation, and flight hardware cost forecasting is treated by the study. This methodology consists of a complete set of mass estimating relationships (MERs) which serve as the control components for the model and cost estimating relationships (CERs) which use MER output as input. To develop this model, numerous MER and CER studies were surveyed and modified where required. Additionally, relationships were regressed from raw data to accomodate the methology. The models and formulations which estimated the cost of historical vehicles to within 20 percent of the actual cost were selected. The result of the research, along with components of the MERCER Program, are reported. On the basis of the analysis, the following conclusions were established: (1) The cost of a spacecraft is best estimated by summing the cost of individual subsystems. (2) No one cost equation can be used for forecasting the cost of all spacecraft. (3) Spacecraft cost is highly correlated with its mass. (4) No study surveyed contained sufficient formulations to autonomously forecast the cost and weight of the entire advanced manned vehicle spacecraft program. (5) No user friendly program was found that linked MERs with CERs to produce spacecraft cost. (6) The group accumulation weight estimation method (summing the estimated weights of the various subsystems) proved to be a useful method for finding total weight and cost of a spacecraft.

## INTRODUCTION

Initial design cost estimates form the premise for budget determination, program approval, and subsequent performance measurement on research spacecraft programs. Unrealistic estimates early in the program are the source of problems for many project managers who are forced to operate within budgets that understate the technical complexity of the job. Cost forecasters consistently report spacecraft cost as a function of the mass; however, the determination of the mass in the initial stage of development still remains a challenge.

The purpose of this study was (1) to extract from the literature those mass estimating relations (MERs) that determine the total mass of a spacecraft by summing the mass of its individual subsystems; (2) to survey cost estimating relationships (CERs) as a function of mass; (3) to normalize and create MER and CER equations in order (4) to develop a computer program that uses MER output as input into CERs producing the cost of a spacecraft as final output.

## MASS ESTIMATING RELATIONSHIPS (MERs)

Forecasting mass properties of a spacecraft vehicle is one of the most important considerations in the design process and yet, one of the most inexact engineering endeavors. While the calculation of propulsion and mission performance are based on widely recognized mathematical forecasting techniques, the estimation of weight is based largely on historical data. The attempt to forecast weight has evolved through the years by collection and correlation of component weights of previously-built vehicles. Advanced vehicle weights are predicted on the basis of component weights of past designs. Although the precise weight of a vehicle is a very complex calculation, mathematical equations for combining the components mass properties into total vehicle mass properties are quite concise. Mass determination for the total vehicle is easily determined once the mass of all subsystems is known. The mass of an individual subsystem is largely a function of the spacecraft geometry; e.g., wetted area, planform area, length, width, volume, etc. These parameters are usually available or can be calculated. This study determines the total weight of spacecraft vehicle by summing the weights of all of its subsystems.

## COST ESTIMATING RELATIONSHIPS (CERs)

Historically, early estimates of spacecraft projects cost have been considerably less than the final actual cost. Spacecraft have been very expensive to produce because of stringent weight and performance requirements, heavy emphasis on reliability, and small production quantities. Various parametric cost estimating models have been developed from experience of the past 30 years, and those models reproduce the cost of the traditional spacecraft with acceptable accuracy. Due to the limited data base of manned space vehicles, a spacecraft cost estimating procedure based on historical data often contains errors. Mathematical relationship errors will exist in any estimating procedure which attempts simplification of actual cause and effect by empirical approximation. A good cost model, of course, is one that strives to minimize these inevitable errors. Cost regression equations for spacecraft subsystems are typical of the type

$$Y = AX^b \quad \text{or} \quad Y = A + BX^c$$

Where Y = cost and X = weight or some other subsystem characteristic. Those cost models that were shown to predict the cost of historical vehicles to within 20 percent of the actual cost were selected or developed for this study. The source of these cost models is reported in the next section of this paper.

## LINKING THE MERs AND CERs

The Mass Estimating Relationship/Cost Estimating Relationship (MER/CER) Program is a computer program for sizing subsystems and vehicle weights and costs for advanced planetary manned vehicles and boost rockets. The major components of the program include: (a) MERs taken from (1) The Mass Properties Systems and Formulation of the NASA Langley Research Center and (2) Handbook for Weight Estimating and Forecasting of Manned Space Systems During Conceptual Design for NASA Johnson Space Center (JSC); and (b) CERs extracted from (1) Marshall Space Flight Center (MSFC) Launch Vehicle Cost Model, (2) MSFC Space Station Cost Model, and (3) NASA's Advanced Planning Cost Model (NAPCOM) prepared by MSFC. The output from each MER in every subsystem becomes the input into the appropriate CER to produce a final cost.

Utilization of previous studies and systems was limited primarily to raw data and formulations used or developed in the earlier works. In a few cases, discrepancies were discovered in listings of raw data and in the calculating of the regressions. In these cases, additional data were used from independent sources and new regressions were calculated to resolve the discrepancies.

The JSC Weight Handbook provided regression curves based on early Shuttle studies and proposals. The MERCER Program converted these curves to mathematical relationships suitable for entry in the EXCEL Program. These equations required system-by-system testing with data from the "as built" Shuttle. The greatest numbers of modifications to the original equations resulted from these tests; however, an independent regression of rocket engine weight versus thrust showed the JSC Handbook curve (and equation) to be more easily applied (broader application) to the MERCER Program than the elaborate and (selectively specific) rocket engine MER in the LaRC paper. Yet, the LaRC body mass relationships proved more accurate than those offered by the JSC Weight Handbook. The MERCER Program permits use of alternate MERs and CERs which may be compared or averaged to enhance accuracy and forecasting credibility.

A final evaluation of the MERCER Program utilized a previous system weight and cost study done by the APDO for the Crew Emergency Rescue Vehicle (CERV) Program. In addition, an "as built" vehicle, Lunar Module, was entered as a test article to confirm MERCER system credibility. Again, an 80% accuracy criteria served as the desired result. Comparing the MERCER result with the two test cases showed better than 80% agreement in weight and cost.

## MERCER PROGRAM APPLICATION

The MERCER Program strives to use features resident in EXCEL and the Macintosh system in a user-friendly fashion. Among these features is the "GO TO" instruction. Clicking on "GO TO" opens a listing of every MER and CER subsystem in the entire MERCER Program so that quick access to specific subsystem entry data as well as weight, and cost results is achieved.

The MERCER Program has a fundamental feature: To compute from an initial specification a forecasted weight for each system of an advanced manned space vehicle or booster rocket; to input the forecasted weight into a corresponding cost equation for forecasting cost of each advanced vehicle system; and finally, to calculate the total forecasted cost.

The MERCER Program features facilitate this fundamental operation. Initial input data is entered in ledger fashion in a single column of the EXCEL spreadsheet matrix. The input data consists of both listed constants selected by the user based on primary space vehicle specifications and the MER input variable (volume, wetted area, planform area, thrust, etc.) The MERCER equation is listed adjacent to the entry data column to assist the user. Again, a designated ledger column serves for listing of all MERs and CERs. This column displays subsystem calculated weights and costs.

Total cost includes two categories: non-recurring design development, test, and evaluation (DDTE) cost and recurring flight hardware (FH) cost. Each subsystem has two cost forecasting equations listed on separate MERCER columns: one for design and development (DD) cost, the other flight FH cost. In some cases, DD cost is designated DD&T with the "T" indicating tooling. In some cases FH cost is designated FH&A with the "A" indicating assembly. Regardless of the listing of "T" or "A" with DD and FH, these are regressions of the same overall cost elements as those listed DD or FH and are treated identically.

DD cost and TE cost are treated separately by MERCER. Subsystem DD costs are summed and used to compute a total vehicle test and evaluation (TE) cost. Again, in accounting ledger fashion, subtotals are displayed for summed subsystem total DD cost, total subsystem FH cost, total TE cost, total FH assembly/test/management cost, and total FH cost. In like fashion, subsystems weights are summed in ledger fashion identifying a total vehicle weight.

MERCER provides a Phase A cost forecast of total vehicle DDTE and FH cost using the NAPCOM CERs. Though MERCER is not organized like the NAPCOM spreadsheet, NAPCOM's CERs are resident in MERCER. The NAPCOM CERs are not modified by MERCER other than normalization to 1989 equivalent dollars. Three NAPCOM equations (Manned Module Cost, Booster Cost, and Orbital Transfer Vehicle Cost) are listed in MERCER. The total MERCER vehicle weight serves as the input to the selected NAPCOM CER. The NAPCOM cost forecast may then be compared to the subsystem based cost estimate generated by MERCER.

## SUMMARY AND CONCLUSION

Advanced Manned Spacecraft weight may be adequately estimated and costed for initial feasibility study utilizing regression mathematics within a programmed methology. The Mass Estimating Relationship/Cost Estimating Relationship Program (MER/CER) is such a system developed by this study

for the Advanced Projects Definition Office (APDO) of the New Initiatives Office (NIO). Adequate techniques sizing of subsystem and vehicle weights and costs for advanced planetary manned vehicles and boost rockets were accomplished. Content of the methology includes two independent mass property estimating systems, three independent cost estimation systems, and mass and cost estimation relationships developed by the study. Dry weights are expressed in pounds and costs in 1989 million-dollar units.

# A PRELIMINARY DESIGN OF INTERIOR STRUCTURE AND FOUNDATION OF AN INFLATABLE LUNAR HABITAT

Final Report

NASA/ASEE Summer Faculty Fellowship Program -1989

Johnson Space Center


| | |
|---|---|
| Prepared by: | Paul K. Yin, Ph.D.,P.E. |
| Academic Rank: | Assistant Professor |
| University and Department: | Texas A&M University @ Galveston<br>Department of Marine Engineering<br>P.O.Box 1675<br>Galveston, Texas 77553-1675 |
| NASA/JSC | |
| Directorate: | Engineering |
| Division: | Advanced Programs Office |
| Branch: | Systems Definition |
| JSC Colleague: | Clarence Bell, Ph.D. |



| | |
|---|---|
| Date Submitted: | August 18, 1989 |
| Contract Number: | NGT 44-001-800 |

## ABSTRACT

A preliminary structural design and analysis of an inflatable habitat for installation on the moon has been completed. This work was an extension of a concept conceived in the Advanced Programs Office of the Johnson Space Center. The concept takes the shape of a sphere with a diameter of approximately 16 meters. The interior framing provides five floor levels and is enclosed by a spherical air-tight membrane holding an interior pressure of 14.7 psi (101.4kpa). The spherical habitat is to be erected on the lunar surface with the lower one third below grade and the upper two thirds covered with a layer of lunar regolith for thermal insulation and shielding against radiation and meteoroids.

The total dead weight (earth weight) of the structural aluminum, which is of vital interest for the costly space transportation, is presented. This structural dead weight represents a preliminary estimate without including structural details.

The design results in two versions, one supports the weight of the radiation shielding in case of deflation of the fabric enclosure and the other assumes that the radiation shielding is self supporting.

To gain some indication of the amount of structural materials needed if the identical habitat were installed on Mars and Earth three additional design versions were generated where the only difference is in gravity. These additional design versions are highly academic since the difference will be much more than in gravity alone. The lateral loading due to dust storms on Mars and wind loads on Earth are some examples.

The designs under the lunar gravity are realistic. They may not be adequate for final material procurement and fabrication however as the connection details, among other reasons, may effect the sizes of the structural members.

All the computer input data, plots of the computer model, and output results are kept with the Advanced Programs Office of the JSC. For more information on these data please contact Mike Roberts at (713)483-0123. The author can be reached at (409)740-4473 for further interpretations.

## INTRODUCTION

The human presence and the development of a permanent base on the moon is envisioned as the next stepping stone to Mars and toward long term space exploration[1]. Options for human habitation on the moon have been conceived and studied recently by NASA. One of the options, which appears promising, is an inflatable spherical habitat. This concept is seriously explored by the Advanced Programs Office of the Johnson Space Center[2]. With the basic concept and various design requirements reasonably defined, a realistic design of the interior structure and the exterior foundation is needed for further development of this concept.

With the design of the regolith shielding yet to be developed, two design versions were generated with one supporting the shielding and the other assuming that the shielding is self supporting.

The interior framing and the exterior support structure, all of high-strength structural aluminum 2219, have been modeled using IDEAS/FRAME, a structural analysis computer program developed by the Structural Dynamics Research Corporation (SDRC)[3]. Since the membrane enclosure does not carry any vertical load under the lunar gravity the flexible membrane is not included in the stiffness model.

Under the expected live loads on each of the five floors and the dead weight of the structure (with the lunar gravity properly accounted), all the load carrying members have been sized to their minimum sizes satisfying the Specification for the Design, Fabrication and Erection of Structural Steel for Buildings published by the American Institute of Steel Construction (AISC)[4] except the foundation mat which provides a factor of safety of 4 against the yield strength of the aluminum and the ultimate bearing capacity of the lunar soil[5,6].

To provide some indication of the impact on the structural dead weight if the identical habitat were installed on Mars or on Earth three additional design versions were generated, two under Martian gravity and one under Earth gravity.

## DESCRIPTION OF THE CONCEPT

Since the interior of the habitat must provide a replica of the earth's atmosphere at approximately sea level the most efficient shape would be that of a sphere from both

the view points of the interior space and the membrane stress in the wall of the enclosure due to the inside pressure of 1 atm[2].

To accommodate a crew of 12 and various other architectural requirements[7] the diameter of the habitat was selected to be 16 meters which provides enough total vertical distance for five floor levels. While the inside air pressure will be contained by a spherical flexible enclosure, the five floors will be provided by some structural framing.

The flexible enclosure together with part of the interior framing will be so designed that it can be folded down into a canister for space transportation and field erection on the surface of the moon. The habitat is to be installed with its lower one-third below grade and its upper two-thirds covered by a one-meter layer of the lunar regolith as the thermal and radiation shielding (Fig.1).

The habitat is intended for permanent human habitation and mission operations for a duration longer than six months.

## DESIGN REQUIREMENTS

In addition to the various requirements described in references [2] and [7], listed below are some specific design considerations:

- The total structural dead weight should be minimized.
- The design satisfies the Specification for the Design, Fabrication, and Erection of Structural Steel for Buildings by the American Institute of Steel Construction (AISC)[4].
- The design provides structural redundancy to allow for load redistribution in case of damage and thus preventing catastrophic collapse until the damage is repaired.
- Interchangeabilities among structural members should be maximized for expediency of field erection and minimization of inventory of spare structural members.
- The framing configuration should be suited for space transportation and field erection.
- The habitat can be installed anywhere on the surface of the moon.

## STRUCTURAL FRAMING

The interior framing is to provide 5 floor-levels with a central vertical core of open space for vertical traffic and air circulation. These are provided by the five horizontal framings and the six central columns defining the central core of the open space. To create maximum degree of interchangeability among structural members it has been decided to maintain the structure axi-symmetrical about its vertical center line and to have six identical vertical-radial planes of "frames" without diagonal bracings to provide maximum usable open spaces between levels. These six vertical frames are 60-degree apart about the vertical axis of symmetry of the entire structure. Loads are transferred from the interior structure to the exterior support structure across the air-tight membrane at the six "hard" points at the first floor level as well as at the bottom ends of the six central columns. The global torsional rigidity and the structural redundancy are provided by the secondary bracings in the planes immediately next and "parallel" to the surface of the spherical membrane.

All horizontal members are of rectangular tubulars with their strong axes horizontal and all the six vertical central columns are of hexagonal tubulars. All secondary braces are of pipe tubulars and so are the six vertical exterior support columns. All members are of commercially available sizes (Figs.1,2)[4].

## STRUCTURAL MATERIALS

The same material used for the frame of the Lunar Rover, Aluminum 2219[8], is used for the design. Extensive selection of material is beyond the scope of this design exercise. Better choice of alternative material is possible, such as, Aluminum Lithium developed more recently which is 10% lighter than 2219 with comparable strength. Relevant properties of the Aluminum 2219 are[9]:

| | |
|---|---|
| Specific weight: | .101 lb./cu.in. |
| Ultimate strength: | 66 ksi(455,070 kpa) |
| Yield strength: | 51 ksi(351,645 kpa) |
| Modulus of elasticity: | 10.6x10E6 psi(73.1x10E9 kpa) |

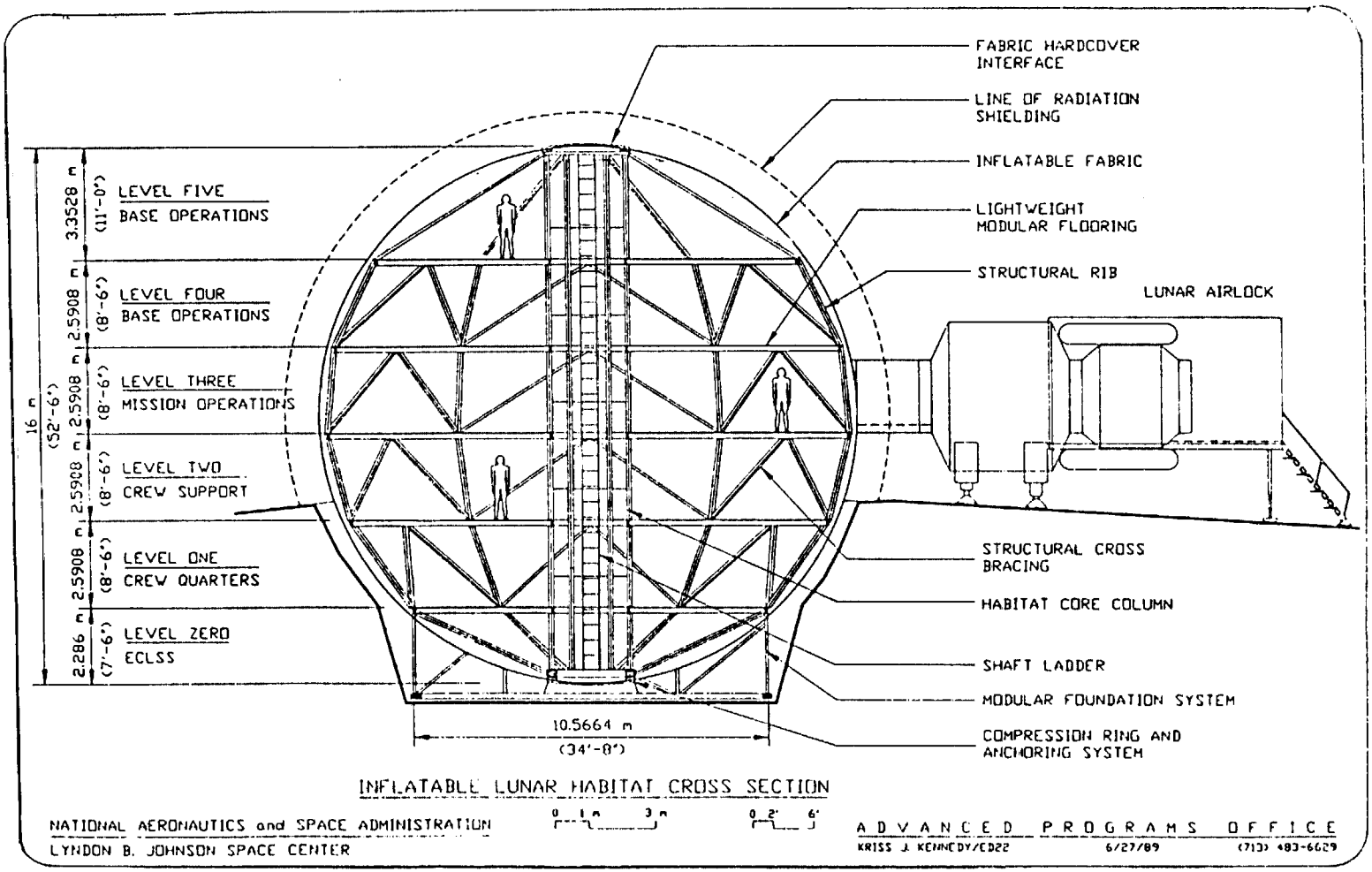


Fig. 1 - Typical Elevation

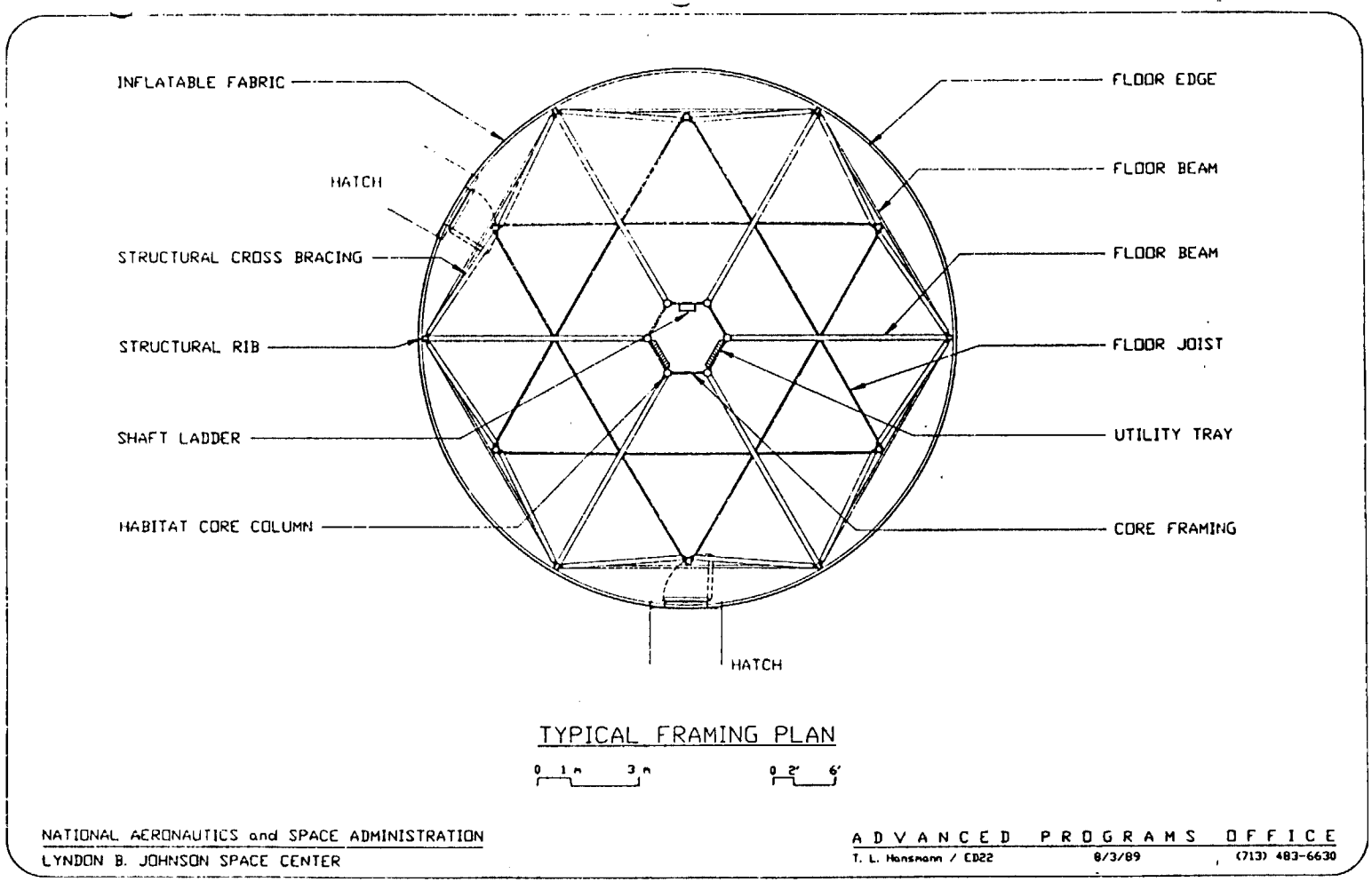


Fig. 2 - Typical Framing Plan

## DESIGN LIVE LOADS

The design live loads are the best estimate of the expected area loadings due to the weight of various equipment, furnitures, people, etc[7]. Since the live loads were realistic estimates and area specific, no additional carry-down factors were applied for the structural analysis and design. The design live loads are given in Table 1.

Table 1.- DESIGN LIVE LOADS.

| floor | earth psf | total earth lbs | total lunar lbs | total lunar kn |
|---|---|---|---|---|
| 1st | 50- 60 | 55,500 | 9,250 | 41 |
| 2nd | 40-125 | 170,100 | 28,350 | 126 |
| 3rd | 60-125 | 187,700 | 31,283 | 139 |
| 4th | 60-125 | 194,800 | 32,467 | 144 |
| 5th | 50-100 | 136,000 | 22,667 | 101 |
| all | | 744,100 | 124,017 | 552 |
| roof | Regolith shielding: | | 77,344 | 344 |

## RESULTS

Results are presented first of the mat foundation, then followed by the bill of materials for the case where the weight of the radiation shielding is not supported by the interior structure, and thirdly of the comparisons among all design cases.

### The Mat Foundation

The design of the mat foundation is summarized below:

- Factor of safety: 4 against soil ultimate bearing capacity and 4 against yield strength of the mat
- Total foundation reaction: 128,000 lbs. (569 kn)
- Total bearing area: 10,000 sq.in. (6.452 sq.m)
- Total dead weight of the mat: 1,310 earth lbs. (594 kg)
- Depth below grade: 16.4 ft (5 m)
- Lunar surface soil properties:
  Apparent density[5]: 100 lb/cu.ft (1,600 kg/cu.m)
  Ultimate bearing capacity[6]:76 psi (524 kpa)

Bill of Materials

Table 2 summarizes the total amount of material for each size and shape of all the structural members. All hexagonal tubulars are represented by pipe tubulars of equivalent strength and weight.

TABLE 2.- BILL OF MATERIALS.

| section | width in. | height in. | wall th. in. | total wt. earth lb. | t. mass kg. |
|---|---|---|---|---|---|
| rect. tubular | 2 | 3 | .1875 | 2,426.0 | 1,100.2 |
| " " | 2 | 4 | .1875 | 534.5 | 242.4 |
| " " | 2 | 5 | .2500 | 1,479.0 | 670.7 |
| " " | 3 | 5 | .3125 | 1,307.3 | 592.9 |
| pipe " | 3.5(o.dia.) | | .2160 | 3,093.0 | 1,402.7 |
| pipe " | 4.5(o.dia.) | | .2250 | 494.8 | 224.4 |
| all sections total(interior & suppt.) | | | | 9,335.0 | 4,233.6 |

Additional Cases

The comparisons among all different design cases are given in Table 3.

TABLE 3.- TOTAL DEAD WEIGHT OF STR. ALUM. FOR ALL CASES.

| | Moon | Mars | Earth |
|---|---|---|---|
| No rad. shielding, earth lbs. | 9,335 | 11,620 | 28,625 |
| kg. | 4,234 | 5,270 | 12,982 |
| Sppt. rad. shielding, earth lbs. | 10,490 | 14,660 | N/A |
| kg. | 4,757 | 6,649 | N/A |
| Gravitational constant, in/sec.sq. | 64.33 | 146.4567 | 386.000 |
| m/sec.sq. | 1.62 | 3.6882 | 9.721 |

CONCLUDING REMARKS

Using Aluminum 2219 for the structural framing subject to a set of estimated live loads under the lunar gravity, the total structural dead weight is 9,335 earth pounds equivalent to a mass of 4,234 kg. This total amount of

structural material includes both the framing inside the 16-meter diameter air-tight enclosure and the exterior support framing with the mat foundation. The structure is analyzed and designed to the Specification for the Design, Fabrication, and Erection of Steels for Buildings by the American Institute of Steel Construction (AISC)[4] except the mat foundation which provides a factor of safety of 4 against yielding of the aluminum or the lunar soil at the depth of 5 meters. The structure may be considered as a "fully stressed design" using the most efficient structural shapes in author's judgement. The total structural dead weight is increased to 10,490 earth pounds or 4,757 kg if the structure was to support a one-meter thick radiation shielding of lunar regolith.

Keeping all the design parameters the same except the gravity, the total structural material is increased by 24.5% under the Martian gravity and 206.6% under the Earth gravity. These results indicate merely the trend of increase in structural dead weight under the influence of gravity knowing that lateral loads, which are absent on the moon but present on both Mars and Earth, are not accounted.

All the summaries in weight may vary as a result of structural details, packaging for shipping, and necessary adjustments for field erection.

In view of the costly space transportation the design can and should be further optimized by way of, for example, using materials lighter than Aluminum 2219 with comparable relevant properties (such as Alum. Lithium), more suitable design specification other the that of AISC, more precise live loads, subgrade modulus for the design of foundation, and finally, a computer program for automatic design optimization.

Being situated remotely on the moon, on-site repairability of structural damage for unforeseeable reasons must be ensured by providing structural redundancy. Question on adequate degree of this redundancy can be answered rationally by performing the so-called collapse analysis. The result is a probability assessment of catastrophic collapse of the structure and its comparison with a certain maximum allowable level.

ACKNOWLEDGMENT

The author owes many thanks to his NASA Colleague, team mates, and all others in the Advanced Programs Office and in JSC in general for their valuable help in various ways.

## REFERENCES


1. Davidson, W.L.,and Stump, W.R., "Lunar Stepping-Stones to a Manned Mars Exploration Scenario," Symposium on Lunar Bases & Space Activities in the 21st Century," Paper No. LBS-88-195, 1988.

2. Roberts, M.L., "Inflatable Habitation for the Lunar Base," Symposium on Lunar Bases & Space Activities in the 21st Century, Paper No. LBS-88-266, 1988.

3. Structural Dynamics Research Corporation (SDRC), User's Guide, I-DEAS, Frame.Engineering Analysis, Vol. 1, Level 4, 1988.

4. American Institute of Steel Construction, Inc., Manual of Steel Construction, 8th Edition, 1980.

5. Mitchell, J.K. et.al., "Mechanical Properties of Lunar Soil: Density, Porosity, Cohesion, and Angle of Internal Friction," Proceedings of the Third Lunar Science Conference, Vol. 3, pp 3235-3253, The M.I.T. Press, 1972.

6. Vesic, A.S., "Bearing Capacity of Shallow Foundations," Foundation Engineering Handbook, Van Nostrand Reinhold Co, 1975.

7. Kennedy, K.J., "Interior Design of the Lunar Outpost," submitted to the 2nd International Conference on Engineering, Construction, and Operations in Space, 1990.

8. Morea, S.F., "The Lunar Roving Vehicle - A Historical Perspective," Symposium on Lunar Bases & Space Activities in the 21st Century, Paper No. LBS-88-203, 1988.

9. Joseph T. Ryerson & Son, Inc., Ryerson Data Book -Steel, Aluminum, and Special Metals, 1971.

NASA
National Aeronautics and Space Administration

# REPORT DOCUMENTATION PAGE

| 1. Report No. | 2. Government Accession No. | 3. Recipient's Catalog No. |
|---|---|---|
| NASA CR 185601 | | |

| 4. Title and Subtitle | 5. Report Date |
|---|---|
| NASA/ASEE Summer Faculty Fellowship Program--1989<br>Volume 2 | December 1989 |
| | 6. Performing Organization Code |
| 7. Author(s) | 8. Performing Organization Report No. |
| William B. Jones, Jr. and Stanley H. Goldstein, Editors | |
| 9. Performing Organization Name and Address | 10. Work Unit No. |
| Texas A&M University<br>College Station, TX 77843 | 11. Contract or Grant No.<br>NGT 44-001-800 |
| 12. Sponsoring Agency Name and Address | 13. Type of Report and Period Covered |
| National Aeronautics and Space Administration<br>Washington, D.C. 20546 | Contractor Report |
| | 14. Sponsoring Agency Code |

15. Supplementary Notes

16. Abstract

The 1989 Johnson Space Center (JSC) National Aeronautics and Space Administration (NASA)/ American Society for Engineering Education (ASEE) Summer Faculty Fellowship Program was conducted by Texas A&M University and JSC. The 10-week program was operated under the auspices of the ASEE. The program at JSC, as well as the programs at other NASA Centers, was funded by the Office of University Affairs, NASA Headquarters, Washington, D.C. The objectives of the program, which began nationally in 1964 and at JSC in 1965, are (1) to further the professional knowledge of qualified engineering and science faculty members; (2) to stimulate an exchange of ideas between participants and NASA; (3) to enrich and refresh the research and teaching activities of participants' institutions; (4) to contribute to the research objective of the NASA Centers

Each faculty fellow spent at least 10 weeks at JSC engaged in a research project commensurate with his/her interests and background and worked in collaboration with a NASA /JSC colleague. This document is a compilation of the final reports on the research projects performed by the faculty fellows during the summer of 1989. Volume 1 contains reports 1 through 13, and Volume 2 contains reports 14 through 26.

| 17. Key Words (Suggested by Author(s)) | 18. Distribution Statement |
|---|---|
| | Unclassified - Unlimited |

| 19. Security Classification (of this report) | 20. Security Classification (of this page) | 21. No. of pages | 22. Price |
|---|---|---|---|
| Unclassified | Unclassified | 338 | NTIS |

For sale by the National Technical Information Service, Springfield, VA 22161-2171

JSC Form 1424 (Rev Aug 89) (Ethernet Jan 88)
U.S. Government Printing Office:1989-761-014/00212